UNIVERSITY OF CALIFORNIA, MERCED

Membrane-Bound Kinesin Transport and its Applications in Active Matter

A dissertation submitted in partial satisfaction of the requirements for the degree
Doctor of Philosophy

in

Physics

by

Joseph David Lopes

Committee in charge:

Professor Kevin Mitchell, Chair
Professor Linda S. Hirst
Professor Ajay Gopinathan
Professor Bin Liu

2019

The Dissertation of Joseph David Lopes is approved, and is acceptable in quality and form for publication on microfilm and electronically:

Bin Liu

Ajay Gopinathan

Linda S. Hirst

Kevin Mitchell, Chair

University of California, Merced

2019

Dedication

To my fiancée Kelly

I wouldn't have been able to pursue my Ph.D. if it wasn't for your love, support, and sacrifice.

To my Mom and Dad

For encouraging me to pursue what I loved.

To my Brother

I hope you enjoy reading this as much as I'll enjoy reading yours.

To my Grandfather

For fostering my curiosity about the world, I hope I've made you proud.

To my Grandmothers

For their support and patience.

To my advisor Linda S. Hirst

I couldn't ask for a better mentor, through triumphs and failures you showed me the way.

To my antagonist Sheida T. Riahinasab

It was never a dull day in the lab with you around, thank you for the memories.

To my friend Charles N. Melton

You made the lab feel like a second home

Table of Contents

List of Figures viii
Acknowledgments xiv
Curriculum Vitae xv
Abstract xviii
Introduction 1
1.1 Active Matter 1
1.2 Lipid Membranes 3
1.3 Microtubules 8
1.4 Kinesin 9
Background and Theory 11
2.1 Kinesin Motor Transport 11
2.2 Multiple Motor Transport 13
2.3 Membrane Bound Motor Transport 17
2.4 Active Matter and Biology 21
2.5 Active Nematic Systems 22
Formation of Lipid Nanotubes from Kinesin Anchored Vesicles 26
3.1 Introduction 26
3.1.1 Kinesin 26
3.1.2 Lipid Membrane 27
3.1.3 Drag Force 28
3.2 Methods 30
3.2.1 Materials 30
3.2.2 GUV Formation 31
3.2.3 Flow cell For Nano-Tubulation 32

3.2.4 Lipid Bilayer from SUV Deposition 33
3.2.5 Fluorescence Microscopy and FRAP 34
3.3 Results 38
3.3.1 Diffusivity of Membrane Bilayer 38
3.3.2 Tubule Formation from Diffusive GUVs 39
3.4 Discussion 40
3.4.1 Tubulation as a Function of Bending Rigidity 40
Clustering of Membrane Bound Kinesin to Microtubules 41
4.1 Introduction 41
4.2 Methods 42
4.2.1 Materials 42
4.2.2 Microtubule Preparation 42
4.2.3 Lipid Membrane Preparation 42
4.2.4 Flow Cell Preparation 43
4.2.5 Microtubule Gliding Experiments 43
4.2.6 DGS-NTA Clustering 43
4.2.7 Motor Clustering 43
4.2.8 Imaging and Data Analysis 44
4.2.9 Confocal Microscopy 44
4.3 Results 45
4.3.1 Motor Proteins Non-Specifically Bind to NTA Head Group. 45
4.3.2 Direct Observation of Motor Clustering on Microtubule 46
4.3.3 Membrane Supported Gliding Velocity is Time Dependent 49
4.3.4 Velocity Increase Observed at .1 and .05mM ATP Concentrations 51
4.3.5 Microtubule Gliding Velocity is Not Caused by Lipid Clustering 51
4.3.6 Gliding Velocity Increase Continues After Temporary Suspension 52
4.4 Discussion 54
4.4.1 Kinetics of Diffusive Kinesin 54
4.4.2 Effects of Kinetics on Gliding Velocity After Long Time Scales 58
4.4.3 Increasing Gliding Velocity Over Time Before Steady State 59
Active Nematics from Membrane Bound Microtubules 61
5.1 Introduction 61

5.2 Methods 62
5.2.1 Materials 62
5.2.2 Microtubule Purification and Preparation 62
5.2.3 Motor Protein Purification and Preparation 63
5.2.4 Lipid Membrane Preparation 63
5.2.5 Flow Cell Preparation 64
5.2.6 Dilute Microtubule Gliding Experiments 64
5.2.7 Microtubule Gliding Experiments with Unlabeled Filaments 64
5.3 Results 65
5.3.1 Formation of Active Nematic 65
5.3.2 Formation of the Network Phase 68
5.3.3 Localization of Kinesin 71
5.4 Discussion 72
5.4.1 Membrane Based Active Nematic 72
5.4.2 Membrane Diffusivity and the Formation of Network Phase 73
Conclusions and Future Work 75
References 77

List of Figures

Figure 1. Active mater. Collective motion of shearing microtubules whose interaction cause the folding and internal fracture of a nematic domain. The fracture line terminates with a pair of oppositely charged disclination defects (A-D) (red arrow tracks ½ disclination; blue arrow tracks -½ disclination) 15 s; scale bar 20 mm. Collective motion demonstrated in Janus particles with different electrical charge conditions obtained from [16]. By redistributing the charge's particles placed in a flowcell of oscillating electric field will move in plane, creating collective group motion, growth or both (F). Image obtained from [10]..... 2
Figure 2. Biomimetic Vesicles. Shearing microtubules confined to giant unilaminar vesicles (GUVs) have been shown to produce motion and shape defects. Confocal images showing the z-projection of the vesicle shape (A), with corresponding 3D schematics shown in (B). Image obtained from [22]..... 3
Figure 3. 18:1 (Δ9-*Cis*) PC (DOPC) Lipid. The double bond indicates that this lipid is unsaturated, creating a kink in its tail structure that impacts it's packing order by taking up a larger volume. DOPC image obtained from [23]..... 4
Figure 4. Self-Assembly driven by hydrophobicity. Lipid molecules have a polar head group and a non-polar tail comprised of long carbon chains. When these molecules are placed in a polar solvent, the tails disrupt the water molecules around them and reduce the possible number of configurations (A). As the lipids randomly diffuse in solution, when their tails make contact, it reduces the area exposed to water, making a smaller "water cage" (B). This process continues until only the polar heads are exposed to water, reducing the entropic cost of the system while forming an ordered structure. Image obtained from [13]..... 5
Figure 5. Lamellar and micellar phase of lipids. Shapes are based not only on concentration of lipids but the curvature of the lipids when packed together. Lipids with more cylindrical volume based on the size of the lipid head and tail structure are predisposed to low curvatures shapes. Lipids with volumes closer in shape to a cone are predisposed to micelle phases. Image obtained from Wikipedia and [27]..... 6
Figure 6. Lipid gel phase and fluid phase. Lipids in the gel phase, $L_{\beta'}$, are tightly packed and have significantly reduced diffusivity compared to the fluid phase, $L_{\alpha'}$. Image obtained from [13]..... 6
Figure 7. Lipid Phase Diagram. The blue region denotes areas with both gel and liquid ordered phase coexistence, red is the coexistence of liquid ordered and liquid disordered phase, and green is the coexistence of the liquid disordered and gel phase. The region between the colored areas has all three phases coexisting. The tie-lines on a phase diagram are lines in the two-phase region which the different phase fractions have consistent compositions. Image obtained from [28]..... 7
Figure 8. Lipid Raft. Due to the difference in the lipids excluded volume, the lipid specimens will separate in plane into a state with the lowest free energy. The blue lipids denote a lipid with

saturated bonds, forming long, straight tails. Cholesterol preferentially packs in these rafts between the lipid tails. The bulk is comprised of lipids with unsaturated tails that take up a larger volume. 8
Figure 9. Microtubules and the dimer subunits. The microtubule is formed from the self-assembly of alpha and beta tubulin dimers into long strand protofilaments. The polymers then assemble into the tube structure above. Image obtained from Wikipedia. 9
Figure 10. Kinesin-1 motor protein. Kinesin protein are responsible for intracellular transport of vesicle cargo along microtubules. The motor head is on the left-hand side, and ATP hydrolysis drives to the kinesin to walk along the microtubule. On the right, the light chain attaches to the vesicle. Image obtained from [2]. 10
Figure 11. Brownian Ratchet. The potential during the off phase of a Brownian ratchet is constant, allowing the particles motion to be considered purely diffusive. When the potential is applied, it forms a periodic asymmetric profile, guiding particles in a biased direction (A). When the potential is made constant again, the particles are initially concentrated (B), but over time diffuse out into the surrounding space, with a portion of the population reaching beyond the next period of potential, biasing the direction of motion with each application of the potential (C). Image obtained from [48]. 12
Figure 12. Kinesin stepping cycle. The stepping of kinesin motors can be modeled as a four-step process starting with the binding of the motor head to the microtubule. While the lead motor domain attaches to the microtubule, ATP binds to the head causing the (red) linker to contract and pull the motor forward (A). While this (yellow) linker contraction occurs, the rearmost detached head (red) diffuses, biased forwards due to the contraction (B). This motor protein then binds to the surface of the microtubule while the rearmost motor head is unbound by the hydrolysis of ATP (C), allowing the rearmost head to diffuse, restarting the cycle (D). Image obtained from [50]. 13
Figure 13. States of collective cargo transport. Motor proteins regularly bind and unbind from microtubule filaments due to the nature of their stepping cycle. When motors are bound to a cargo, the motor proteins that unbind have a potential to rebind to the filament. Each cargo can be considered as a state with n motor proteins bound to a filament, walking at v_n speed, with a potential to transition to a new state at rate $\boldsymbol{\varepsilon_n}$ or $\boldsymbol{\pi_n}$ (A). If we consider the bound vs unbound state (B), we can see that at state n=0, there is a rate $\boldsymbol{\pi_0}$, for the system to transition to the bound state and a potential for the state n=0 to be transitioned to from state n=1 at rate $\boldsymbol{\varepsilon_1}$. Image obtained from [52]. 14
Figure 14. Diagram of membrane bound microtubule transport. Kinesin motor proteins are bound to a fluidic lipid membrane by biotin-streptavidin linkage. When ATP is added to the system the motor proteins “walk”. Since the kinesin are bound to the surface of the membrane the microtubule instead glides in the opposite direction of motor stepping. Image obtained from [56]. 18
Figure 15. Quantification of velocity and net force. The velocity of slipping, how much the motor protein is displaced during stepping, is subtracted from the velocity of stepping to relate it to the gliding velocity (A). The net force on the microtubule is defined as the force of each motor multiplied by the number of motors. Image obtained from [56]. 19

Figure 16. Computational results from Vicsek et al. The Viseck model gave particles a constant velocity whose direction was the average of the neighboring particles with some noise. By varying the noise and velocity you can see a transition from isotropic to nematic phase. Particles start with random alignment and if they have high coherence and low particle density will random clusters, (B). If coherence is lowered but density is increased the particles will move randomly with some alignment, (C). Lastly if the particles have high density and coherence then they will be strongly aligned (D). Image obtained from [64]. 23
Figure 17. Model of particle motion and their phase behaviors. Polar active particles are directed particles that are asymmetric in shape (A), apolar particles are symmetric particles that move in either direction (B), and the self-propelled rod is a symmetric particle that moves in one direction (C). These particles then produce either polar (D) or nematic phases (E, F). Image obtained from [57]. 24
Figure 18. Density waves in polar filaments. When myosin motors drive polar actin filaments, there motion prevents cross over, and an intermolecular force allows the filaments to align. When the density of filaments increases we can see (A) the formation of dense regions that spontaneously emerge. With the increase in density, the regions grow (B), until a critical density is achieved, and the filaments form waves (C). Image obtained from [62]. 25
Figure 19. Formation of lipid tubules by anchored GUVs. When GUVs are bound to a microtubule by a motor protein, the application of drag force will cause the GUV to deform and extract a tubule. This tubule can be stabilized by other motors anchoring the tubule to additional microtubules. Image obtained from [8]. 29
Figure 20. Lipid molecular diagrams. These lipid molecules, DOPC (A), DGS-NTA (B), and DOPE-NBD (C), form homogenous fluid membranes at room temperature because of their identical unsaturated tail structures. When DPPC (A), DGS-NTA (B), and DOPE-NBD (C) are mixed, the rigid tail structure of DPPC forces the membrane to be in the gel phase at room temperature. Images obtained from Avanti Inc. 31
Figure 21. GUV electroformation. GUVs are formed when a you take two pieces of ITO glass (A) and coat the surface with dried out lipids. When the dried-out lipids are enclosed and hydrated (B), the lipid will slake off the surface. When a sinusoidal electric field is induced by a generator at the proper frequency and voltage (C) GUVs will form from the dissolved sheets of lipid. 32
Figure 22. Flow cell. Flow cells are constructed from cleaned glass slide, coverslip, and double-sided sticky tape. Two ends are left open for the inflow and outflow of solution and are approximately 25 µl in volume. 33
Figure 23. Fluorescence recovery after photo bleaching (FRAP). Initially the lipid bilayer is imaged and used to measure the total intensity of the area (A). The membrane in then bleached by passing the light through an aperture, overexposing a small region (B). The Lipids of the bleached area will slowly exchange with unbleached lipids at the interface (C), until the entire area has exchanged with the background. Image obtained from Wikipedia. 35
Figure 24. Plot of Time vs. Normalized Intensity. The plot represents the intensity curve from FRAP experiments on DOPC/DGS-NTA (5 mol%) lipid membranes. The red line is the Soumpasis equation fit used to extract the diffusion coefficient, D, of the membrane. The D value for the plot shown here is 9.01±.58 $\frac{\mu m^2}{s}$. Image obtained from [8]. 38

Figure 25. Fluorescence microscopy of GUVs and nanotubes. DPPC/DGS-NTA (5 mol%) form crumpled vesicles (A) while DOPC/DGS-NTA (5 mol%) form spherical vesicles (B). DOPC/DGS-NTA (5 mol%) vesicles form tethered GUV (C) when flow is induced, and these tethers are anchored onto labeled microtubules (D). Lipid nanotube can bind to additional motors and remain extended (E). Scale bar: 10 μm. Image obtained from [8]..... 39
Figure 26. Confocal microscope diagram. Confocal microscopes operate much the same as a standard fluorescence microscope, using a source of filtered light source to send a specific wavelength of light into the sample. The sample's fluorophores become excited and emit photons of a higher wavelength that then must pass through a pinhole aperture. This aperture only allows light from a set focal plane to pass through to the detector..... 45
Figure 27. Kinesin non-specifically binds to DGS-NTA lipids. Confocal images of the lipid membrane after introduction of GFP labeled kinesin-1, whose concentration in solution was 0 nM (A), 100 nM (B), 200 nM (C), and 300 nM (D) to quantify non-specific binding. Scale bar represents 50 μm. (E) Average intensity of GFP signal plotted against motor protein concentration, with error bars representing the standard error of the mean (SEM). This plot demonstrates the increased motor concentration on the surface with the increased presence of motor proteins in solution. 46
Figure 28. Membrane-coupled motors accumulate on static microtubule. (A) Cartoon schematic of motor protein clustering on a microtubule. (B - E) Fluorescence images of GFP labeled kinesin clustering on an immobile microtubule recorded at 15, 45 and 75 minutes and (F - H) corresponding 1D line profiles of image intensity after background subtraction, corresponding to peaks of intensity. (I) Normalized GFP intensity as a function of time calculated from the average area under the peak for 45 microtubules error bars indicate standard error of the mean. Scale bar is 5 μm. 48
Figure 29. Microtubule gliding velocity is influenced by membrane coupling. Cartoon schematics of gliding, microtubules gliding while coupled to a fluid membrane substrate (A) and gliding on a solid substrate (B). Representative gliding trajectories of microtubules and their associated velocity histograms on membrane (C, D - F) and on glass (G, H - J) taken after initial introduction of ATP (C, D), 102 min after (E, I), and 192 min after (F, J). Solid lines represent best fit to a Gaussian distribution. Mean velocities of microtubule gliding for motors coupled to the lipid bilayer 1mM ATP concentration (K) is plotted against time. Shaded bars represent the average gliding velocity of motors coupled to glass on the coverslip (K), with the width representing one standard deviation. Error bars indicate standard deviation. 50
Figure 30. Average gliding velocity at 0.1 and 0.05 mM ATP. Mean velocities of microtubule gliding for motors coupled to the lipid bilayer at 0.1 mM (A) and 0.05 mM (B) ATP concentrations plotted against time. Shaded bars represent the average gliding velocity of motors coupled to glass on the coverslip, with the width representing one standard deviation. Error bars indicate standard deviation. 51
Figure 31. Lipid clustering does not influence microtubule gliding velocity. Graph of average gliding velocity after lipids were given 120 minutes to cluster onto motor proteins (A). Velocities are normalized for with average glass gliding velocity on coverslip and error bars indicate standard error of the mean. 52

Figure 32. Arresting microtubule gliding motion does not alter the increase in microtubule gliding velocity. Gliding velocity distributions after the addition of 1mM ATP and 20 minutes afterwards are contrasted between continuous gliding (A) and "paused" gliding (B). Velocities from continuous membrane gliding experiment are shown as histograms (A, B). Membrane gliding was repeated with the additional step of removing ATP (C) after initial observation period (E). ATP was re-introduced 20 minutes later, and gliding resumed (F). Histograms are fitted with a Gaussian distribution. 53
Figure 33. Membrane-coupled motors disassociate rapidly with the introduction of ATP. Experimental measurements of GFP intensity as a function of time for 45 microtubules using the methods described in Fig. 25. Data shown for (*a*) 0.05 mM and (*b*) 1 mM ATP, where ATP is introduced to induce gliding at 120 mins. Error bars indicate standard error of the mean. Theoretical fits (dashed lines) are performed separately for kinesin aggregation without ATP (Blue) and the decay of the microtubule-bound kinesin signal after ATP addition (Orange). (*c*) Rates $\boldsymbol{k_a^{eff}}$ (inset) and $\boldsymbol{k_d^{eff}}$ extracted from our fitting model (Equations 3b and 5b) for ATP concentrations 0.05mM and 1mM (Orange) show a general trend of increasing off rate ($\boldsymbol{k_d^{eff}}$) with increasing ATP concentration. Both growth rates ($\boldsymbol{k_a^{eff}}$) are approximately the same (dark blue). The fitted effective off-rates are compared with expected $\boldsymbol{k_d^{MM}}$ values calculated assuming Michaelis-Menten kinetics (light blue). 54
Figure 34. Membrane-coupled motors glide at lower speeds with lower ATP concentrations. Gliding experiments were carried out at 3 different ATP concentrations, 1mM (A), 0.1mM (B), and 0.05mM (C). Microtubule gliding velocities were recorded at steady state after 2 hours. Error bars represent the standard error of the mean. Estimates for gliding velocities at 1 mM and 0.05 mM ATP are $V_{MT}(1mM) \approx 281.5\frac{\boldsymbol{nm}}{\boldsymbol{s}}$ and $V_{MT}(0.05mM) \approx 133.2\frac{\boldsymbol{nm}}{\boldsymbol{s}}$. 58
Figure 35. Labeled microtubules as tracers. Labeled filaments are dispersed with unlabeled filaments to show the general direction of flow, without producing to much fluorescence signal to obscure imaging. 65
Figure 36. Transport of microtubules on membrane coupled kinesin can induce "snuggling". When filaments are bound to a membrane, the slippage of kinesin will result in an overall reduction of force [56]. If two or more filaments collide, then they may not have to force required to cross each other and align via "snuggling" [12]. 66
Figure 37. Formation of an active nematic from isotropic due to "snuggling" effect. When microtubules are initially added to the flow cell they are randomly mixed during initial gliding and form the active nematic after 40 minutes of gliding when gliding under the conditions of 0.5mM ATP and 0.51 µg/µl filament density. To better visualize this, we perform a z-stack of 10 frames to show the trajectory of the microtubules. 67
Figure 38. Activity dependence of active nematic phase. Our model for the formation of an active nematic is based on the reduction of motor activity. By reducing ATP concentration we can reduce the activity of kinesin and control the force of interactions. Comparing our initial active nematic (A), we find that by reducing the ATP concentration to 0.1 mM, an active nematic forms at reduced filament concentration (B, C). 68
Figure 39. Intermediate network phase. When filament density is at 0.26 µg/ µl and an ATP concentration of 0.5mM the network phase occurs. This phase consists of streams of filaments

that persist for long time scales and have local orientation (A). Over time these streams will exhibit a global rotation (B, C, D) that is counterclockwise. Image comprised of a z-stack of 10 frames taken 10 seconds apart. 69
Figure 40. Qualitative Phase Diagram of Active Matter System. The red dots denote areas where the system is an active nematic, with an overall unified orientation. Blue triangles denote the existence of a network phase, where the filaments form streams of independent orientation. Black squares denote areas of isotropic flow, where filaments lack orientation. 70
Figure 41. Formation of vortices in Network phase. In some instances, instead of forming streams of random local orientation, the filaments will form vortices that persist for tens of minutes. 71
Figure 42. Localization of kinesin. At the start of gliding we can see that the fluorescent signal of our labeled kinesin is uniform (A). After the system has been gliding for a long time and streams of filaments form (B), we can see a localization of the GFP signal (C). After 15 minutes we can see that the GFP signal has grown in intensity and expanded (D). 72

Acknowledgments

There have been many people who have helped me along this journey, friends and family who have inspired me and challenged me in equal measure. I would like to acknowledge my advisor Linda S. Hirst who showed me what it takes to be a great mentor and professor. I would like to acknowledge Jing Xu, though you no longer mentor me I wouldn't be the experimentalist I am without your influence. I want to thank my committee members: Professors Kevin Mitchell, Bin Liu, and Ajay Gopinathan, for there assistance and guidance. I am also grateful to David Quint, for providing guidance on all matters theoretical, computational, and post-doctoral. To my labmates Kai Lor, Amanda J. Tan, and my friend Melissa Xu, for teaching me the esoteric secrets of motor proteins and lipids. To my labmates Sheida T. Riahinasab and Charles N. Melton for helping with the "sturm und drang" of graduate school. Finally, I want to thank my fiancée Kelly Thomas for encouraging me through this entire process.

I want to acknowledge the NSF for funding my research; NSF#DMR 1808926

As well as acknowledge the NSF-CREST Center for Cellular and Biomolecular Machines (CCBM), for funding my research; NSF-CREST: Center for Cellular and Biomolecular Machines at UC Merced HRD-1547848.

Lastly, I want to acknowledge the Health Sciences Research Institute (HSRI) at UC Merced for funding my research.

Curriculum Vitae

Joseph Lopes
Ph.D. Candidate
Hirst lab, Merced CA (916) 276-1882 jlopes2@ucmerced.edu
linkedin.com/in/joseph-david-lopes

Skills

Main

- Coding simulations in C/C++ and Python
- Linux OS experience, R, ROOT, NumPy, Fiji, Origin, and SciPy
- Quantitative Fluorescence Microscopy Fluorescence Recovery after Photobleaching
- Confocal Microscopy
- Formation of supported lipid membrane bilayers using SUV deposition
- Formulation/formation of lipid GUV using electrophoresis and PAPYRUS method
- General biochemistry for protein preparation, kinesin purification, and biopolymer formation
- Microtubule gliding assay
- Protein binding kinetics and membrane biophysics
- Total Internal Reflective Fluorescence (TIRF) Microscopy,
- Lipid tubule formation

Broader impact skills.

- Peer mentoring
- Designed experiments for high school science outreach
- Team building

Education

Ph.D. Physics

- University of California, Merced, Hirst Lab 2013-2019. Membrane Bound Kinesin Transport and its Applications in Active Matter

B.S, Physics

- University of California, Davis, 2013

Experience/Employment

Graduate Teaching Assistant and Researcher.

University of California, Merced, 2013-2019

Merced, California

- Lead Labs for PHYS 10, introduction to modern physics course
- Lead Discussions/Labs for PHYS 8 Honors, introduction to classical mechanics course
- Lead Discussion/Labs for PHYS 19, introduction to electrodynamics
- Lead Lab Sections for PHYS 160, a modern physics experimental lab course for physics seniors.

Undergraduate Volunteer Researcher

University of California, Davis, 2012-2013

Davis, California

- Assisted in the growth of colloidal nanowires and their testing, design and construction of colloidal growth setups, and coding programs to analyze testing data.

Student Assistant

Medical Board of California, 2010-2012

Sacramento, California

- Worked in the Consumer Information Unit, answering calls made by doctors, consumers, and applicants. I also helped to work the front desk and sort incoming medical license application documents.

Publications, Talks, Presentations, and Awards

Publications

- **In Progress** - "Phase Behavior of Membrane Coupled Active Nematic" Joseph Lopes, Fereshteh Memarian, Amanda J. Tan, Kevin Mitchell, and Linda S. Hirst
- **In Submission** - "Effect of Membrane Diffusion on Kinesin Kinematics" Joseph Lopes, David Quint, Dail E. Chapman, Melissa Xu, Ajay Gopinathan, and Linda S. Hirst
- **"A Simple Experimental Model to Investigate Force Range for Membrane Nanotube Formation"** C. Lor, J. D. Lopes, M. K. Mattson-Hoss, J. Xu and L. S. Hirst, FRONTIERS IN MATERIALS, BIOMATERIALS, 3, 6 (2016)

Talks

- "Substrate Mobility Produces Velocity Time Dependence in Microtubule Gliding", American Physical Society (APS) March Meeting 2018
- "Substrate mobility produces velocity time dependence in microtubule gliding", APS Far West 2017
- "Effect of membrane coupling on multiple-kinesin transport", APS March Meeting 2017
- "Effect of membrane coupling on multiple-kinesin transport", APS Far West Section 2016
- "The effects of lipid membrane mobility on microtubule gliding", APS Far West Section 2015
- "Interplay between group function of kinesin based transport and lipid bilayer mobility", APS March Meeting 2015
- "Interplay between group function of kinesin based transport and the planar lipid bilayer's recovery time after photobleaching", APS Far West 2014

Poster Presentations

- "Membrane Diffusivity Driven Microtubule-Based Active Nematics", Gordon Research Conference: Complex Active and Adaptive Material Systems, 2019
- "Effect of membrane coupling on multiple-kinesin transport", American Society for Cell Biology (ASCB), Annual Meeting 2017
- "Effects of membrane mobility on microtubule gliding", Biophysical Society Annual Meeting 2016
- "Effects of membrane mobility on microtubule gliding", ASCB Annual Meeting 2016

Awards and Accolades

- Carl Storm Underrepresented Minorities Fellowship, Gordon Research Conference, 2019
- Physics Graduate Group Summer Fellowship, 2018
- Physics Graduate Group Summer Fellowship, 2017
- Center for Cellular and Bio-Molecular Machines (CCBM), Spring Fellowship, 2017
- Center for Cellular and Bio-Molecular Machines (CCBM), Fall Fellowship, 2017
- ASCB, Minorities Affairs Committee (MAC) Travel Award, 2017
- Physics Graduate Group Summer Fellowship, 2016
- Physics Graduate Group Summer Fellowship, 2015
- GRAD-EXCEL Peer Mentor
- CREST CCBM Scholar

Abstract

Membrane-Bound Kinesin Transport and its Applications in Active Matter
Joseph David Lopes
University of California, Merced, 2019
Committee Chair: Kevin Mitchell

Understanding the intricacies of biological systems from a first principal approach has provided much insight into the function of cellular systems. The self-assembly of lipid membranes and the far-from-equilibrium nature of protein biochemistry has given rise to a new field of physics, active matter, that considers biological systems as hierarchical far-from-equilibrium phases. In this thesis, I describe experiments that investigate the impact of membrane diffusivity on intracellular transport. The results from these experiments then inspired the development of a novel form of active matter that is capable of altering its environment.

Motor proteins, specifically kinesin, are responsible for the transportation of cellular cargo. This cargo is held inside of a lipid vesicle, and how the vesicle's membrane affects kinesin-based transport has been a hotly debated topic. Recent *in-vitro* experiments suggest that transport of lipid vesicles is enhanced by the diffusivity of the membrane cargo itself. In this thesis work, I designed a system in which fluorescently labeled motor proteins are bound to a planar lipid bilayer. This two-dimensional bilayer demonstrates the diffusivity of a spherical vesicle without exhibiting the elastic or geometric effects found in small vesicles that could contribute to transport. When studying individual microtubules, we see several interesting phenomena. We observe that motor proteins are diffusive when bound to a membrane and therefore they can cluster onto a stationary filament. When we add ATP to induce gliding, the motors unbind, and by measuring the bound population density we show that motor protein disassociation from the filament is a diffusion limited process. Surprisingly when gliding on a membrane we also observed that the gliding velocity increases over time before reaching a steady state.

The next phase of the research presented in this thesis was to study if densely packed filaments on a membrane could form an active nematic. Interestingly, when bound to a diffusive membrane, sufficiently large concentrations of gliding filaments can align and move collectively. Furthermore, the results of this experiment are quite striking when the density of filaments is insufficient to form an active nematic phase. Below a certain filament density, we see the formation of a network phase of filament streams that have their own local orientation. These streams can persist for up to an hour and can also exhibit a global rotation. This could be due to the localization of the motor protein, as we see them clustered around streams of filaments. This is quite significant as we have a two-dimensional active matter system that is the product of a diffusive environment, but in turn alters that environment.

This thesis demonstrates the complex interactions motor proteins can have with lipid membranes and their subsequent impact on transport. We take advantage of these properties to design a novel active matter system that restructures its environment to reinforce its steady state.

Chapter 1

Introduction

1.1 Active Matter

Active matter is a growing field of study that intersects biophysics, soft matter, and statistical mechanics [1]. Active matter research focuses on particles that produce their own internal movement and whose interactions yield collective motion. These particles take in energy from their surroundings, producing non-equilibrium activity such as collective motion, growth, and replication [1]. In this thesis, I have investigated motor proteins and their interactions with microtubules to act as building blocks for active biological materials. In nature, motor proteins take energy from ATP hydrolysis and convert it to directed walking motion along the body of microtubules [2], allowing for the transport of intracellular cargo [3, 4, 5, 6, 7, 8, 9]. Beyond the immediate biological applications, they can be viewed in more general terms as self-propelled macromolecules with collective motion. Just like living organism have hierarchies of structure and function active matter systems can also have hierarchies. The action of motor proteins collectively propelling microtubules is a form of active matter, while the nematic phase produced by the microtubules is another level of collective action.

Collective motion occurs when individual participants in an ensemble of material exhibit coordinated motion [1]. Animals, cells, and self-propelled particles all move collectively, and this motion is based upon local interactions between participants [10]. This collective motion can further be produced in sets of hierarchies of that correspond to the particle's interaction [10, 11, 12]. For an example of this hierarchy in nature we can look at ourselves. Human eukaryotic cells are organizations of biological building blocks such as lipids and proteins. These cells organize into tissues and organs, which organize into a human being, and groups of humans organize socially. Replicating hierarchal organization in inorganic materials would provide a wealth of knowledge in how living systems developed and requires an interdisciplinary approach with active matter and another field of physics, soft matter. Soft matter is the study of condensed matter structures that are highly susceptible to temperature changes. Its most notable contributions to our understanding of biology are self-assembly, how hierarchical structures developed as the lowest energy state [13]. While most common objects exist in the solid, liquid, or gas phases, soft matter materials form intermediate phases and that are particularly susceptible to changes at or near room temperature [13]. These intermediate phases allow for the self-assembly of structures, based on the local interactions of diffusive particles.

There have been many novel models of active matter produced in the last 15 years, from systems as diverse as chemically driven particles to fire ant colonies [14, 15]. One of the most investigated systems involves propulsion of microtubules by the motor protein

kinesin. Microtubules are macromolecules with a long, rod like shape, allowing them to form active nematic phases either in bulk or confined in-plane. The nature of an active matter systems motion is dependent on the meditation of particle interactions and how they are confined. Microtubules confined to an oil/water interface bound together by kinesin that propel them will shear with the addition of ATP [10]. As the motor proteins "walk", the microtubule moves in the opposite direction, resulting in the two bound filaments moving against each other. Their confinement to the 2-dimensional interface inhibits their ability to cross, causing the bulk to mix, producing defects (Fig 1. A – D). These defects will move away from each other based on their topological charge, with ½ disclination moving away from -½ disclination. This system clearly demonstrates hierarchical directed motion in active matter. The most basic directed motion is of the motor protein from ATP hydrolysis, then we have the directed motion of the filaments through their interactions, and lastly the orientation of the defects displays a collective directed preference. Another unique example of collective motion can be seen using Janus particles, which are small spheres that have a conductive half and a nonconductive half. These particles are placed in an ionic buffer sandwiched between an oscillating electric field [16]. The field drives the motion of the ions, and the ions interaction with the Janus particle is based on the distribution of charge on the particle surface, causing the particles to move perpendicular to the field. This distribution not only induces collective swarming motion perpendicular to the field, but can induce a "pure growth" phase, and phases that are a combination of the former and latter (Fig 1. E, F).

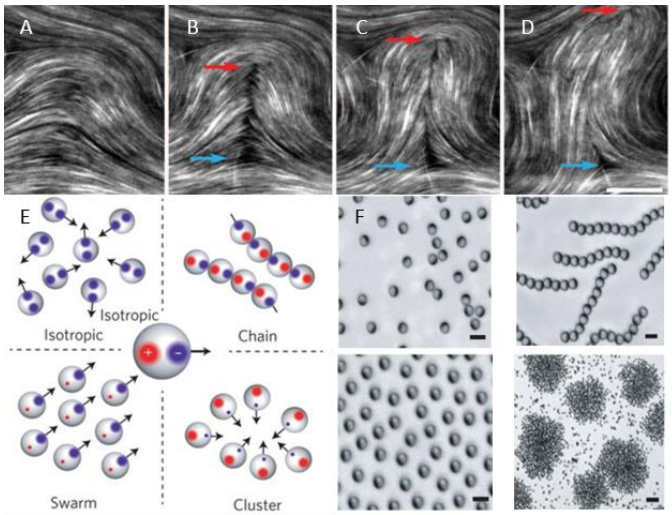

Figure 1. Active matter. Collective motion of shearing microtubules whose interaction cause the folding and internal fracture of a nematic domain. The fracture line terminates with a pair of oppositely charged disclination defects (A-D) (red arrow tracks ½ disclination; blue arrow tracks -½ disclination) 15 s; scale bar 20 mm. Collective motion demonstrated in Janus particles with different electrical charge conditions obtained from [16]. By redistributing the charge's particles placed in a flowcell of oscillating electric field will move in plane, creating collective group motion, growth or both (F). Image obtained from [10].

One aspect of active matter that is promising is the potential for developing predictive models in biology. By synthetically creating complex, ordered, and dynamic assemblies, we can better understand the structures of cells from a first principles approach [17]. While soft matter science has provided insight into the nature of self-assembly that is vital to biology, such as membrane formation [13, 18], polymer organization [13, 19], and protein folding [13, 20], these experiments cannot fully replicate the complexity of biological systems, such as the necessity to take in energy and maintaining non-equilibrium states. Current work involving motor proteins, microtubules, and lipid membranes [10, 11, 12, 21] have been promising avenues of research in this regard, for instance the usage of active nematic microtubules to drive the warping of vesicles in a periodically driven motion [22] (Fig. 2).

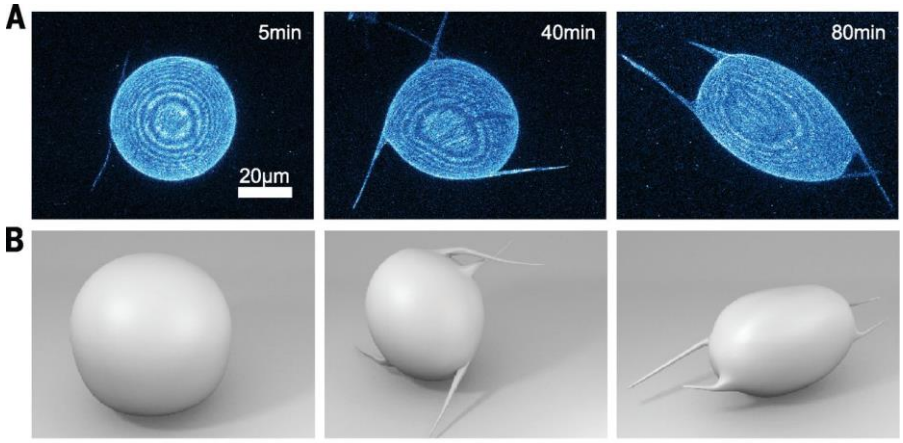

Figure 2. Biomimetic Vesicles. Shearing microtubules confined to giant unilaminar vesicles (GUVs) have been shown to produce motion and shape defects. Confocal images showing the z-projection of the vesicle shape (A), with corresponding 3D schematics shown in (B). Image obtained from [22].

The system I investigated involves the self-assembly of lipid molecules, motor proteins, and microtubules to create planar hierarchical collective motion. The motor proteins take in ATP to drive the system, the nematic nature of the microtubule creates collective motion, and lastly the lipid membrane formed a tunable, reconfigurable environment. This system represents a system of active matter based not only on particle interactions within the active matter but also the interaction of the active matter with the surrounding environment. In the long term, researchers hope to form general theories beyond molecular autocatalysis to address the emergence of organic life based on the development of non-equilibrium states. By researching a system that is active and interacts with its environment we are one step closer to a general understanding of this.

1.2 Lipid Membranes

Cells are the key building blocks of life and their existence is made possible by a dynamic cellular membrane composed of lipid molecules. These membranes are responsible not only for the formation of the boundaries of the cell, but organization of organelles in eukaryotic cells, the regulation of material uptake into cells, interactions between the cell and the surrounding environment, and most importantly maintaining the electrical potential difference between the interior and exterior of the cell [13]. These biological membranes typically comprise of two sheets of lipid molecules, referred to as a bilayer [13]. While seemingly simple in construction, membranes contain a wide range of lipid molecules and trans-membrane proteins that continuously change and alter the properties of the cell. Remarkably, we can easily create analogs of the cell membrane *in-vitro*, by taking lipid molecules and suspending them in solution through a variety of techniques and allowing them to form vesicles through self-assembly [13]. These *in-vitro* lipid membranes can vary from a simple single lipid type, to complex mixtures that include not only lipid molecules but sterols, fatty acid salts, and trans-membrane proteins. The diversity of structures possible through simple mixing is due to the nature of the lipid molecule interaction with polar solvents.

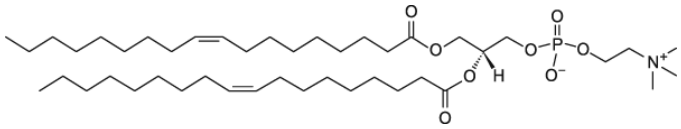

Figure 3. 18:1 (Δ9-*Cis*) PC (DOPC) Lipid. The double bond indicates that this lipid is unsaturated, creating a kink in its tail structure that impacts it's packing order by taking up a larger volume. DOPC image obtained from [23].

The amphiphilic nature of the lipid molecule drives self-assembly [13]. This property is not only the basis for creating *in-vitro* cellular and organelle analogs for experimentation, but the basis for the formation of cells in nature. By having a hydrophilic molecular head group and a hydrophobic tail group (Fig. 3), a lipid's molecular configuration leads to the existence of multiple possible phases in water. The range of lyotropic phases possible depends on the concentration of lipid in the solvent [13]. This self-assembly is due to the hydrophobic effect. When lipids are added to water, their non-polar alkyl chains will not form hydrogen bonds with the water, forcing the water to form a cage around the lipid tail (Fig. 4). This forced ordering will decrease the local entropy of the water and costs free energy. However, water can form hydrogen bonds with the lipid's polar head group. If enough lipids are added to water they can organize so that the heads conceal the tails, decreasing the total free energy of the system. The most biologically relevant structures are the micellar, hexagonal, and lamellar phases [24, 25, 26]. These phases form the membranes that compartmentalize cells, and due to the hydrophobic effects can contain trans-membrane proteins based on their own localized hydrophobicity. Not only can lipids form large three-dimensional structures but lipid molecules within the membrane are able to move in plane via diffusion. This diffusion means that we can treat

a lipid membrane as a two-dimensional fluid depending on the rigidity of their tail structures [13, 26].

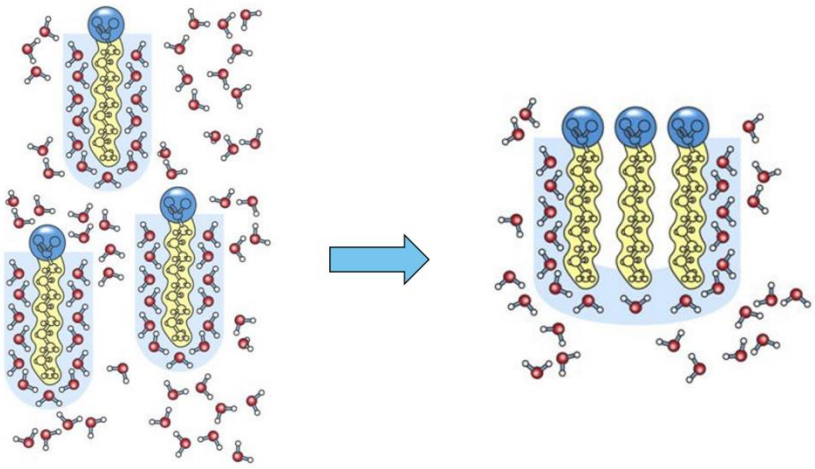

Figure 4. Self-Assembly driven by hydrophobicity. Lipid molecules have a polar head group and a non-polar tail comprised of long carbon chains. When these molecules are placed in a polar solvent, the tails disrupt the water molecules around them and reduce the possible number of configurations (A). As the lipids randomly diffuse in solution, when their tails make contact, it reduces the area exposed to water, making a smaller "water cage" (B). This process continues until only the polar heads are exposed to water, reducing the entropic cost of the system while forming an ordered structure. Image obtained from [13].

The general molecular structure of the lipid is responsible for the formation of lipid membranes. However, in plane diffusion allows for further potential for the membranes to self-assemble due to entropic forces. Lipid molecules can reorganize in-plane by this diffusion, with both head and tail groups contributing to the overall shape and structure of the membrane. Lipid tail rigidity alters lipid in-plane diffusion by affecting the packing order [13, 26]; a lipid with an unsaturated tail (Fig. 3) has a 'kink' that increases the number of tail conformations. This allows for the tail to take up a greater average volume as it thermally fluctuates, reducing the packing order in the membrane and increasing membrane fluidity. These effects change the diffusivity of the membrane and below a certain temperature, membranes made of multiple lipids can separate in-plane based on this packing order. Beyond just in-plane ordering, the average volume a lipid occupies, called a packing parameter, can also affect the intrinsic curvature of the membrane, driving the lipids to form micelles, vesicles, or membranes [13, 26] (Fig. 5).

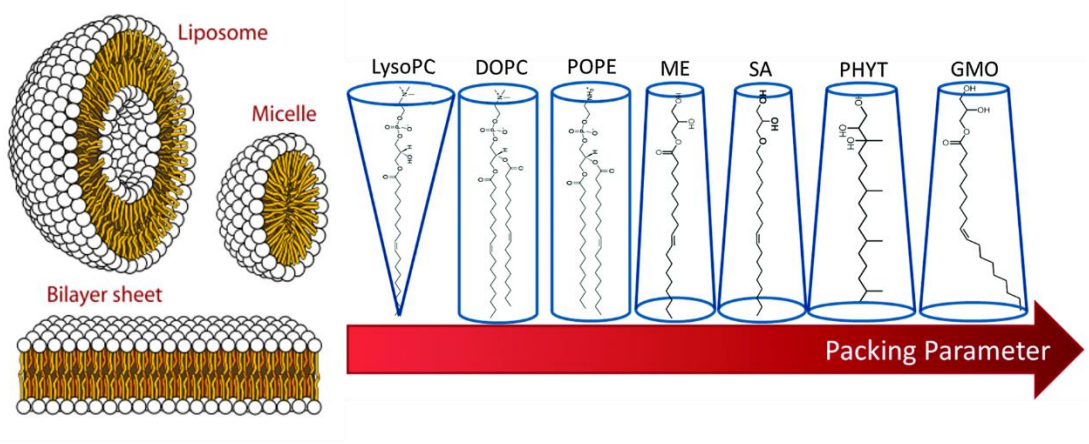

Figure 5. Lamellar and micellar phase of lipids. Shapes are based not only on concentration of lipids but the curvature of the lipids when packed together. Lipids with more cylindrical volume based on the size of the lipid head and tail structure are predisposed to low curvatures shapes. Lipids with volumes closer in shape to a cone are predisposed to micelle phases. Image obtained from Wikipedia and [27].

Packing order can also give rise to the lipid membrane's thermotropic phases. Membrane diffusivity is highly dependent on the lipid phases. In this thesis we work with lipids in the fluid and gel phase. In the lipid fluid phase lipid molecules can freely diffuse and rotate in-plane. Lipids that exhibit the gel phase at room temperature tend to have saturated tails and pack together more tightly, greatly reducing the membranes diffusivity (Fig. 6). By mixing these different lipids, we can form membranes with a variety of co-existing phases.

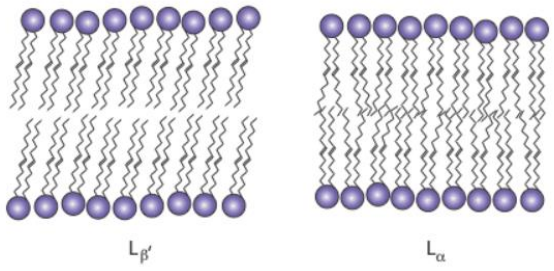

Figure 6. Lipid gel phase and fluid phase. Lipids in the gel phase, $\boldsymbol{L_{\beta'}}$, are tightly packed and have significantly reduced diffusivity compared to the fluid phase, $\boldsymbol{L_{\alpha}}$. Image obtained from [13].

A common way to represent the ratio of lipids needed to form these phases is with a Gibbs ternary phase diagram (Fig. 7), an isothermal diagram that maps the membrane phase behavior.

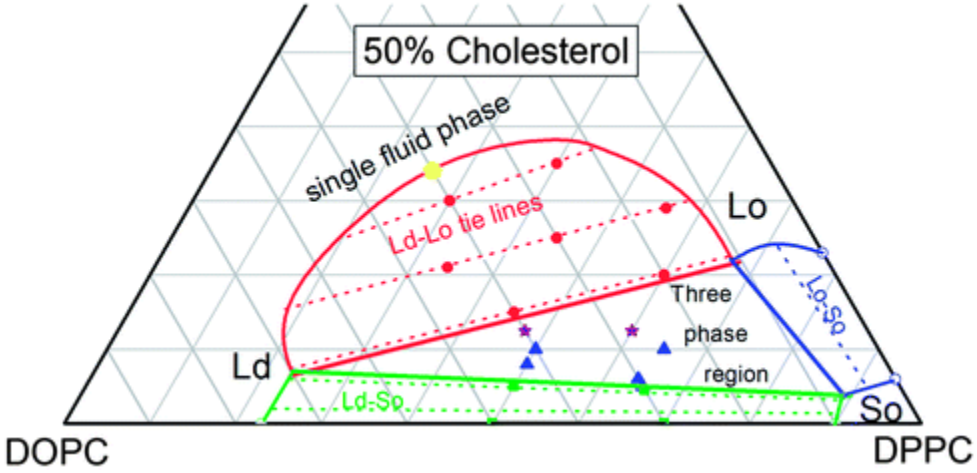

Figure 7. Lipid Phase Diagram. The blue region denotes areas with both gel and liquid ordered phase coexistence, red is the coexistence of liquid ordered and liquid disordered phase, and green is the coexistence of the liquid disordered and gel phase. The region between the colored areas has all three phases coexisting. The tie-lines on a phase diagram are lines in the two-phase region which the different phase fractions have consistent compositions. Image obtained from [28].

Membranes have planar organizational hierarchies based on their packing order. When membranes are composed of different lipid molecules *in-vitro* with concentrations that allow phase coexistence, these phases can segregate into easily seen rafts [29, 30, 31] (Fig. 8). These rafts typically exist as islands of specific lipids whose diffusivity and contents are different from the surrounding membrane. The raft properties depend on temperature and the relative concentration of their components [32]. Their biological existence was originally hypothesized after discovery that glycosphingolipids clustered on the Golgi apparatus before sorting. Lipid rafts have become a major focus of research to understand cell organization through thermodynamics and have been proposed to play vital roles in localizing proteins used in cell signal transduction [29, 33]. However, for this research lipid rafts are considered as a means for the localization of motor proteins, and how it can alter the motility of microtubules.

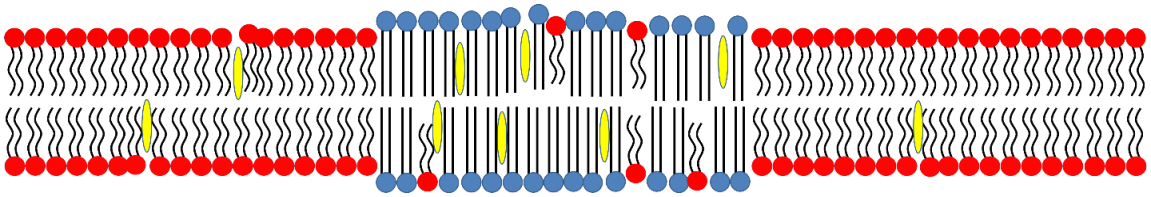

Figure 8. Lipid Raft. Due to the difference in the lipids excluded volume, the lipid specimens will separate in plane into a state with the lowest free energy. The blue lipids denote a lipid with saturated bonds, forming long, straight tails. Cholesterol preferentially packs in these rafts between the lipid tails. The bulk is comprised of lipids with unsaturated tails that take up a larger volume.

1.3 Microtubules

In eukaryotic cells the cytoskeleton is responsible for the mechanical support and framework of the cell. This cytoskeleton, immersed inside the cytoplasm, consists of proteins assembled into filaments. These filaments drive not only the structure of the cell but a variety of cell functions such as cellular division, gene expression, motility, and intracellular transport. The component of the cytoskeleton responsible for intracellular transport are microtubules. Microtubules act as the "highway" of intramolecular transport in larger cells, such as neurons, by which motor proteins walk and carry cargo [4, 5, 6, 7]. They are long biopolymers made of repeating α/β tubulin heterodimers [34, 35], globular proteins that in the presence of GTP self-assemble and de-polymerize due to hydrolysis [36]. These polypeptide subunits form long protofilaments, which then polymerize into a hollow tube structure with a width of 24 nm and a length measured in microns [34] (Fig. 9). When interacting with microtubule associated proteins (MAPS), the microtubules play in integral part in cell organization and are present in all eukaryotic cells. In eukaryotic cells these biopolymers act as the scaffolding, radiating out from the centrosome and organizing the cytoplasm [35].

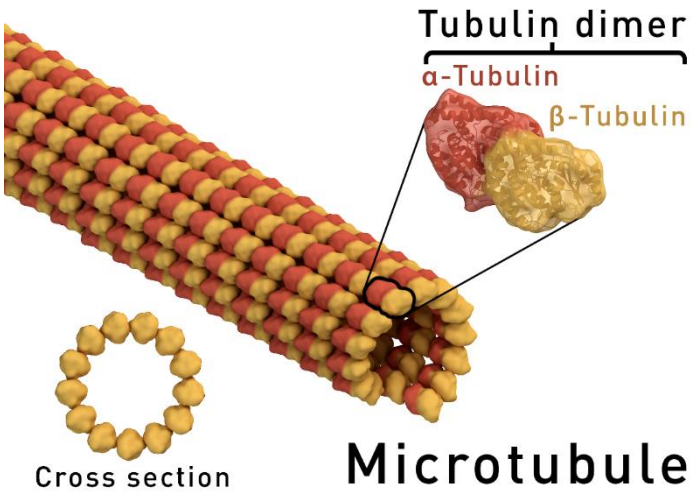

Figure 9. Microtubules and the dimer subunits. The microtubule is formed from the self-assembly of alpha and beta tubulin dimers into long strand protofilaments. The polymers then assemble into the tube structure above. Image obtained from Wikipedia.

In-vivo, the microtubule exhibits constant change [35]. While they are structurally strong, they continually grow and shrink depending on the needs of the cell and we can replicate this process *in-vitro*. This far from equilibrium behavior is called dynamic instability [37, 38, 39]. This process occurs as the tubulin dimers combine via GTP hydrolysis, growing out from the plus ends of the microtubule [38], as understood by the GTP cap model. In this model GTP binds to one tubulin dimer at a time, with the binding to α-tubulin being non-exchangeable and forms the α/β subunit, while binding to β-tubulin is exchangeable. When forming the subunit, the β-tubulin then polymerizes to another subunit and after a period the GTP will hydrolyze [37, 39]. GTP hydrolysis into GDP causes a conformational change that can force the protofilaments to bow outward allowing for rapid depolymerization if not stabilized. However, the rate of hydrolysis is slower than polymerization, as multiple subunits polymerize on the growing end a cap of GTP bound subunits keeps the microtubule together. This lag in reaction time allows for microtubule growth, even in low concentrations of tubulin. When growing microtubules, the length of microtubules can be controlled via tubulin dimer concentration, temperature, and can be stabilized for long periods of time using Taxol.

1.4 Kinesin

Motor protein is the collective term for a variety of nano-machines used by the body for transport, cellular division, muscle contraction, and cellular motility [2-12, 40-43]. Motor proteins are activated by ATP hydrolysis and convert the chemical energy into mechanical work [2-12, 40-43], such as walking or contraction. In our experiments, the motor protein responsible for axonal transport, kinesin, is used. These Kinesin-1 (Fig. 10),

are bound to the lipid surface through a histadine (HIS) tag [8, 44] and walk independently of each other. The structure of our kinesin motors is a truncated body, allowing for tight coupling to the surface and has two globular heads on the other that allows for walking. The globular heads are the motor domain, releasing from the surface due to ATP and initiating a power stroke, to allow for walking. The kinesin used in our research are anterograde transport, i.e., they will walk towards the plus end of the microtubule.

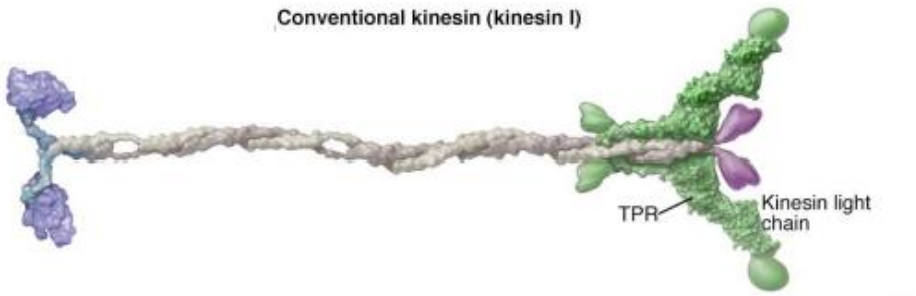

Figure 10. Kinesin-1 motor protein. Kinesin protein are responsible for intracellular transport of vesicle cargo along microtubules. The motor head is on the left-hand side, and ATP hydrolysis drives to the kinesin to walk along the microtubule. On the right, the light chain attaches to the vesicle. Image obtained from [2].

Chapter 2

Background and Theory

2.1 Kinesin Motor Transport

To understand the work and overall research goals presented in this thesis we will first go over the underlying physics of the main players; the motor proteins, microtubules, and lipid bilayers. Their physics and the physics of their interactions to produce intracellular transport are what motivated my research initially, and their unique properties are what propelled me to investigate active nematics. The physics of lipid self-assembly was understood largely by the 1970's [26], however these structures are formed at room temperature without the external input of energy. It wasn't until the mid 80's with the discovery of the molecular motor [45] as a means of cellular transport, and the discovery of the dynamic growth of the microtubule, did scientists truly appreciate the far from equilibrium nature of cellular organization.

Intracellular transport is powered by molecular motor proteins. For our research, we focused on understanding how the membrane of a motor proteins cargo affects its transport. To understand how lipid membranes affect the transport of cargo, we must first understand the nature of the motor protein, its interaction with the microtubule, and its interaction with other motor proteins. The simplest starting point is the motor protein itself and modeling its motion as a "Brownian ratchet" [46] (Fig. 11). By taking in chemical energy from the surrounding medium, the motor protein has directed motion, and thus can be modeled as a system where the random motion of an object is biased by the application of a periodic asymmetric potential [47]. Imagine you had a collection of particles in a fluid, when the potential is flat, the particles simply diffuse around in the medium. However, with the application of an asymmetric potential, the particles will localize to a certain point. As the potential is removed particles will diffuse out from the central point (Fig. 11a), some beyond the local boundary of the removed potential and the others still within its boundary. When the potential is reapplied, the particles that went beyond the local boundary are driven forward again by the potential (Fig. 11b, 11c), while the remaining particles are re-focused. This out of equilibrium system can be applied to single molecule motion as well, where instead of moving a collection of particles we are moving parts of a molecule in a cyclic process.

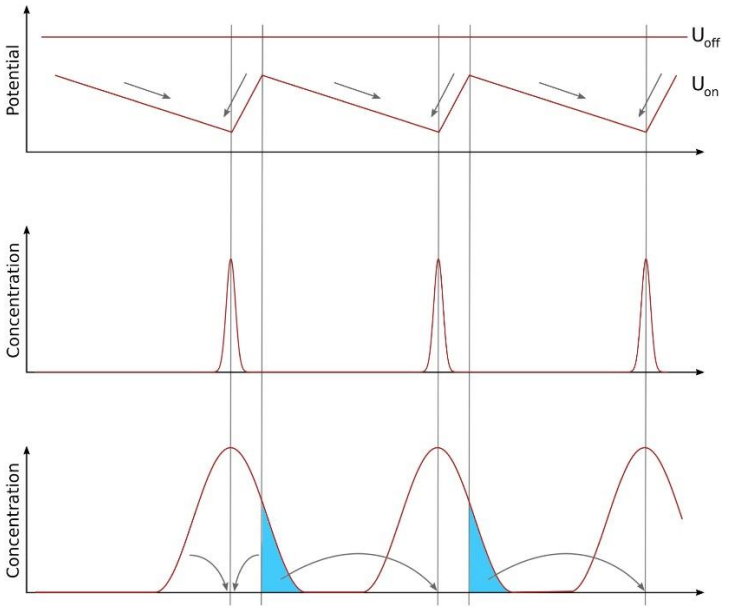

Figure 11. Brownian Ratchet. The potential during the off phase of a Brownian ratchet is constant, allowing the particles motion to be considered purely diffusive. When the potential is applied, it forms a periodic asymmetric profile, guiding particles in a biased direction (A). When the potential is made constant again, the particles are initially concentrated (B), but over time diffuse out into the surrounding space, with a portion of the population reaching beyond the next period of potential, biasing the direction of motion with each application of the potential (C). Image obtained from [48].

In the case of a single molecular motor, ATP causes the protein to transition between two conformational states, each with two sub-steps, that interact with a microtubule filament in different ways. Specifically, in these experiments I used a member of the kinesin motor family called kinesin-1. This motor is called "conventional kinesin" [48] and is considered the representative member of the kinesin superfamily. Kinesin have two head domains; these domains attach to the microtubule and bind strongly to the biopolymer. When the protein undergoes a conformational change, the kinesin will take an 8nm step [49]. This "walking" is conventionally modeled in a head over head pattern, with each head moving over the other after its partner has bound to the microtubules structural lattice, allowing for processive motion (Fig. 12). As the motor protein's lowest energy state is to be bound to the microtubule protofilaments in between the α and β heterodimer, to take a step an ATP molecule must bind to the lead motor head [48]. When ATP binds to the lead head domain, this causes the neck linker that connects the head to the body of the motor to contract and pull the motor forward. While the lead head undergoes a conformational change, the rear most motor head hydrolyzes the ATP, releasing energy to detach it from the microtubule surface (Fig. 12a). The combined effort of the contraction of the lead linker and the diffusion of the rear head causes a step to be made (Fig. 12b). Step length is independent of ATP concentration, though the concentration can increase the step frequency [48, 50]. The motor head moves past the still bound head and binds to

the lead of the microtubule. Once bound to the microtubule it will bind a molecule of ATP, while the now rearwards facing head's ATP hydrolyzes into ADP and restarts the cycle, (Fig. 12c, 12d). This stepping motion is biased towards the plus end of the microtubule, with a kinesin-1 motor taking 100 steps on average before it falls off the microtubule. This motion is, 90% of the time [41], toward the plus end of the microtubule so long as there isn't a load pulling it backwards [46].

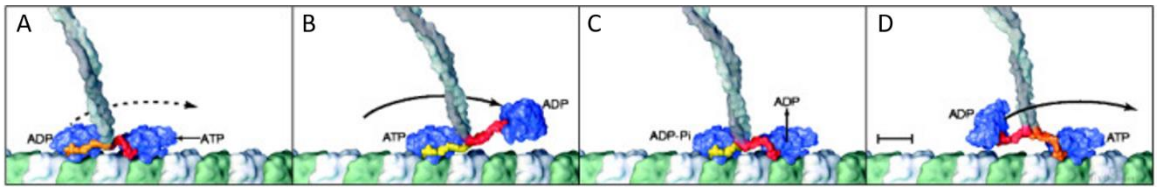

Figure 12. Kinesin stepping cycle. The stepping of kinesin motors can be modeled as a four-step process starting with the binding of the motor head to the microtubule. While the lead motor domain attaches to the microtubule, ATP binds to the head causing the (red) linker to contract and pull the motor forward (A). While this (yellow) linker contraction occurs, the rearmost detached head (red) diffuses, biased forwards due to the contraction (B). This motor protein then binds to the surface of the microtubule while the rearmost motor head is unbound by the hydrolysis of ATP (C), allowing the rearmost head to diffuse, restarting the cycle (D). Image obtained from [50].

2.2 Multiple Motor Transport

When we look at transport *in-vivo*, cargo doesn't simply move forward at a set speed [41], from this we can immediately see that cargo properties can impact transport. Because of this, looking at the properties of a single motor is insufficient to understand transport phenomena. For example, cargos exert a load force that affects their transport, if the force is too great there will be no forward motion and the cargo will "stall" [41]. By binding kinesin-1 to silica bead cargos, and controlling the force exerted on these beads with optical traps, the stall force for a single kinesin cargo has been found empirically to be 5-7pn [41]. However, even attaching cargo to single motors *in-vitro* and observing their motion doesn't give one the full picture, as *in-vivo* measurements produce different results. One major difference is that *in-vivo* the population of motor proteins is dynamic, allowing for multiple motors to bind to and carry a single cargo. Not all motors are walking in the same direction however, such as the motor dynein, which leads to tug-of-wars between different variants of motor protein [51]. Additionally, other proteins can bind to the surface of the microtubule, acting as road blocks that pause the stepping of kinesin. For this research, I focused on the actions of groups of kinesin motors, and their interactions when bound to a surface comprised of a lipid membrane.

A single motor protein only exerts piconewtons of force, so ensembles are needed to drive cargo through the cytoplasm of the cell [48]. Beyond inducing greater force, having teams of motor proteins carrying cargo has been shown to increase the travel distance of transport, as the random total disassociation of a single motor is recoverable by keeping it in proximity of the filament [52]. However, increasing the bound motor protein density too much causes exclusion forces between motors, which reduce the transport velocity [52]. To understand this phenomena Klumpp and Lipowsky proposed a two-state statistical model that factored in the binding/unbinding rate of motor protein to a microtubule and the number of motors. They were able to model the general velocity and travel distances produced by a team of motors for hard cargos with and without large forces applied. This transition rate model considers a single cargo of N motors, and within this ensemble of motors, n number are bound to the filament, presenting a system with a total of N+1 macrostates. Each of these macrostates has a multiplicity modeled in equation 1.

$$\frac{N!}{(N-n)!\,n!} \quad (1)$$

This is a two-state system, where each motor is either bound or unbound. The rate of motor unbinding is given as the value ε_n with the rate of binding being denoted as π_n, the velocity of the cargo then is denoted as v_n (Fig. 13).

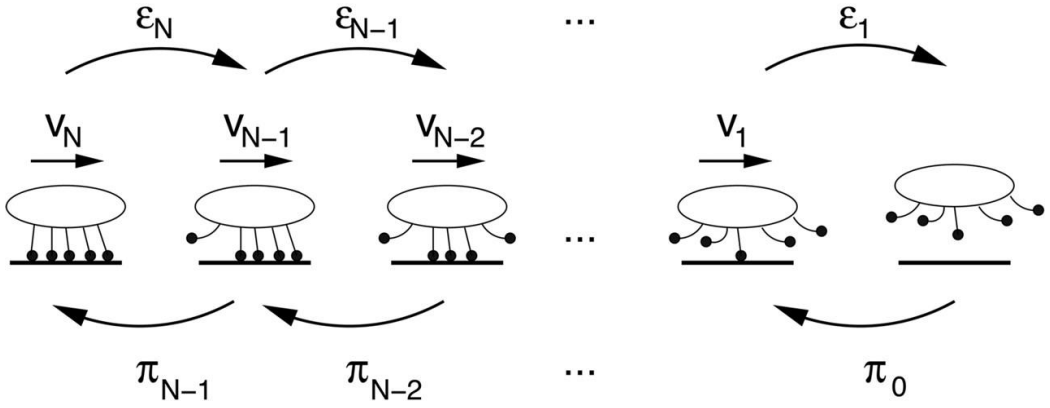

Figure 13. States of collective cargo transport. Motor proteins regularly bind and unbind from microtubule filaments due to the nature of their stepping cycle. When motors are bound to a cargo, the motor proteins that unbind have a potential to rebind to the filament. Each cargo can be considered as a state with n motor proteins bound to a filament, walking at v_n speed, with a potential to transition to a new state at rate $\boldsymbol{\varepsilon_n}$ or $\boldsymbol{\pi_n}$ (A). If we consider the bound vs unbound state (B), we can see that at state n=0, there is a rate $\boldsymbol{\pi_0}$, for the system to transition to the bound state and a potential for the state n=0 to be transitioned to from state n=1 at rate $\boldsymbol{\varepsilon_1}$. Image obtained from [52].

This model provides us with the ability to describe the probability that the cargo would be in a specific state using a master equation, equation 2, where n denotes the number of bound motors in the state. The state can vary from n=0, the state where the cargo is no longer bound, to n=N, the state where all motors bind the cargo to the filament.

$$\frac{\partial}{\partial t}P_n = \varepsilon_{n+1}P_{n+1} + \pi_{n-1}P_{n-1} - (\varepsilon_n P_n + \pi_n P_n) \quad (2)$$

The probability of the system changing states, either a motor rebinding or unbinding to the filament, is understood as thus. Consider we are in the state n=0, where all motor proteins are unbound to our filament and transport velocity is zero. In this state our rate of change, $\frac{\partial}{\partial t}P_n$, is zero and our equation reduced to.

$$\varepsilon_{n+1}P_{n+1} = \pi_n P_n \quad (3)$$

By characterizing all possible states in terms of P_0, and normalizing the sum of possible states to be 1, we can then define each state of n in terms of the n=0 state.

$$P_0 = \frac{\varepsilon_1 P_1}{\pi_0} \quad (4)$$

$$P_1 = \frac{\pi_0 P_0}{\varepsilon_1} \quad (5)$$

$$\varepsilon_2 P_2 = \pi_1 P_1 \quad (6)$$

$$P_2 = \frac{\pi_1 P_1}{\varepsilon_2} = \frac{\pi_1 \pi_0 P_0}{\varepsilon_2 \varepsilon_1} \quad (7)$$

$$P_n = P_0 \prod_{i=0}^{n-1} \frac{\pi_i}{\varepsilon_{i+1}} \quad (8)$$

This distribution of states, defined by equation 8, can be used to understand the distribution of velocities of our system when the total sum of states is set to 1.

$$\sum_{n=0}^{N} P_n = 1 \quad (9)$$

$$P_0 \sum_{n=0}^{N} \prod_{i=0}^{n-1} \frac{\pi_i}{\varepsilon_{i+1}} = 1 \quad (10)$$

$$P_0 = \left[1 + \sum_{n=0}^{N-1} \prod_{i=0}^{n} \frac{\pi_i}{\varepsilon_{i+1}}\right]^{-1} \quad (11)$$

Using this notation, we can find the average number of states that our cargos exist in, and from this we can consider that each state has a corresponding velocity of transport v_{eff} using the average number of bound motors, N_b, modeled in equation 12.

$$N_b = \sum_{n=1}^{N} \frac{nP_n}{1 - P_0} \quad (12)$$

$$v_{eff} = \sum_{n=1}^{N} \frac{v_n P_n}{1 - P_0} \quad (13)$$

Assuming in this model that motors are well spaced, and there is no motor-motor interaction we can consider the velocity of a cargo transported by N motors. As the velocity of transport is proportional to the unbinding rate of the motor protein we can consider the walking distance from relating the on and off rates with the density.

$$\varepsilon_{eff}(1 - P_0) = \pi_{eff} P_0 \quad (14)$$

$$\langle \Delta x_b \rangle \approx \frac{v}{\varepsilon_{eff}} = \frac{v}{N\pi_{ad}} \left[\left(1 + \frac{\pi_{ad}}{\varepsilon}\right)^N - 1\right] \quad (15)$$

For the case of strongly bound motor proteins, where $\frac{\pi_{ad}}{\varepsilon}$ is about 5, distance traveled scales quickly with the number of motor proteins N without changing the velocity of the cargo. This is directly applicable to transport systems such as the microtubule gliding assay, where in the microtubule is carried across a surface with a large team of motors, with a travel distance that is many times larger than the length of any one filament. Additionally, the velocity of transport remains constant for these systems when the load of the cargo is zero. However, as the force increases the velocity drops, with larger N teams able to better resist the velocity drop from cargo loads. This behavior is also seen in glass gliding experiments, where the velocity of microtubule gliding remains mostly unaffected by motor density [9]. While this explains the long run distances of motor proteins, the cargo

carried *in-vivo* are comprised of lipid vesicles, which are dynamic. This means that the cargo can change shape due to the elasticity of a lipid vesicle, motors can interact with each other through the membrane, and motors can move along the surface of the vesicle due to the surface diffusivity. However, since our theoretical model is reduced to a cargo on a filament, we can flip the script, with the filament being transported by the kinesin. This means that we can use the gliding assay as an approximation of cargo transport, isolating the effect of diffusivity from the geometry and elastic deformation of the vesicle. In chapter 4, we will explore how this alters the transport of individual filaments and the consequences diffusivity has on motor protein binding. In chapter 5, we will observe the behavior of dense populations of filaments gliding on a lipid bilayer covered surface.

2.3 Membrane Bound Motor Transport

Experiments in collective transport have mostly focused on *in-vitro* work transporting silica cargo along microtubules [53], however experiments involving the transportation of lipid cargos using myosin Va have revealed some interesting results [54]. In these experiments, myosin Va motors transported lipid vesicles along actin filaments. By controlling the lipid diffusivity and number of motor proteins, they could control transport properties. While transport rates involving a single motor protein were equivalent between lipid vesicles and hard quantum dots, teams of motor proteins produced a higher transport velocity when carrying disordered lipid vesicles, a result that has also been seen in lipid covered beads transported by kinesin [55]. However, transport of lipid vesicles in the gel phase exhibited significantly reduced velocities compared to transport of lipid vesicles in the disordered phase. While this could be attributed solely to the diffusivity of the membrane, as the gel phase reduced diffusivity is more akin to a hard surface, it was also found that transport velocity was increased in fluid vesicles with increased diameter. However, increasing the diameter of vesicles in the gel phase vesicles exhibited no such velocity change. Due to the complex nature of vesicle transport we must isolate the effects of diffusivity on transport from the potential elasticity of a vesicle.

In a recent paper, Grover et al. developed a model of transport velocity based on membrane diffusion from gliding experiments [56]. This model shows how motor protein number and membrane diffusion, independent of the geometry of the cargo, can alter transport velocity. Despite the motor protein being quite large compared to the lipids of the membrane and potentially being bound to more than one lipid, motor proteins can still diffuse along the lipid membrane. By fluorescently labeling the motor protein and using total internal reflection microscopy (TIRF) they observed that the kinesin exhibits diffusive motion. This diffusivity has been measured to be about half that of the actual membrane diffusivity as recorded from fluorescence recovery after photobleaching (FRAP) measurements.

The gliding experiments in [56] produced two main results that contributed to a model of membrane bound transport (Fig. 14). The first is that gliding on a fluid membrane produces lower velocity than on glass that is tunable by motor density and membrane

diffusivity. The second observation is that when microtubules encounter each other they have a propensity to "snuggle" and align with another instead of crossing [12]. This same phenomenon is seen in glass gliding experiments when a polymer, such as poly (ethylene glycol) (PEG), is added to the solution exerting a depletion force on the microtubule that keeps the head from crossing over another microtubule [12]. These findings indicate that membrane diffusivity reduces the velocity of gliding and the net force exerted onto the microtubule.

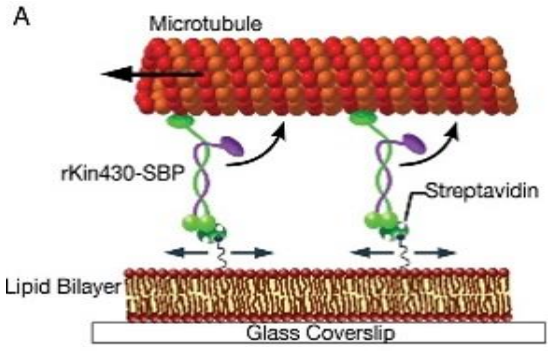

Figure 14. Diagram of membrane bound microtubule transport. Kinesin motor proteins are bound to a fluidic lipid membrane by biotin-streptavidin linkage. When ATP is added to the system the motor proteins "walk". Since the kinesin are bound to the surface of the membrane the microtubule instead glides in the opposite direction of motor stepping. Image obtained from [56].

When the motor protein "walks" and drives the microtubule forward, there is an equal and opposite reaction onto the motor protein from the microtubule. In the case where motor proteins are bound to glass, this force translates momentum into the glass slide where it dissipates. However, with a motor protein bound to a diffusive lipid, the motor can be displaced, resulting in a reduced net force. This reduction in net force means that the microtubule may be unable to force itself over an object. Additionally, as less force is applied to a microtubule moving through a fluid medium, its gliding velocity is decreased. By considering the effect of the lipid membrane on the force exerted on a microtubule gliding with fixed velocity, and the force of friction opposing this motion, Grover et al. [56] constructed a model for the velocity dependence on membrane diffusion and motor density (Fig. 15). On glass the microtubule gliding velocity is equal and opposite to the stepping velocity of a kinesin, due to it being a processive motor protein, and the kinesin stepping velocity is the upper bound of gliding velocity. When modeling the stepping velocity of a microtubule gliding on a lipid membrane, we can subtract the velocity of the motor protein as it slips giving us equation 16.

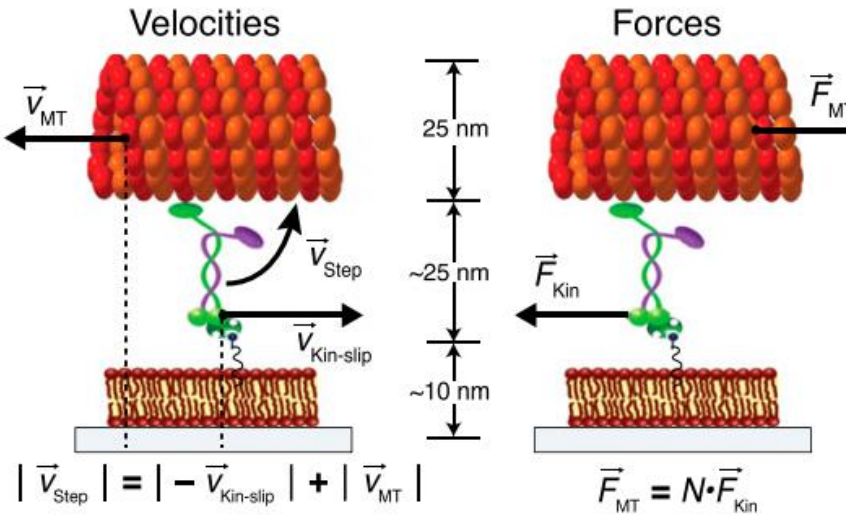

Figure 15. Quantification of velocity and net force. The velocity of slipping, how much the motor protein is displaced during stepping, is subtracted from the velocity of stepping to relate it to the gliding velocity (A). The net force on the microtubule is defined as the force of each motor multiplied by the number of motors. Image obtained from [56].

$$\vec{v}_{MT} = -\vec{v}_{step} + \vec{v}_{Kin-slip} \quad (16)$$

Where $\vec{v}_{MT}$ is the velocity of microtubule gliding, $\vec{v}_{step}$ the velocity of a walking motor protein, and $\vec{v}_{Kin-slip}$ the velocity of a motor protein's displacement. If we consider the microtubule gliding velocity to be approximately constant, then the net force acting on the microtubule would be zero. Since the motor proteins exert a force on the microtubule in proportion to their numbers, the opposing force on the microtubule would be the friction force of the fluid medium.

$$N \cdot \vec{F}_{Kin} + \vec{F}_{MT} = 0 \quad (17)$$

Where the force of the microtubule on the motors, $\vec{F}_{MT}$, is equal and opposite to the force of the motor protein, $\vec{F}_{Kin}$, times N motors. By considering the microtubule as a rod whose length greatly exceeds its radius, the drag coefficient is given by equation 18, with the drag force being the velocity of gliding multiplied by this coefficient.

$$\gamma = \frac{2\pi\eta L_{MT}}{\ln(\frac{2h}{r_{MT}})} \quad (18)$$

$$\vec{F}_{MT} = \gamma \cdot \vec{v}_{MT} = \frac{2\pi\eta L_{MT}}{\ln\left(\frac{2h}{r_{MT}}\right)} \cdot \vec{v}_{MT} \quad (19)$$

Where $\vec{v}_{MT}$ is the velocity of the microtubule, L_{MT} is the length of the microtubule, r_{MT} is the radius of the microtubule, h is the height of the microtubule, and η is the viscosity of water. By using the Einstein-Smoluchowski equation [56] they were able to derive a drag co-efficient for the motor protein in relation to its diffusivity. Using this co-efficient and the stepping velocity of the motor protein, the force applied by the motor protein is given by equation (20).

$$\gamma = \frac{K_b T}{D_{Kin}} \quad (20)$$

$$\vec{F}_{Kin} = \gamma \cdot \vec{v}_{Kin-slip} = \frac{K_b T}{D_{Kin}} \cdot \vec{v}_{Kin-slip} \quad (21)$$

Where D_{Kin} is the diffusion constant of the kinesin, K_b is the Boltzmann's constant, and T is the temperature. By combining equations 17, 19, and 21 we can relate the velocity of gliding with the diffusivity of the membrane and the density of motor proteins. For the case of gliding with static velocity, this can be simplified to relate the velocity of microtubule gliding with the net velocity of motor protein stepping, shown in equation 23.

$$N \cdot \frac{K_b T}{D_{Kin}} \cdot \vec{v}_{Kin-slip} + \frac{2\pi\eta L_{MT}}{\ln\left(\frac{2h}{r_{MT}}\right)} \cdot \vec{v}_{MT} = 0 \quad (22)$$

$$\vec{v}_{MT} = -N \cdot \frac{\frac{K_b T}{D_{Kin}}}{\frac{2\pi\eta L_{MT}}{\ln\left(\frac{2h}{r_{MT}}\right)}} \cdot \vec{v}_{Kin-slip} \quad (23)$$

Where $\vec{v}_{Kin-slip}$ is the velocity of the kinesin slipping with respect to the membrane. Equation 23 can be simplified by grouping the constants into one coefficient c, equation 24. Equation 25 relates the velocity of gliding as a fraction of the motor proteins stepping velocity, with the properties of the membrane. If we consider that the total number

of motor proteins divided by the length of the microtubule is the motor density, we can relate the ratio to the density of motor protein and the diffusivity of the membrane in equation 26.

$$c = \frac{2\pi\eta}{\ln(\frac{2h}{r_{MT}}) \cdot K_b T} \quad (24)$$

$$\frac{\vec{v}_{MT}}{\vec{v}_{Step}} = -\frac{1}{1 + \frac{c \cdot D_{Kin} L_{MT}}{N}} \quad (25)$$

$$\frac{\vec{v}_{MT}}{\vec{v}_{Step}} = -\frac{1}{1 + \frac{c \cdot D_{Kin}}{\rho}} \quad (26)$$

Experimental results from this work show that when the density of motor proteins is increased, the gliding velocity increases proportionally, plateauing with gliding velocity comparable to a microtubule gliding on a hard substrate. Similarly, by increasing the membrane diffusivity the velocity drops accordingly. The key result of this research shows that the diffusivity of the membrane alone can greatly impact transport, although there are still many other factors that impact the transport of cargo *in-vivo*. Additionally, a finding of this work was to show that when gliding is performed on a diffusive membrane, filaments will align when they encounter one another, similar to "snuggling" [12]. This inspired me to make a novel active matter system entirely dependent on the diffusivity of the membrane.

2.4 Active Matter and Biology

Active matter as a field related to soft matter physics has developed greatly over the last couple of years, and through that development has shifted its focus. A field that once focused on simply understanding the basic statistical mechanics of far from equilibrium systems has now expanded to understanding living systems from first principles [57]. Active matter systems are defined as systems of internally powered particles [1, 57] whose interactions produce collective motion. The microtubule and motor protein are excellent examples of active matter as the motor protein motion is due to ATP hydrolysis driving conformational changes in the protein, which when in contact with a microtubule will cause "walking" behavior [2, 45, 46, 50]. Instead of having motors walking along a microtubule, we can have microtubules propelled by the motor protein, or shear relative to another microtubule. These systems can show hierarchies of dynamics due to microtubule-microtubule interactions [10, 11, 12, 22]. Using reconstituted biochemical

building blocks has become an integral part of the field for the very reason that they are both natural examples [58] of active matter systems and their usage allows us to better understand how life came to be [59].

Traditional non-equilibrium systems such as a heated pot of water or the sun's energizing of our atmosphere produce phenomena ranging from formation of convection cells to rich chaotic weather systems. However, if one were to look at the pot of water, one would note immediately that the water is comprised of dead molecules, excited by an external input of energy through a solid barrier [59]. When compared to a cell, we note that while the energy is taken in externally, it is broken down internally, powering the machinery of the cell. This machinery forms hierarchies of interaction until you reach the cell itself. The rich variety of biological systems has limitations however, and the information we can get from *in-vivo* observations are clearly restrictive when one considers their origins. When one observes *in-vivo* systems, it can be very difficult to isolate variables as the interaction of multiple factors allows the system to function. Additionally, biological systems are highly conserved due to their evolutionary nature, produced by genetic mutation and drift, re-enforced by natural selection [60]. This limits our observations to only those systems that have survived billions of years of evolutionary development. Taking the building blocks and reconstituting them into *in-vitro* systems, we can explore unique examples of active matter beyond those that serve a biological function.

Due to the historical focus on the cytoskeleton and its function in cell division and motility, motor-driven biopolymers are a favorite for *in-vitro* studies. From the perspective of the physics of active matter, the cytoskeleton forms as an energy dissipative ensemble of motors and biofilaments, and this property makes for exciting *in-vitro* studies. Motor proteins and biofilaments combine to form various structures such as asters and vortices after the addition of ATP [10, 11, 22, 61, 62, 63]. Motor driven filaments have furthermore been confined to lipid membrane vesicle, forming an active nematic that produced synthetic motility and shape change [22]. This active nematic phase, produced by motor proteins propelling microtubules whose interactions produce short-range order, is the focus of our research into active matter.

2.5 Active Nematic Systems

In liquid crystal physics, the nematic state is a phase that exists between the solid and liquid phases. This fluid phase exhibits short range orientational order [13] due to the physical anisotropy of the molecule, be it a collection of rod-like or disc-like shaped particles. An active nematic is when we have a collection of these anisotropic particles that can move under their own power and interact with each other. In its most basic form we can model an active nematic system as a collection of particles that can step forward at a set velocity. When a particle takes a step, the direction of each particle step is in the same direction as the average of its neighbors. This is the Viseck model (Fig. 16), originally conceived as a means of understanding the flocking and swarming of animals and other biological entities. This simple computational model has been expanded upon to cover a

variety of experimental systems. When particles are at a high number density and move with low noise, they spontaneously transition from a random isotropic state, to a nematic phase. In such a system the momentum of the particles is not conserved between particle-particle interactions [57]. This is true of our experimental system as well. When microtubules glide on a substrate, they do so through an interaction with the motor proteins, which allows for the transfer of momentum to the substrate.

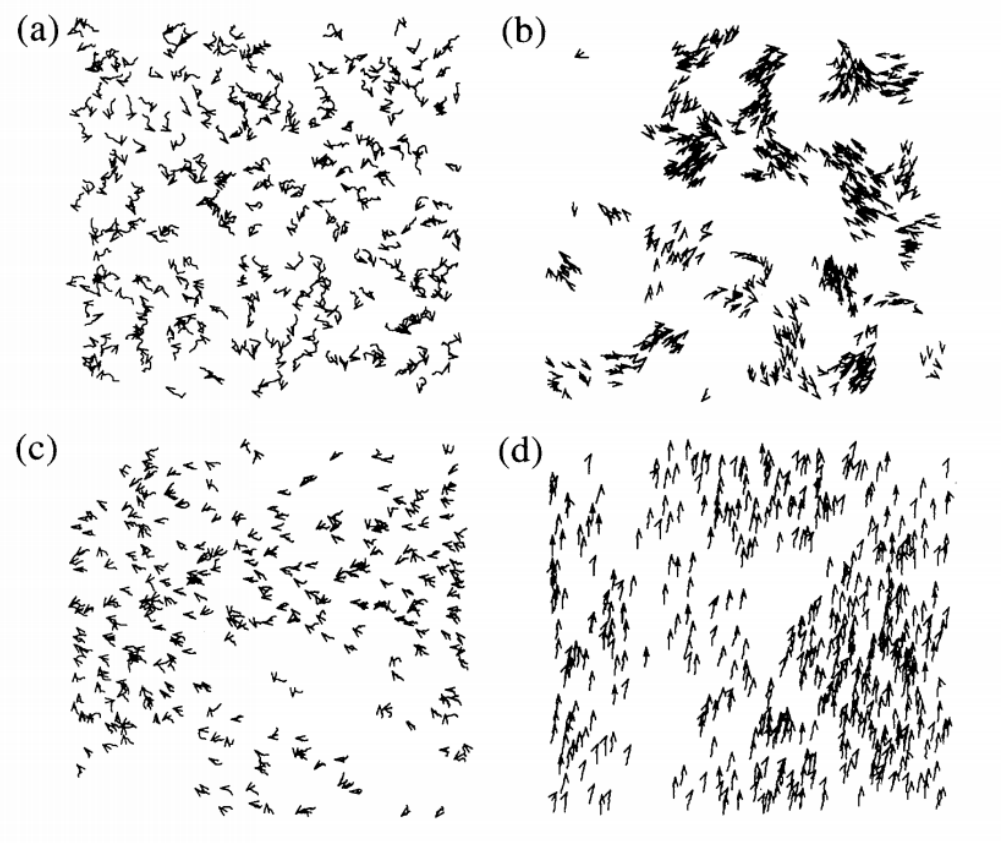

Figure 16. Computational results from Vicsek et al. The Viseck model gave particles a constant velocity whose direction was the average of the neighboring particles with some noise. By varying the noise and velocity you can see a transition from isotropic to nematic phase. Particles start with random alignment and if they have high coherence and low particle density will random clusters, (B). If coherence is lowered but density is increased the particles will move randomly with some alignment, (C). Lastly if the particles have high density and coherence then they will be strongly aligned (D). Image obtained from [64].

In the Vicsek model, the particles have defined heads and tails, however when experimenting with microtubule-based active nematics often the particles are polar in direction but not in alignment. This is because gliding against each other in a positive and

negative direction yields alignment regardless of if the filaments were moving in the same direction. In an active nematic system, if our particle's physical anisotropy is uniaxial, such as in a rod, then there is no difference between one end or the other. Similar to calamitic liquid crystals, which form a nematic phase with particles pointing in either the x or –x direction (Fig. 17) [13], we can see the formation of an active nematic phase from rod-like particles moving either in the x or -x directions. Despite their movement producing an average momentum of zero, they can produce dynamic and complex phase behaviors.

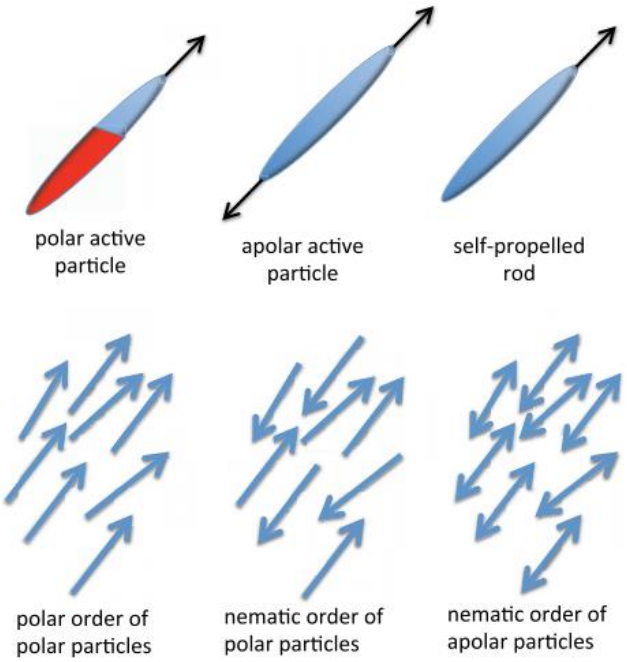

Figure 17. Model of particle motion and their phase behaviors. Polar active particles are directed particles that are asymmetric in shape (A), apolar particles are symmetric particles that move in either direction (B), and the self-propelled rod is a symmetric particle that moves in one direction (C). These particles then produce either polar (D) or nematic phases (E, F). Image obtained from [57].

In previous experiments, filaments gliding on a substrate induced into an active nematic have yielded phase behaviors beyond the simple nematic phase when filament density is at its highest. Between the isotropic and nematic phases exists a variety of phases that form based on the density of motors, persistence length and size of filaments, as well as the type of motor driven assemblage [62]. In experiments of non-processive heavy meromyosin driven F-actin filaments above a critical filament density, clusters of high density aligned gliding would spontaneously emerge from the isotropic domain. It is important to note that in these experiments, the filaments glided in a uniform direction forming a polar order due to the nature of the myosin motor. This uniformity further

increases in filament density and extends the lifetime of these local congregations into high density waves. These waves form perpendicular to the direction of motion with filaments at the trail and leading edge of the wave exchanging with filaments at the isotropic domains (Fig. 18).

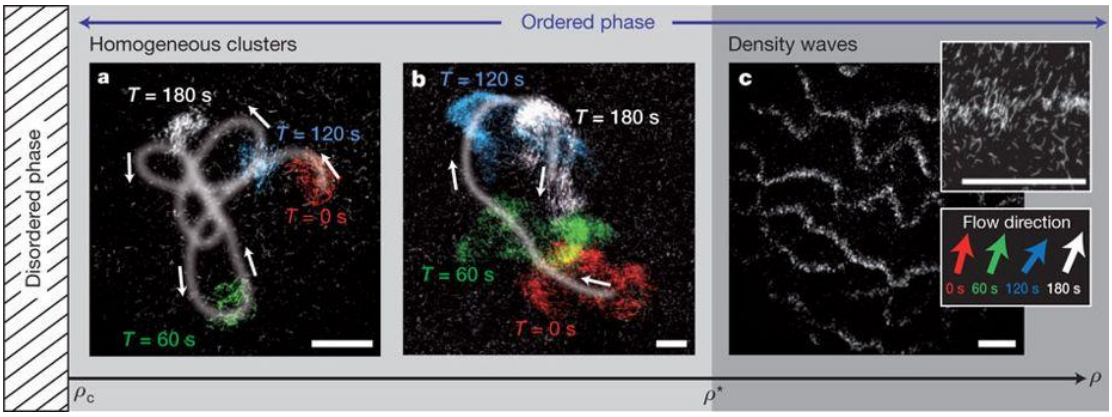

Figure 18. Density waves in polar filaments. When myosin motors drive polar actin filaments, there motion prevents cross over, and an intermolecular force allows the filaments to align. When the density of filaments increases we can see (A) the formation of dense regions that spontaneously emerge. With the increase in density, the regions grow (B), until a critical density is achieved, and the filaments form waves (C). Image obtained from [62].

Another consequence of this apolar nature is that increases in density form circular vortexes of motion around defect points. Experiments using kinesin driven microtubules in PEG have produced similar density fluctuations along the direction of gliding, due to the apolar nature of the filaments motion. Lastly, systems of dynein drive microtubules have produced large numbers of filament vortex rings [63].

An important question is how do motor proteins bound to a membrane alter the active matter's characteristics? Motor protein diffusion not only allows for the formation of an active nematic, but also allows for the localization of motor proteins, the introduction of thermal noise, the relaxation of defects, as well as additional hierarchal possibilities associated with the formation of lipid rafts. In this thesis I aim to understand how motor proteins interact with the membrane and impact transport. In addition, I investigate how the motor-membrane system can be used to make a novel form of active matter.

Chapter 3

Formation of Lipid Nanotubes from Kinesin Anchored Vesicles

3.1 Introduction

This research project set out to measure the length of lipid nanotubules extracted from kinesin anchored giant unilamellar vesicles (GUVs), and I specifically worked on characterizing the lipid membranes used to form vesicles. In nature motor proteins actively pull nanotubules from lipid membranes, however the force of this extraction is still not well understood. To test the force required to pull out a nanotubule, GUV's were added to a flowcell containing static kinesin bound to microtubule. These motor proteins would then bind to the vesicle via a lipid with a special head group. When a flow was induced, the GUV would be carried along and extract nanotubules from its surface, allowing for a simple method of nanotubule formation. Before this project, previous research had looked at kinesin proteins walking along microtubules and extracting nanotubules from membranes [65, 66]. By leaving the motor proteins static on the microtubule, we can find the force required to extract nanotubules without the potential confounding effects of ATP concentrations creating osmotic pressures or dynamics of motor protein walking. To characterize the lipid membrane, I used fluorescence recovery after photobleaching (FRAP) to find the diffusivity of our novel lipid mixture that was used to make the GUVs [67]. A simple model was then developed to characterize the force required for nanotubule extraction and the number of kinesins required for extraction. Using this experimental data, our group developed a theoretical model incorporating the fluidity of the lipid membrane, as the fluidity impacts not just the elasticity of the membrane, but the shapes allowed by the GUV, and the ability for kinesin to move laterally on the GUV surface. The result of this research was the determination of our lipid membrane having a diffusion constant of $D = 9.01 \pm 0.58 \frac{\mu m^2}{s}$. We also determined that a minimum of ~7 pN of drag force is needed form a nanotubule from vesicles with diameters of 2 μm. This calculated force is physiologically feasible and matches experimental data of the range of a kinesin motor protein during stepping.

3.1.1 Kinesin

As described in chapters 1 and 2, kinesin motor proteins are the primary drivers of intracellular transport in cells [3, 4, 5, 6, 7, 8, 9]. Teams of kinesin motor proteins transport cargo along microtubule highways from the nucleus of the cell. By utilizing ATP hydrolysis, the motor protein undergoes conformational changes that drive its motion along

the microtubule. In the absence of ATP, the motor protein will bind to the microtubule with a force of ~5 pN [68], scaling linearly with motor number when teams of motors are present. Lipid nanotubules are also known to be important structures involved in cellular communication and transport, and their formation is associated with the presence of kinesin motor proteins [69]. Understanding the forces required to extract nanotubules allows for a better understanding of these fundamental biological processes.

3.1.2 Lipid Membrane

As mentioned in chapter 1, lipid membranes are formed from the self-assembly of amphiphilic molecules [13]. These molecules, consisting of a polar head group and a fatty acid tail, organize into spherical structures such that the tail groups are kept out of contact with water molecules. We can consider the wall of the vesicle to consist of two leaflets [26], the hydrophobic tails are on the inside, and the polar head groups on the outside. This forms a structure that is elastic, whose molecules are free to diffuse laterally in plain, and capable of self-healing when ruptured. While the self-assembly process forms these structures as the lowest energy configuration, these vesicles are an integral part of dynamic living systems that exist out of equilibrium. The lipid membranes make it possible to compartmentalize the functions of the cell, maintain chemical gradients, and transport chemical compounds within the cell [26]. Native cellular membranes are complex, consisting of a wide range of lipid molecules that are both saturated or unsaturated, contain cholesterol, and embedded transmembrane proteins. All these constituent parts affect the diffusivity, shape, and function of the membrane as well as allowing for the formation of more exotic hierarchical structures called rafts. Despite these complexities, we can still model these vesicles through *in-vitro* studies by using only a couple of lipids and no imbedded proteins. For this study we used a mixture of 94.95 mol % 1,2-dioleoyl-sn-glycerol-3-phosphocholine (DOPC) for the bulk composition (Fig. 20), 5 mol % 1,2-dioleoyl-sn-glycero-3-[(N-(5-amino-1-carboxypentyl)iminodiacetic acid) succinyl] (ammonium salt) (DGS-NTA) lipid to bind to our kinesin through an electron switch mechanism [44], and 0.05 mol % of 1,2-dioleoyl-sn-3-phosphoethanolamine-N-(7-nitro-2-1,3-benzoxadiazol-4-yl) (ammonium salt) (DOPE-NBD) lipid to fluorescently label our vesicle. All three lipids have 18 carbon length tails with one double bond, making them all unsaturated lipids with similar packing properties. This allows us to form GUVs (large scale version of a liposome) with well-known elasticity and simplify our analysis. For our gel phase lipid, we replaced the DOPC in our lipid mixture with 1,2-dipalmitoyl-sn-glycero-3-phosphocholine (DPPC) a lipid with an unkinked tail that forms a gel phase at room temperature.

3.1.3 Drag Force

For this experiment, we use the drag force of fluid flow to pull our GUV while it remains anchored to the surface by teams of kinesin attached to microtubules. In the presence of a fluid flow, the vesicle either forms nanotubules, remains static, or detaches completely from the surface. When unsaturated lipids are placed in water, they preferentially form into spherical vesicles. To deform this shape a force is applied to the vesicle at a specific point and instead of simply pulling a cluster of lipid molecules out, exposing the oily tail groups to water, the vesicle will deform and form a tubule [70]. The length and stability of this tubule is based on the elasticity of the membrane. If the energy cost to form a long tubule remains less than that of exposing the lipid tails to solution [71] the membrane won't rupture. Since the GUVs were in a sustained flow of fluid during the experiment, we can use equation 27, Stoke's law, to estimate the force on our vesicle (Fig. 19).

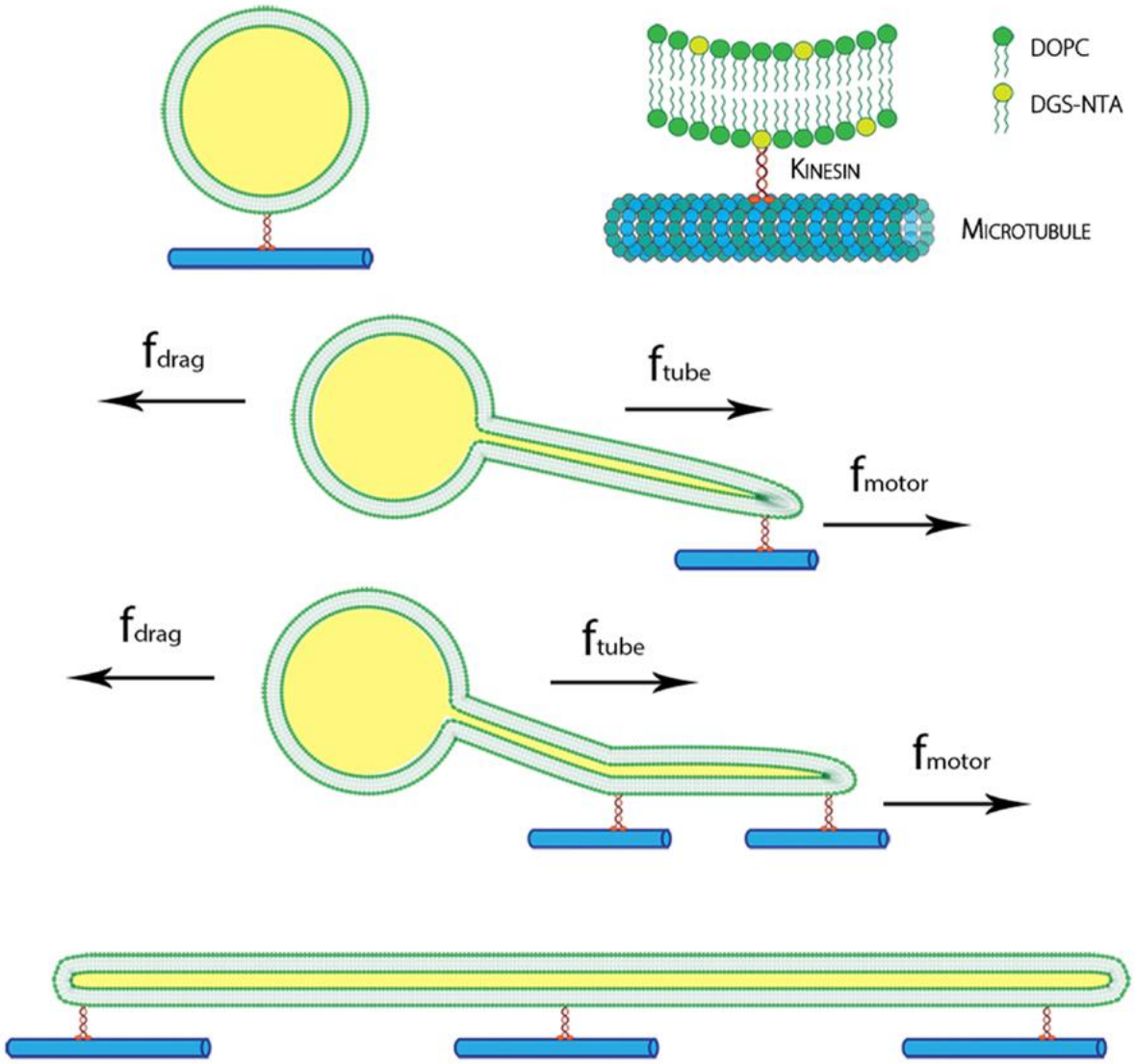

Figure 19. Formation of lipid tubules by anchored GUVs. When GUVs are bound to a microtubule by a motor protein, the application of drag force will cause the GUV to deform and extract a tubule. This tubule can be stabilized by other motors anchoring the tubule to additional microtubules. Image obtained from [8].

$$f = 6\pi\eta r v \quad (27)$$

This equation states that the force on our vesicle is equal to 6π multiplied by v the velocity of the fluid flow, the radius of the GUV as given by r, and the viscosity of the

solution η. For our system our medium is water, however the viscosity of water near the surface of a boundary requires the use of equation 29, Faxen's law, to calculate [72, 73].

$$\eta = g \quad (28)$$

$$g = (1 - \frac{9R}{16h} + \frac{R^3}{8h^3} - \frac{45R^4}{256h^4} - \frac{R^5}{16h^5})^{-1} \quad (29)$$

Where *h* is the height of the GUV from the surface of the flowcell and *R* is the radius of the GUV. Our g value is estimated to be 2.36, with our GUV radius of 1 μm and a value of 100 nm for the height of our guv. Testing the system with glass beads or rigid membrane GUVs composed of DPPC lipids in gel phase, one can see that instead of tubules forming, the objects simply detach or remain stationary to the surface. For the lipid vesicles made of DOPC lipids in fluid phase, we see the formation of tubules. The force of tubulation is given by equation 30 [74].

$$f = \frac{2\pi k}{r} \quad (30)$$

Where r is the radius of the pulled tubule and k is the bending rigidity, in our system the value of k for DOPC is 85 pNnm and 1100 pNnm respectively [75, 76]. While we used fluorescence microscopy to view the tubule, the radius of the tubule couldn't be measured due the resolution limit of the equipment and had to be estimated to be 20-100 nm.

3.2 Methods

3.2.1 Materials

All of our lipids, 1,2-dipalmitoyl-sn-glycero-3-phosphocholine (DPPC), 1,2-dioleoyl-snglycero-3-phosphocholine (DOPC), 1,2-dioleoyl-sn-glycero-3-[(N-(5-amino-1-carboxypentyl)iminodiacetic acid) succinyl] (ammonium salt) (DGS-NTA), and 1,2-dioleoyl-sn-3-phosphoethanolamine-N-(7-nitro-2-1,3-benzoxadiazol-4-yl) (ammonium salt) (DOPE-NBD) were purchased from Avanti Polar Lipids in chloroform and used without further purification (Fig. 20). Lyophilized tubulin was purchased from Cytoskeleton (Cat.T240). Recombinant kinesin protein (K560) was purified [77]. Silicon beads of 2.47 μm (SS04N) and 4.56 μm (SS06N) in water were purchased from Bangs Laboratories, Inc.

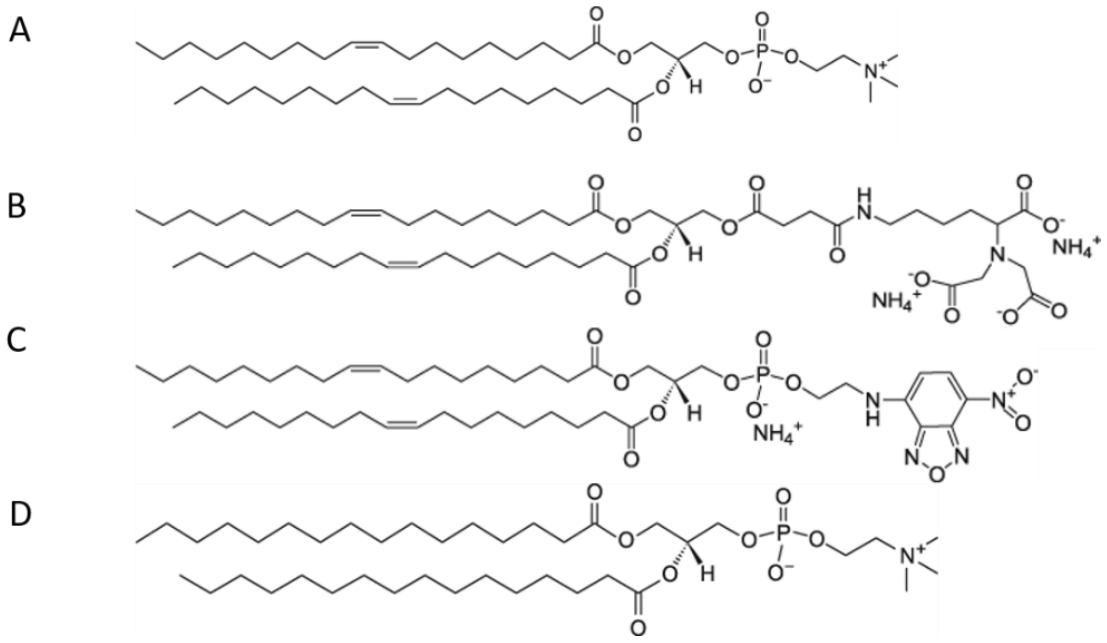

Figure 20. Lipid molecular diagrams. These lipid molecules, DOPC (A), DGS-NTA (B), and DOPE-NBD (C), form homogenous fluid membranes at room temperature because of their identical unsaturated tail structures. When DPPC (A), DGS-NTA (B), and DOPE-NBD (C) are mixed, the rigid tail structure of DPPC forces the membrane to be in the gel phase at room temperature. Images obtained from Avanti Inc.

3.2.2 GUV Formation

When dried lipids are dissolved in sufficient concentration in aqueous solution, they will come off the surface in sheet like bilayers. If an alternating electric field is applied normal to the surface, GUVs will form in a process called electroformation [78]. To produce these conditions, a dried layer of lipid molecules coats the surface of a nonconductive side of Indium Tin Oxide (ITO) glass in a 5-point star pattern and is then hydrated with an aqueous solution that contains sucrose to weigh the vesicles down to the surface during experimentation. To keep this solution on the slide, a plastic O-ring is placed on top and covered with another piece of ITO glass. This glass was previously cleaned in a sonicated bath of acetone, then ethanol, and then dried with N_2 gas. The entire ensemble is sealed with vacuum grease and screwed into place via a holder. To form the GUVs, the sample is placed in an oven, set to 45 ℃, and electrodes affixed to the conductive side of the glass. Using a function generator, one applies an oscillatory sinusoidal voltage with a peak of 2 V and a frequency of 7.5 Hz for a total time of 3 hours (Fig. 21). This process rehydrates the lipids and causes the layers of lipid molecules to come off the surface in sheets. By constantly oscillating in solution the membrane sheets will form large vesicles

of approximately 1-10 µm in diameter. Lipid GUVs are then extracted via pipette and placed in a centrifuge tube and refrigerated at 4 ℃. These GUVs were made of a lipid mixture that contains 94.95 mol% DOPC, 5 mol% DGS-NTA, and 0.05 mol% DPPE-NBD.

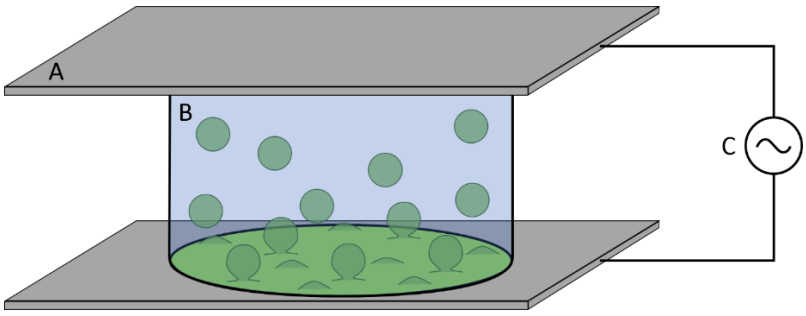

Figure 21. GUV electroformation. GUVs are formed when a you take two pieces of ITO glass (A) and coat the surface with dried out lipids. When the dried-out lipids are enclosed and hydrated (B), the lipid will slake off the surface. When a sinusoidal electric field is induced by a generator at the proper frequency and voltage (C) GUVs will form from the dissolved sheets of lipid.

3.2.3 Flow cell For Nano-Tubulation

For the nano-tubulation experiments a flow cell was used as the platform (Fig. 22). A flow cell is a small chamber of approximately 20 µm made from taking a microscope slide, applying 2 pieces of double-sided sticky tape, and adding a glass coverslip. This provides a chamber with an inlet and an outlet that is cost effective, disposable, and easily mass produced for high throughput experimental processes. The disadvantage of this method is that, compared to microfluidic chambers controlled by pumps, we are unable to control the volume of fluid exchange and are forced to pull water through using filter paper. However, given that we know the time needed for complete volume exchange of our applied buffer we can approximate the flowrates and track particles as they flow through the fluid.

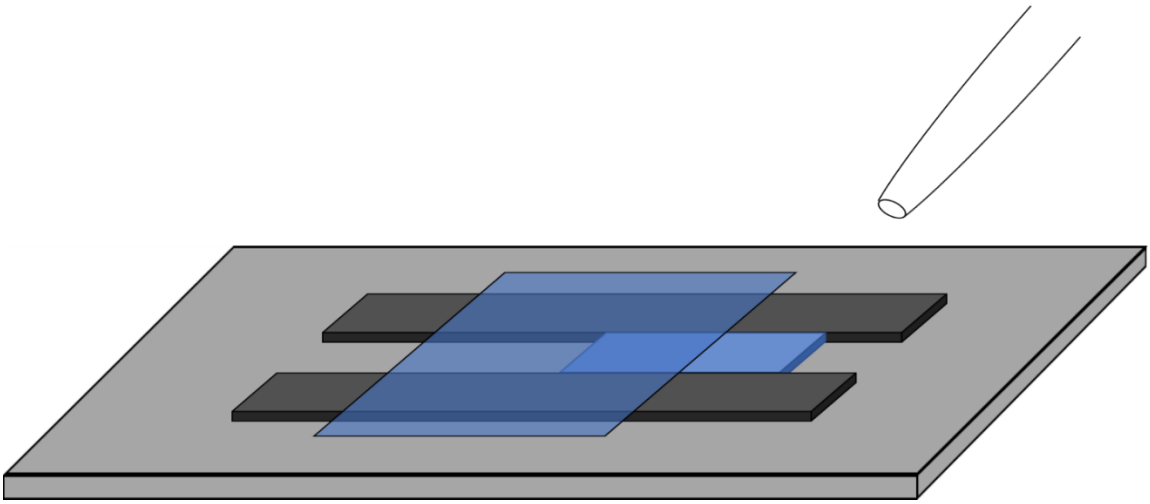

Figure 22. Flow cell. Flow cells are constructed from cleaned glass slide, coverslip, and double-sided sticky tape. Two ends are left open for the inflow and outflow of solution and are approximately 25 µl in volume**.**

3.2.4 Lipid Bilayer from SUV Deposition

While the lipid GUV's were mostly comprised of DOPC, 5% of the molar composition was DGS-NTA lipid and 0.05% was DPPE-NBD. This lipid has an identical tail structure to DOPC, however the differences in head size affect the diffusion constant. To more accurately assess the diffusion constant, D, for GUVs containing 5 mol% DGS-NTA and .05% DPPE-NDB, we used fluorescence recovery after photo bleaching (FRAP) on supported lipid bilayers. To form these lipid bilayers a method called small unilaminar vesicle (SUV) deposition was used to coat the surface of a glass coverslip with a single layer bilayer. To reduce the interaction between glass and lipid bilayer, a cushion of Bovine Serum Albumin (BSA) was used. For this process we first took our stock lipid mixtures, DOPC, DGS-NTA, and DPPE-NBD, which are stored in chloroform and combined in a clean glass vial. The vial is then placed under vacuum for 5 hours, so that all chloroform has been removed from the lipid and a dry film coats the bottom surface. Nanopore water is added to the vial to rehydrate the lipids to their final concentration and stored in a refrigerator at 4 ℃.

To form the lipid bilayer a small space is placed on a microscope slide and a drop of 5mg/ml BSA solution added. This is then placed in an oven set to 45 ℃ for 2 hours to allow for even coating of the surface with the protein. The stock vial of water dissolved lipids was then tip sonicated for 1 minute. The constant vibrations and heat from the tip break up the lipid vesicles in the solution, forming SUVs. This formation can be visually confirmed when the cloudy solution turns clear as the SUV's are too small to scatter light. 10 µl of SUV solution was then removed from the vial, mixed with 10µl of 10mM $MgCl_2$ and drop cast onto the BSA coated slide. The slide is then incubated at 45 ℃ for 45 minutes.

As the slide is being incubated the temperature allows for the vesicles to randomly impact the surface of the slide, breaking apart and coating the surface. As the impact number grows, the fusion of the SUVs onto the surface forms a single bilayer. The sample is then covered with a coverslip and sealed with wax before the bilayer is observed using fluorescence microscopy.

3.2.5 Fluorescence Microscopy and FRAP

Fluorescence microscopy is used to image our experiments [67]. In fluorescence microscopy the sample is doped with a fluorophore, a molecule or structure that when stimulated by specific wavelengths will excite an electron to a higher energy state. When this electron relaxes, a photon of a longer wavelength than the initial excitation is emitted and observed. To measure the diffusivity of the membrane, a technique called FRAP was used to assess the single bilayer diffusivity. As our lipid membrane consisted of a small percentage of fluorescently labeled lipid, we can take images of this fluorescence and measure its intensity. Over time, as the labeled lipid is constantly excited, the fluorophore will break down, reducing the net intensity of our membrane (bleaching). This reduction in intensity, while normally a nuisance that is combated with anti-bleaching agents, can be used as an important experimental tool. To understand this, imagine that the lipid membrane is an infinite sheet [67, 79], where the lipid molecules are capable of diffusing randomly in the x and y direction, due to random thermal motion. In this sheet, a small circular region of about 10-20 μm is overexposed by an intense beam of light. Due to this overexposure, the fluorophores on the molecules have been bleached and one would observe a dark spot. Over time at the boundary of the bleached region, there is an exchange of lipid molecules, with the bleached lipids diffusing into the bulk of the sheet and the unbleached lipids replacing them (Fig. 23). The time of this recovery phase can then be used to quantify the diffusive constant of the lipid.

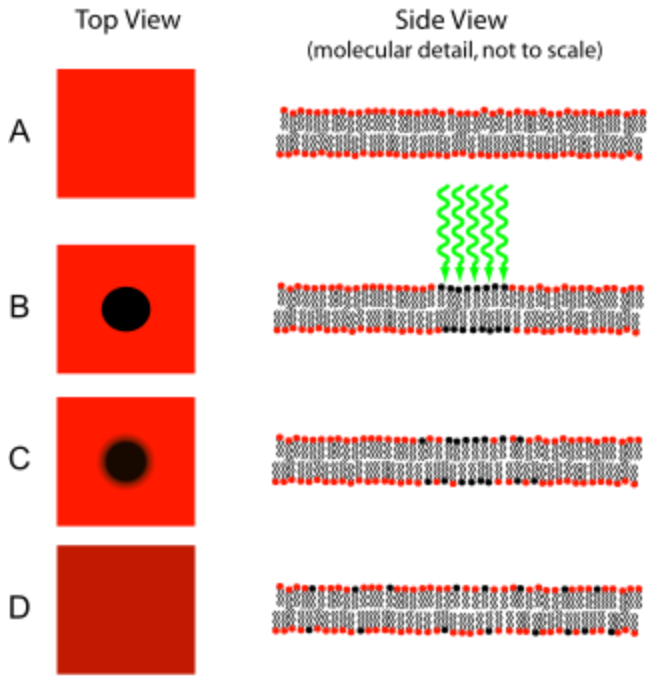

Figure 23. Fluorescence recovery after photo bleaching (FRAP). Initially the lipid bilayer is imaged and used to measure the total intensity of the area (A). The membrane in then bleached by passing the light through an aperture, overexposing a small region (B). The Lipids of the bleached area will slowly exchange with unbleached lipids at the interface (C), until the entire area has exchanged with the background. Image obtained from Wikipedia.

To quantify the diffusive constant from the recovery measurements, we must use the Soumpasis equation [79]. This theoretical model is based on calculating the diffusion of bleached molecules leaving a circular region, with the fluorescence intensity recovery as a function time, $F_k(t)$, is given by equation 31 and considering the total concentration of lipids, given by equation 32.

$$F_k(t) = \frac{q}{A}\int I(r)\, C_k(r,t) d^2r \quad (31)$$

$$C_k(r,t) + C_k^*(r,t) = C_0 \quad (32)$$

Where in equation 32 q is the laser efficiency, A the attenuation of the laser, I the intensity of bleaching, and $C_k(r,t)$ the concentration of unbleached lipids with r taken as the center of the bleached region. If we take the total population of unbleached $C_k(r,t)$ and bleached $C_k^*(r,t)$, and add them then we have the total concentration of lipids C_0.

Equations 33 and 34 give us our boundary conditions. The bleached population is zero far away from the center of bleaching, and zero at t=0.

$$C_k^*(\infty, t) = 0 \quad (33)$$

$$\begin{bmatrix} C_k^*(r,0) = 0 & r > \omega \\ C_k^*(r,0) = C_0(1 - e^K) & r \leq \omega \end{bmatrix} \quad (34)$$

$$K = \alpha T I(0) \quad (35)$$

Where ω is the radius of the bleached region and K is equal to the rate of irreversible bleaching multiplied by the intensity, $\alpha I(0)$, and by the width of the beam T. This can be written in an integrable form by considering that the bleaching rate occurs under the conditions of equation 31. Given that the laser profile is a Gaussian we can model the intensity as equation 36, with P_0 the total laser power, and ω is the beam radius. We can consider the diffusion of a concentration, $C_k^*(r,t)$, of particles from a circular region modeled as equation 37.

$$I(r) = \begin{bmatrix} 0 & r > \omega \\ \dfrac{P_0}{\pi\omega^2} & r \leq \omega \end{bmatrix} \quad (36)$$

$$\frac{\partial C_k^*(r,t)}{\partial t} = D\nabla^2 C_k^*(r,t) \quad (37)$$

Where D is the diffusion constant. Equation 37 can then be written in a convenient integral form.

$$C_k^*(r,t) = \frac{1}{2Dt}\int_0^\infty dr' r' C_k^*(r',0) e^{\left(-\frac{r^2+r'^2}{4Dt}\right)} \boldsymbol{I}_o\left(\frac{rr'}{2Dt}\right) \quad (38)$$

Using an identity given by equation 39 and equation 40, equation 38 can be rewritten.

$$\frac{1}{2\gamma} e^{\left(-\frac{\alpha^2+\beta^2}{4\gamma}\right)} \boldsymbol{I}_{\boldsymbol{v}}\left(\frac{\alpha\beta}{2\gamma}\right) = \int_0^\infty ds\, s\, \boldsymbol{J}_{\boldsymbol{v}}(s\alpha)\, \boldsymbol{J}_{\boldsymbol{v}}(s\beta) e^{(-\gamma s^2)} \quad (39)$$

Where $\gamma = Dt$, $v = 0$, $\alpha = r$, $\beta = r'$, $\boldsymbol{J_v}$ are Bessel functions, and $\boldsymbol{I_v}$ are modified Bessel functions.

$$\int_0^\infty r'\boldsymbol{J_0}(sr')dr' = \frac{w}{s}\boldsymbol{J_v}(ws) \quad (40)$$

Combining equation 38, 39, and 40 we see that the concentration over time in the bleached region can be modeled as equation 41.

$$C_k^*(r,t) = wC_0(1-e^{-K})\int_0^\infty dse^{-\gamma s^2}\boldsymbol{J_0}(sr)\boldsymbol{J_1}(ws) \quad (41)$$

And combining equation 41 with equation 36, 35, and 31gives us equation 42.

$$F_k(t) = \frac{q}{AP_0C_0} - 2\left(\frac{q}{AP_0C_0} - \frac{q}{AP_0C_0}e^{-K}\right)\int_0^\infty \frac{dx}{x}J_1^2(x)e^{\left(-\frac{Dt}{w^2}\right)} \quad (42)$$

Where A is the attenuation factor, C_0 the initial concentration of bleached molecules, q the quantum efficiency of adsorption, and K the bleaching parameter. By deriving and re-integrating equation 42 we finally come to the equation 43.

$$f(t) = e^{\left(\frac{-2\tau_d}{t}\right)}\left[\boldsymbol{I_0}\left(\frac{2\tau_d}{t}\right) + \boldsymbol{I_1}\left(\frac{2\tau_d}{t}\right)\right] \quad (43)$$

$$\tau_d = \frac{\omega^2}{4D} \quad (44)$$

Where *f(t)* is the measured intensity of the bleached region over time, D is the diffusion constant, ω is the radius of bleaching, and $\boldsymbol{I_0}$ and $\boldsymbol{I_1}$ are modified Bessel functions. Using this equation, we can fit our average intensity data and calculate the diffusion constant of our lipid membrane. The diffusion constant is then found as a fit parameter and given by equation 44. In our experiments the data was averaged between slides and normalized by measuring the base intensity of the membrane, with each region observed in 120 s intervals for a total time of 20 minutes.

3.3 Results

3.3.1 Diffusivity of Membrane Bilayer

The diffusion constant of our lipid bilayer was found to be 9.01±.58$\frac{\mu m^2}{s}$. This is more fluidic compared to the diffusion constant for a bilayer composed of pure DOPC lipid, 8.2$\frac{\mu m^2}{s}$ (Fig. 24). To test the impact of diffusivity on the formation of tubules, DPPC vesicles were also prepared and used. DPPC is a saturated lipid, and as such their lipid tails have no double bonds. Without this double bond, the DPPC lipid is able to more tightly pack, generating higher bending rigidity of 1100 pNnm. Because of this, when DPPC lipids are below a transition temperature of 43 ℃, they are in the gel phase. This gel phase has a very low diffusion value, of the order 0.001 $\frac{\mu m^2}{s}$ [80], meaning that when the membrane forms the lipids will stay in place for long time scales. Additionally, the packing of the lipid is tilted, and because of this rigidity and tilting, DPPC GUVs are not perfectly spherical but crumpled [81]. If the DPPC GUVs are heated to above transition temperature, then they will become spherical. In this study no lipid nanotubes were formed from DPPC vesicles at room temperature when the flow was introduced because of this rigidity. DPPC GUVs as large as 20 μm were flowed into the flow cell channel and allowed to sink to the surface by the gravity of their sucrose interior (see section 3.2.2). Afterward, the channel was washed by filter paper absorption with GUVs either remaining static on the glass or caught and dragged out by the flow.

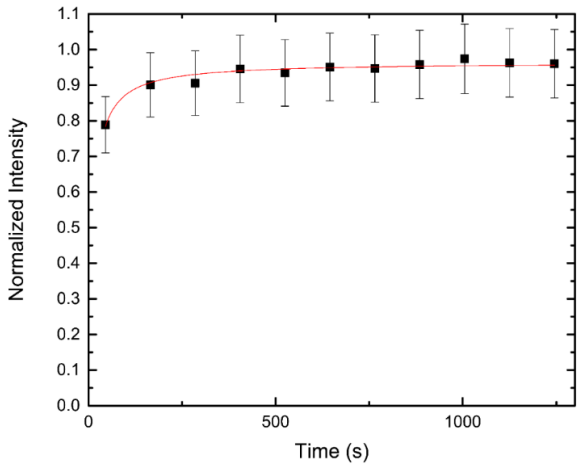

Figure 24. Plot of Time vs. Normalized Intensity. The plot represents the intensity curve from FRAP experiments on DOPC/DGS-NTA (5 mol%) lipid membranes. The red line is the Soumpasis equation fit used to extract the diffusion coefficient, D, of the membrane. The D value for the plot shown here is 9.01±.58 $\frac{\mu m^2}{s}$. Image obtained from [8].

3.3.2 Tubule Formation from Diffusive GUVs

Vesicles made from 94.95% DOPC, 5% DGS-NTA, 0.05% DPPE-NBD are capable of tubulation when tethered to the surface, linking via the DGS-NTA lipid group and the kinesin motor proteins (Fig 25). This tubulation requires a higher flow velocity for smaller vesicles, as smaller vesicles have higher curvature, which necessitates more force. Tubulation occurs for GUVs greater than 4.5 μm in diameter at a low flow rate of 61.3 $\frac{\mu m}{s}$, and GUVs between 2 μm and 4.5 μm in diameter required a higher flow rate of 177.6 ± 18.2 $\frac{\mu m}{s}$. The radius of the tubules could not be determined due to the limit of resolution of our instruments, but past research has found that a typical nanotube is between 20 nm and 110 nm in diameter [82, 83, 84]. Lipid nanotubes were observed to reach lengths of up to 100 μm. Because of the strong surface anchoring, the tubules would remain stable during fluid flow, and sometimes when the flow was removed, not fully retract. This evidence strongly suggests that there were multiple linkages along the nanotube, and as the tubule formed it was possible for it to contact additional kinesin, locking down the microtubule (Fig. 25 E).

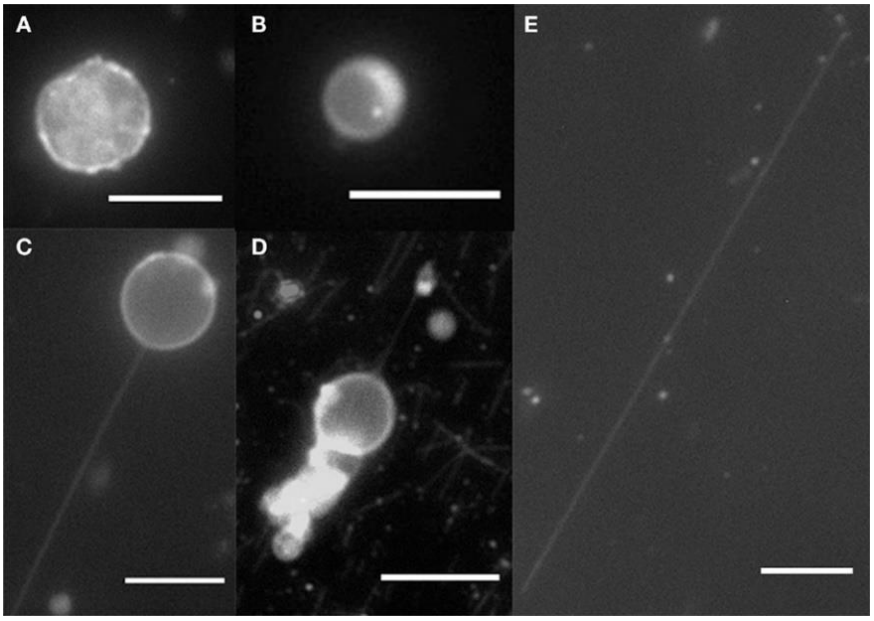

Figure 25. Fluorescence microscopy of GUVs and nanotubes. DPPC/DGS-NTA (5 mol%) form crumpled vesicles (A) while DOPC/DGS-NTA (5 mol%) form spherical vesicles (B). DOPC/DGS-NTA (5 mol%) vesicles form tethered GUV (C) when flow is induced, and these tethers are anchored onto labeled microtubules (D). Lipid nanotube can bind to additional motors and remain extended (E). Scale bar: 10 μm. Image obtained from [8].

3.4 Discussion

3.4.1 Tubulation as a Function of Bending Rigidity

In our experiments we have observe three different cases of $f_{vnet} = f_{drag} + nf_{tube}$ where f_{net} is the net force exerted on the GUV.

1) $f_{net} > nf_{motor}$: This results in the surface bound GUVs to be swept away in the fluid flow, as the net force is greater than the force of the ensembled motors, nf_{motor}. This is more common for larger GUVs, as their large surface cross section generates a larger f_{vnet}.

2) $f_{net} \leq nf_{motor}$: This results in tubulation, as the f_{net} is not strong enough to detach the motors from the surface microtubules. Under a high flow rate of ≈177 μm/s, GUVs less than 5 μm remain anchored to the surface and are not washed from the flow cell. Nanotube formation is dependent on the distribution of kinesin and their total number.

3) $f_{net} \ll nf_{motor}$: This results in no tubule formation as the drag force is insignificant comparted to the force anchoring the GUV to the surface. Too many bound sites on the membrane or in the case of DPPC, stiff membrane, prohibits the GUV from either washing away or pulling out nanotubes

If each kinesin exerts a force of around 5 pN and we also assume that extracted lipid nanotubes are 67.6 nm in radius, we can estimate the number of motor proteins from the force of tubulation. Using the data of measured tubules, and equation 30, we found that nano-tubulation requires a minimum of one or two motors initially in both low and high flow, since the force required 7.2 pN is within the force that a single motor can exert. According to experimental data, if there are more motor/lipid linkages then the GUV does not form a nanotube and remains immobilized. This trend is also observed when we plot the estimated number of motors required for tubulation in relation to the GUV's radius. To extract larger tubules, more motor protein force will be required. This is impractical for several reasons. Primarily motor proteins are distributed randomly on a microtubule, meaning that as the number of motor proteins increases, they have a linear distribution, not clustering around a point. If this occurs instead of a nanotubule forming the energy cost will be too great, and the GUV will simply stretch.

This chapter covered how the diffusivity of the membrane alters the shape of lipid structures and the properties of motor/membrane interactions. In the course of this research I prepared planar bilayers and used FRAP to determine the diffusivity of the membrane and the forces needed for motor proteins to deform a lipid membrane. These same lipid mixtures and techniques will be used in chapter 4 where we use membrane bound proteins to transport microtubules.

Chapter 4

Clustering of Membrane Bound Kinesin to Microtubules

4.1 Introduction

As outlined in chapter 1, within the cell, molecular motors play an important role in the transportation of intracellular cargo [2]. By converting chemical energy into mechanical energy through ATP hydrolysis [41, 49], molecular motors contribute to the highly-organized nature of cellular function. One of the main motor proteins, kinesin-1, carries its cargo along microtubule pathways. This cargo of organelles and protein bodies is contained within a lipid vesicle [7, 85], where kinesin is physically coupled to the lipid membranes of the vesicles they transport either directly or through proteins [51]. Here I asked the question: do the physical characteristics of the vesicle membrane impact transport properties?

To answer this question and quantify the transport properties of lipid bilayer-coupled kinesin, a simple planar experimental model based on the standard gliding assay was used [86, 87]. In the gliding assay, microtubules are typically propelled across a solid motor-decorated surface. This experimental system can be used for investigating kinesin-based transport of cargo along a microtubule, as opposed to the bead-cargo method [4, 88]. Since kinesin cargoes (e.g. lipid vesicles) are large when compared to nanoscale kinesin motors [89], flat experimental geometry can be considered a good model for the biological system I wanted to mimic. As gliding microtubules are transported across a substrate, an analysis of their motion can yield valuable information on the ensemble behavior of the underlying motors - a complex function of binding and unbinding rates and motor-motor interactions.

These experiments demonstrate unusual time-dependent gliding behavior is seen for microtubules transported on a lipid bilayer. To recruit kinesin motors onto the bilayer, 1,2-dioleoyl-sn-glybero-3-[(N-(5-amino-1-carboxypentyl) iminodiacetic acid) succinyl] (ammonium salt) (DGS-NTA) at 10 mol%, unless otherwise specified was added to a lipid bilayer comprised primarily of 1,2-dioleoyl-sn-glycero-3-phophocholine (DOPC). This membrane was designed to exhibit homogeneous fluid behavior while incorporating three carboxyl groups providing nonspecific binding through electrostatic attraction and hydrogen binding sites with the kinesin motors histidine tag [8, 44] (Fig. 25). The lipid membranes are decoupled from the glass substrate by a bovine serum albumin (BSA) cushion providing a fluid membrane environment in which the motors can diffuse laterally.

The results are striking and clear differences in gliding behavior between the glass and membrane substrates were observed. Microtubule gliding velocity for membrane coupled motors increased twofold over time, a trend not seen for the microtubule gliding

on glass substrates. My collaborators and I attribute this result to a gradual build-up of bound motors on the microtubule over the timescale of our experiment; an effect that results in increased gliding velocity, as well as clustering of motor proteins that release in the presence of ATP. Our findings underline the importance of vesicle membrane composition on transport, an aspect of kinesin transport only recently explored [56, 90].

4.2 Methods

4.2.1 Materials

All lipids used in this work were purchased from Avanti Polar Lipids (Alabaster, AL, USA) in chloroform and used without further purification. They include 1,2-dioleoyl-sn-glycero-3-phophocholine (DOPC), 1,2-dioleoyl-sn-3-phosphoethanolamine-N-(7-nitro-2-1,3-benzoxadiazol-4-yl) (ammonium salt) (DOPE-NBD), and 1,2-dioleoyl-sn-glybero-3-[(N-(5-amino-1-carboxypentyl) iminodiacetic acid) succinyl] (ammonium salt) DGS-NTA. Porcine tubulin (Cat. T240), and rhodamine labeled porcine tubulin (Cat. TL590M) were purchased from Cytoskeleton, Inc (Denver, CO, USA). Recombinant penta-histidine-tagged kinesin protein was purified from *Escherichia coli* as previously described [77]. All other chemicals were purchased from Sigma Aldrich (St. Louis, MO, USA).

4.2.2 Microtubule Preparation

Labeled and unlabeled porcine tubulin was dissolved at a ratio of 1:5 at a concentration of 1.5 mg/ml in PEM80 (80 mM PIPES, 1 mM ethylene glycol bis (β-aminoethyl ether), 1 mM $MgSO_4$, pH 6.9), buffer and supplemented with 10 mM GTP and 40 µM Taxol). The tubulin solution is then incubated in a 37 ℃ bath for 12 hours to allow for polymerization after which microtubules are then stored at room temperature in a dark box.

4.2.3 Lipid Membrane Preparation

Lipid mixtures of 89.95 mol% DOPC, 10 mol% DGS-NTA, and 0.05 mol% DPPE-NBD (fluorescent lipid), were mixed in chloroform then vacuum dried to remove all chloroform. Other lipid mixtures used include 80mol% DOPC with 20 mol% DGS-NTA, and 90 mol% DOPC with 10 mol% DGS-NTA. Lipids were then rehydrated with water to final concentration. SUVs were formed via tip sonication [8, 91] and dropcast onto a clean

glass flow cell coated with bovine serum albumin [8]. Then the sample was incubated at 50 ℃ for 1 hour to allow for fusion on the surface forming a single bilayer. The bilayer was observed using fluorescence microscopy. DGS-NTA was selected as a lipid to anchor motor proteins due to its similar tail structure to DOPC, and ability to coexist in a liquid disordered phase.

4.2.4 Flow Cell Preparation

Flow cells [43] are constructed by placing electrical tape on a glass slide cleaned in acetone, methanol, ethanol, and Nanopure water. This forms a rectangular channel. A cover slip cleaned in an identical manner is then added on top of the tape after deposition of lipid membrane and set in place with wax to form the flowcell with a volume of approximately 15 µl. The flowcell is finally sealed with vacuum grease once gliding has been established.

4.2.5 Microtubule Gliding Experiments

Kinesin solutions were introduced at a concentration of 300nM in PEM80 buffer into the flow cell and incubated for 10 min. After allowing 10 minutes for the GFP labeled motors to adhere to the surface, I flowed in the 1:5 rhodamine labelled microtubules diluted in PEM80 (10uM Taxol), which also removed excess motors. Microtubules were then given 10 minutes to adhere to the remaining motors bound on surface. Lastly a motility mix (PEM80 supplemented with 1mM ATP, 1mM DTT, 10uM Taxol, 0.22 mg/ml glucose oxidase, 0.04 mg/ml catalase, 3.68 mg/ml glucose, 2 mM phosphocreatine and 70 µg/mL creatine phosphokinase) [87] to provide a regenerative ATP source and reduce bleaching. The flow cell was sealed with vacuum grease.

4.2.6 DGS-NTA Clustering

Kinesin solution, 300nM in PEM80 buffer, was introduced into the flow cell containing a bilayer with an altered lipid composition that varied the DGS-NTA mol% and incubated for 10 min. After allowing 10 minutes for the GFP labeled motors to adhere to the surface, I flowed in the 1:5 rhodamine labelled microtubules diluted in PEM80 (10uM Taxol), and washed away excess motors that had not adhered to the surface. Microtubules were then given 10 minutes to adhere to the remaining motors bound on surface. Lastly a motility mix (PEM80 supplemented with 1mM ATP, 1mM DTT, 10uM Taxol, 0.22 mg/ml glucose oxidase, 0.04 mg/ml catalase, and 3.68 mg/ml glucose were flowed in to provide ATP and reduce bleaching after 2 hours. The flow cell was sealed with vacuum grease.

4.2.7 Motor Clustering

To determine that motor proteins aggregated onto microtubules the GFP signal intensity of motor proteins was used as a proxy for number of proteins. Microtubules were deposited onto a lipid membrane with adhered motor proteins as in the above experiments. Excess microtubules were removed with a wash buffer (PEM80, 1mM DTT, 10 µM Taxol, 0.22 mg/ml glucose oxidase, 0.04 mg/ml catalase, and 3.68 mg/ml glucose and the chamber sealed with vacuum grease. Images were taken with a widefield fluorescence microscope every 15 minutes in the GFP channel, until three hours passed, and a final image was taken in the Rhodamine channel to confirm that physical location of microtubules was the same as the localized motor proteins.

4.2.8 Imaging and Data Analysis

Microtubule gliding was imaged using a Leica Microsystems Inc. DM 2500P fluorescence microscope, (Buffalo Grove, IL, USA) and a QImaging Retigia Exi camera (Surrey, BC, Canada). In a typical experiment, images were collected at 4-8 observation areas per slide, to produce gliding movies for 1.5 min per area using a 20x or 63x objective. Images were taken at 10 second intervals with a 500 µs exposure time and .69 s delay between frames. All image analysis was carried out using Image Processing and Analysis in Java (ImageJ, http://imagej.nih.gov/ij/). The gliding microtubule gliding velocity was tracked using the MTrackJ plugin for ImageJ (http://www.imagescience.org/meijering/software/mtrackj/). Microtubules were tracked by their leading edge, with an average of 60 microtubules tracked per analysis region.

4.2.9 Confocal Microscopy

For confocal imaging of lipid membranes, a Zeiss LSM 880 with AiryScan+FAST was used, and subsequent analysis carried out using bio-formats in Image j (https://docs.openmicroscopy.org/bio-formats/5.7.0/users/imagej/). Confocal microscopy is a branch of fluorescence microscopy that allows one to only observe the light from a single focal plane [92]. During fluorescence microscopy, light is passed through an excitation filter that only allows specific wavelengths through to the sample. When this light hits the sample, the photon excites an electron in the fluorophore, however all regions of the sample can be excited and emit photons, obscuring details. To limit the light observed to a single focal plane one can use a pinhole aperture (Fig. 26). Using this technique, one can observe more detail and quantify the in intensity of our sample with greater accuracy.

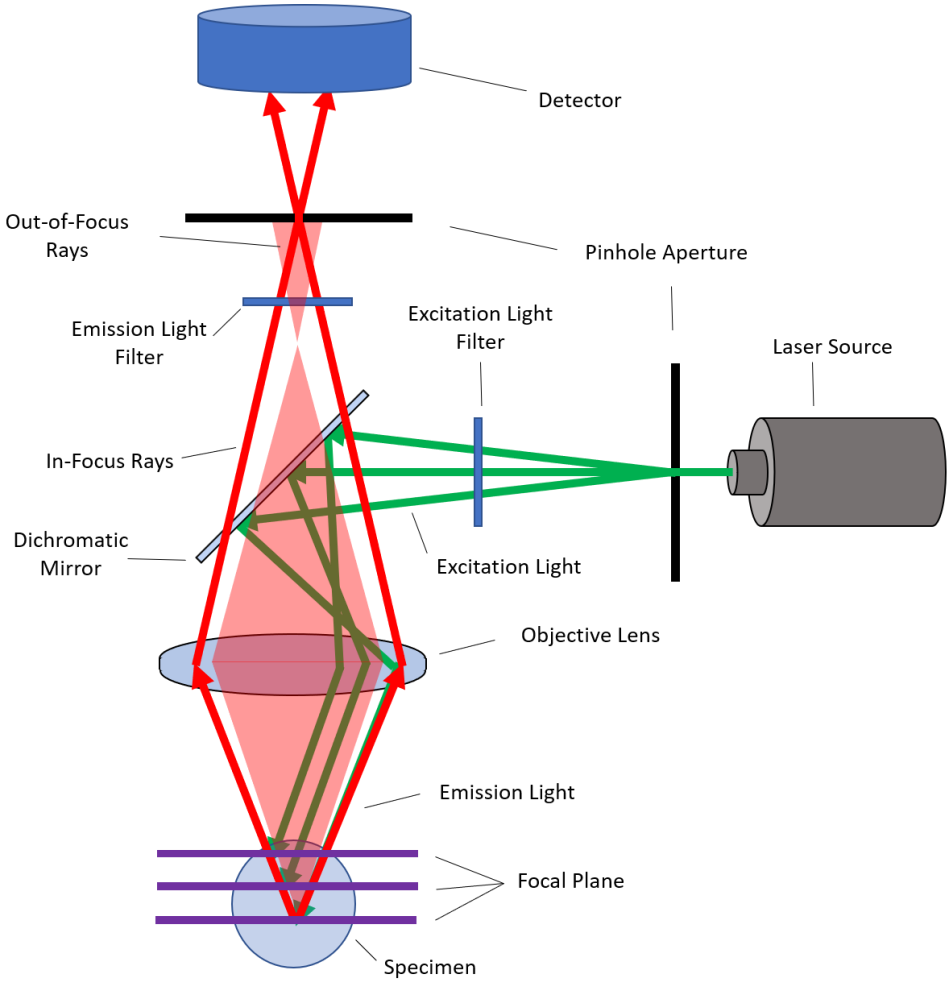

Figure 26. Confocal microscope diagram. Confocal microscopes operate much the same as a standard fluorescence microscope, using a source of filtered light source to send a specific wavelength of light into the sample. The sample's fluorophores become excited and emit photons of a higher wavelength that then must pass through a pinhole aperture. This aperture only allows light from a set focal plane to pass through to the detector.

4.3 Results

4.3.1 Motor Proteins Non-Specifically Bind to NTA Head Group.

GFP labeled kinesin-1 motor proteins were added to a flow cell in a buffer exchange process. These motor proteins bound to the lipid membrane non-specifically, attaching to the NTA group of the lipid molecule. This non-specific binding was assessed using confocal microscopy (Fig. 27), to demonstrate that increased motor protein concentration

in buffer would translate to increased concentration on the surface. Qualitatively we can see that motor proteins bind and remain uniformly distributed on a lipid membrane (Fig. 27 A - D). Buffers containing motor protein at different concentrations was added to the flow cell, and the buffer subsequently exchanged after 10 minutes to remove unbound motors. By using the GFP signal of the motor protein as a proxy for concentration, we see that increased motor concentration on the surface after buffer exchange is a result of increased concentration in solution (Fig. 27 E).

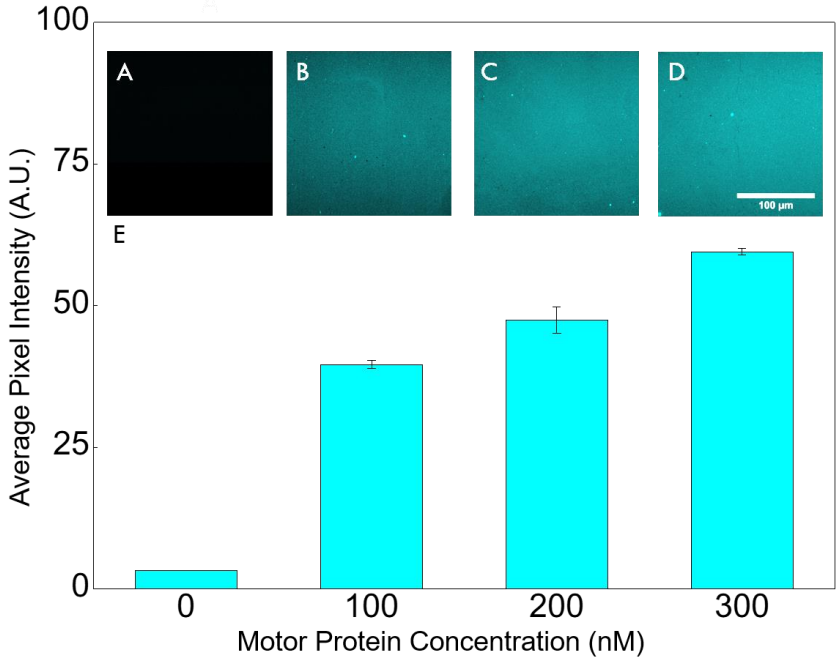

Figure 27. Kinesin non-specifically binds to DGS-NTA lipids. Confocal images of the lipid membrane after introduction of GFP labeled kinesin-1, whose concentration in solution was 0 nM (A), 100 nM (B), 200 nM (C), and 300 nM (D) to quantify non-specific binding. Scale bar represents 50 µm. (E) Average intensity of GFP signal plotted against motor protein concentration, with error bars representing the standard error of the mean (SEM). This plot demonstrates the increased motor concentration on the surface with the increased presence of motor proteins in solution.

4.3.2 Direct Observation of Motor Clustering on Microtubule

While the mobility of individual lipids in the bilayer is well established, comparatively bulky tethered kinesin motors will exhibit a reduced diffusive behavior and predicting the ability of kinesin motors to diffuse across the membrane is non-trivial. To

test the hypothesis that motor proteins diffuse across the membrane, a simple clustering experiment was performed. Since motor proteins bind to microtubules and remain attached in the absence of ATP, as GFP-labeled motor proteins diffuse into and bind to the microtubule the trace of the microtubule should be visible using fluorescence microscopy.

To test the motor clustering hypothesis, I examined GFP intensity as a function of time (Fig. 28) at the position of a microtubule. In support of our hypothesis, the signal in the GFP channel shows a distinct outline of a microtubule that solidified an hour after microtubules were added to the system (Fig. 28 B - D). I then took cross plots of the microtubule to quantify the intensity due to clustering (Fig. 28 E - G). Over an hour-long period, we can see distinct peaks that increase in intensity. To quantify the average increase in intensity I then calculated the area under the curve for each microtubule and averaged the values for each observation time (Fig. 28 H). These results confirm that the motor proteins indeed cluster on the microtubule, creating a higher signal.

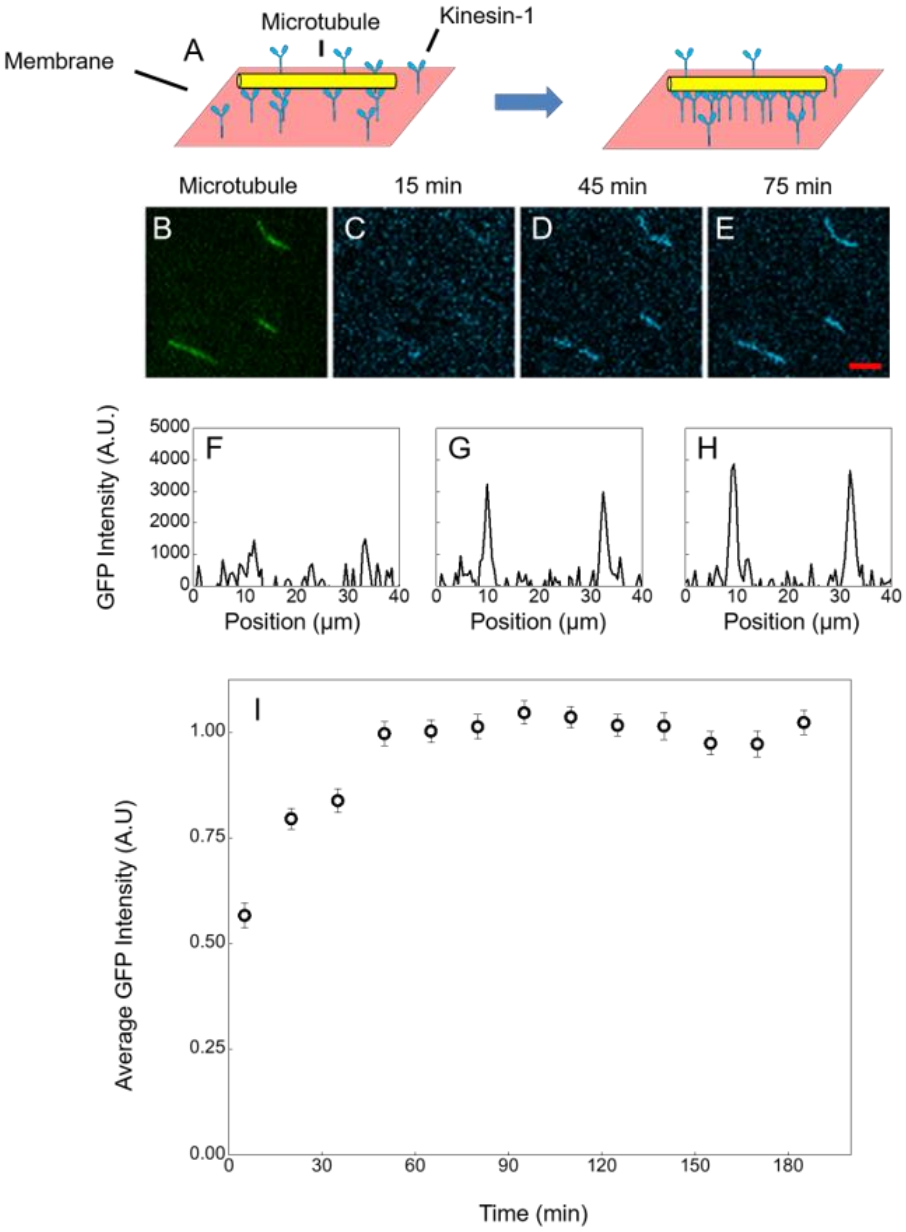

Figure 28. Membrane-coupled motors accumulate on static microtubule. (A) Cartoon schematic of motor protein clustering on a microtubule. (B - E) Fluorescence images of GFP labeled kinesin clustering on an immobile microtubule recorded at 15, 45 and 75 minutes and (F - H) corresponding 1D line profiles of image intensity after background subtraction, corresponding to peaks of intensity. (I) Normalized GFP intensity as a function of time calculated from the average area under the peak for 45 microtubules error bars indicate standard error of the mean. Scale bar is 5 μm.

4.3.3 Membrane Supported Gliding Velocity is Time Dependent

The primary objective of this work was to investigate the effect of bilayer coupling on kinesin-based transport to more closely mimic biological conditions. When coupled to a lipid bilayer, motors are free to diffuse in-plane (Fig. 29). However, when my collaborators and I started this research it was largely unknown how this additional degree of freedom would impact kinesin-based transport. To address this open question, I performed gliding assays on membrane-coupled kinesin motors. Our results, along with the results of Grover et al. [56] demonstrate that membrane-coupling has a substantial effect on microtubule gliding velocity.

Figure 27 demonstrates that when kinesin motors are coupled to a fluid lipid bilayer their gliding velocities vary as a function of time. To perform this experiment, I collected trajectory data for over 100 microtubules, recording both position and velocity as a function of time. The data presented in Figure 29 compares position and velocity data for microtubules on membrane (Fig. 29 C, D -F) and glass substrates (Fig. 29 G, H - J). Considering t=0 min to be the introduction of microtubules to flow cell, I added a motility mix at t=10 min, and made initial observations at t=12 min. We note that the path length traveled by microtubules increased on membrane (Fig. 29 C) with each successive observation. These successive observations were made at t=102 min and t=192 min. To find the average gliding velocity for these time windows I constructed velocity histograms (Fig. 29 D - F). Two2 minutes after introducing motility mix to the flow cell to initiate membrane gliding, I measured an average gliding velocity of $0.16334 \pm 2.6 \times 10^{-3}$ μm/s for the initial time window. This gliding velocity then increased to $0.35105 \pm 5.1 \times 10^{-3}$ μm/s at 102 minutes (Fig. 29 E), and finally $0.3901 \pm 6.5 \times 10^{-3}$ μm/s at 192 minutes (Fig. 29 F). In contrast, when the motors were coupled to the solid glass substrate, I observed no significant change in velocity over the same time periods (Fig. 29 H - J).

As a control, a comparison with a glass substrate was performed in the same flow cell to ensure identical buffer conditions. This was done by constructing a flow cell with a membrane on the slide portion of the flow cell while the glass coverslip remained bare (Fig. 29 A - B). The scatter plot represents the average gliding velocity on the membrane (Fig. 29 K), and the gray bar represents the average gliding velocity on the coverslip. The data shows that the initial average gliding velocity on the membrane is substantially less than that on glass (Fig. 29 K), consistent with results from Grover et al. Over time, the velocity increases until the average gliding velocity approaches that of glass, with lower ATP concentrations taking less time to reach parity (Fig. 30).

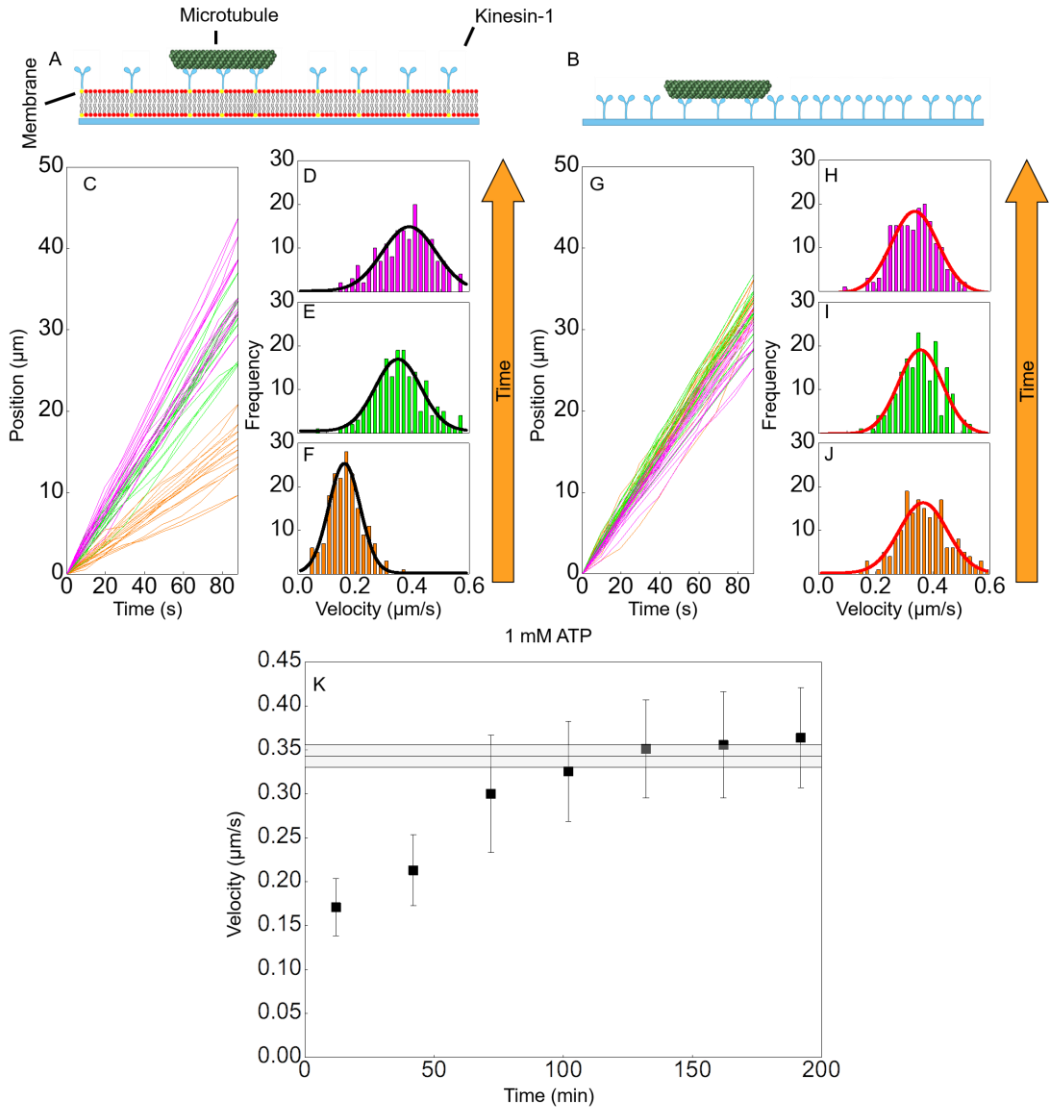

Figure 29. Microtubule gliding velocity is influenced by membrane coupling. Cartoon schematics of gliding, microtubules gliding while coupled to a fluid membrane substrate (A) and gliding on a solid substrate (B). Representative gliding trajectories of microtubules and their associated velocity histograms on membrane (C, D - F) and on glass (G, H - J) taken after initial introduction of ATP (C, D), 102 min after (E, I), and 192 min after (F, J). Solid lines represent best fit to a Gaussian distribution. Mean velocities of microtubule gliding for motors coupled to the lipid bilayer 1mM ATP concentration (K) is plotted against time. Shaded bars represent the average gliding velocity of motors coupled to glass on the coverslip (K), with the width representing one standard deviation. Error bars indicate standard deviation.

4.3.4 Velocity Increase Observed at .1 and .05mM ATP Concentrations

To verify our observation of an increase in microtubule gliding velocity over time while anchored to the membrane, the experiment was reproduced with 0.1 mM ATP (Fig. 30 A) and 0.05 mM ATP (Fig. 30 B)

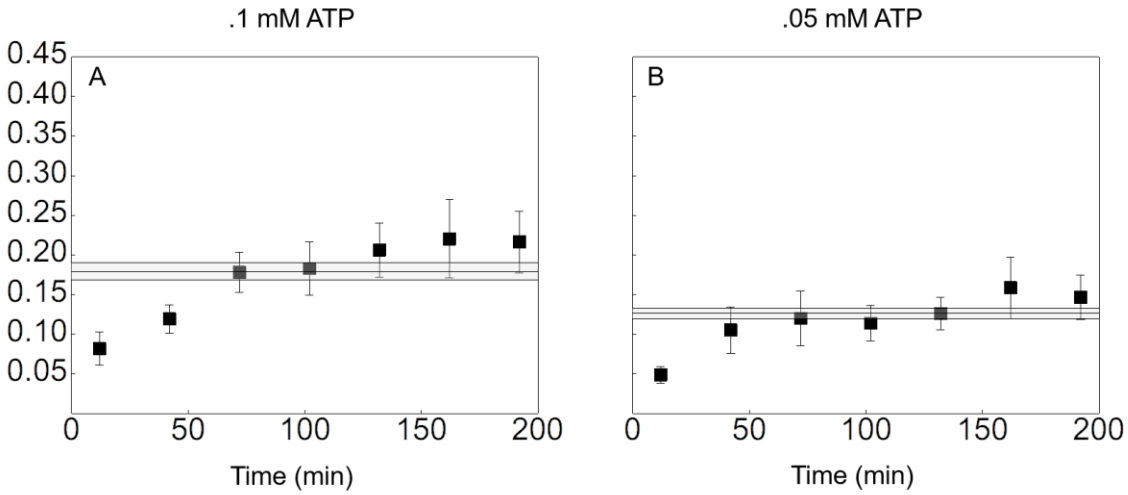

Figure 30. Average gliding velocity at 0.1 and 0.05 mM ATP. Mean velocities of microtubule gliding for motors coupled to the lipid bilayer at 0.1 mM (A) and 0.05 mM (B) ATP concentrations plotted against time. Shaded bars represent the average gliding velocity of motors coupled to glass on the coverslip, with the width representing one standard deviation. Error bars indicate standard deviation.

4.3.5 Microtubule Gliding Velocity is Not Caused by Lipid Clustering

To investigate the mechanism behind the observed increase in velocity, we hypothesized that clustering of motor-binding DGS-NTA lipid could lead to a more solid-like substrate local to the microtubule. The motor protein has a HIS-6 tag, allowing for multiple DGS-NTA lipids to non-specifically bind to a single motor. Such clustering of lipids could create a small motor-rich lipid raft, with an increased hydrodynamic radius.

Such a raft is therefore expected to reduce overall motor mobility in the membrane [31], producing gliding characteristics that trend towards those of a solid glass substrate with increasing radius. To test the possibility that nano-raft formation leads to the observed increase in transport velocity, I prepared slides with lipid membranes and added motor proteins. Excess motors were washed out with buffer and the slide given 120 minutes to sit before the introduction of microtubules, giving the DGS-NTA lipids ample time to cluster

onto the motors. If DGS-NTA raft formation onto the motor protein is the cause of the velocity change once the 1mM ATP motility mix is added to the slide we would expect a constant gliding velocity.

I observed gliding 120 minutes after the addition of the motility mix and the results clearly show that the microtubule gliding velocity increase with time (Fig. 31 A). Despite being given 120 minutes to cluster, there was no variation in the gliding velocity behavior compared to our original experiment (Fig. 29)

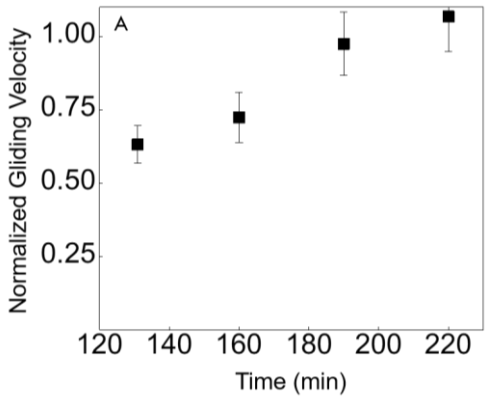

Figure 31. Lipid clustering does not influence microtubule gliding velocity. Graph of average gliding velocity after lipids were given 120 minutes to cluster onto motor proteins (A). Velocities are normalized for with average glass gliding velocity on coverslip and error bars indicate standard error of the mean.

4.3.6 Gliding Velocity Increase Continues After Temporary Suspension

Another potential mechanism for the observed increase in gliding velocity is that the average number of microtubule bound motor proteins varies with time and impacts gliding velocity. The lipid membrane is a 2D fluid, allowing for diffusive motion (Fig. 28) of the coupled motor proteins. After the initiation of gliding, motor proteins may diffuse onto the microtubules and bind on the timescale of our velocity increase (Fig. 29). To test this a "pause" experiment was conducted, in which I looked at whether the microtubules need to be gliding continually to exhibit the velocity increase. By pausing gliding, the system would be static with the exception of the motor proteins diffusive motion.

To carry out the "pause" experiment, motor proteins were coupled to a lipid membrane in a gliding assay. After an initial gliding was observed over a period of eight minutes, the motility mix was replaced with inert buffer, and the microtubules left static. Motility mix was reintroduced 19 minutes afterwards, and I observed gliding again. I determined that the gliding velocity after the "pause" is the same as continuous gliding.

Figure 32 shows velocity histograms for the relevant time periods, (Fig. 32, A, D) for both flow cells and then half an hour afterward (Fig. 32 B, E)

The results are revealing, we find that not only does the average microtubule gliding velocity still increase over time in the paused flow cell, but that it does so at a rate comparable to the standard non-paused experiment. Despite the arrest of motor protein activity, an identical increase in velocity occurs. Since the only mechanism for motor motion in our system after removal of the ATP is diffusion, taken together with the DGS-NTA clustering experiment (Fig. 28), we can conclude that motor clustering on the microtubule via membrane diffusion is likely responsible for the increased velocity.

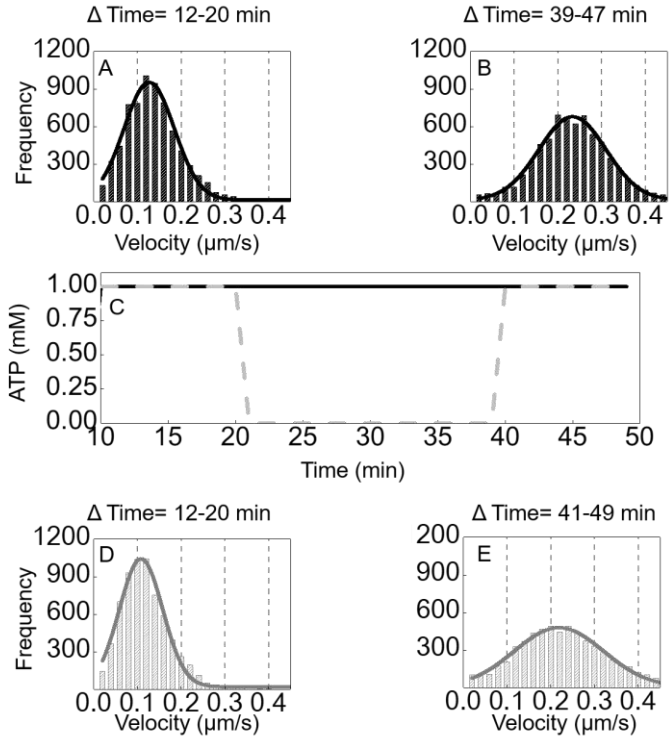

Figure 32. Arresting microtubule gliding motion does not alter the increase in microtubule gliding velocity. Gliding velocity distributions after the addition of 1mM ATP and 20 minutes afterwards are contrasted between continuous gliding (A) and "paused" gliding (B). Velocities from continuous membrane gliding experiment are shown as histograms (A, B). Membrane gliding was repeated with the additional step of removing ATP (C) after initial observation period (E). ATP was re-introduced 20 minutes later, and gliding resumed (F). Histograms are fitted with a Gaussian distribution.

4.4 Discussion

4.4.1 Kinetics of Diffusive Kinesin

Having verified the effects of membrane diffusion on kinesin binding in the absence of ATP, we then performed a second experiment in which ATP was introduced into the system. Fig. 33 shows GFP intensity (measured in the same way as for Fig. 28) as a function of time before and after ATP introduction. ATP was introduced to the flow cell at two different concentrations (1 mM and 0.05 mM) after which time we observed a steep decay in GFP intensity and the onset of gliding motion, consistent with rapid kinesin unbinding.

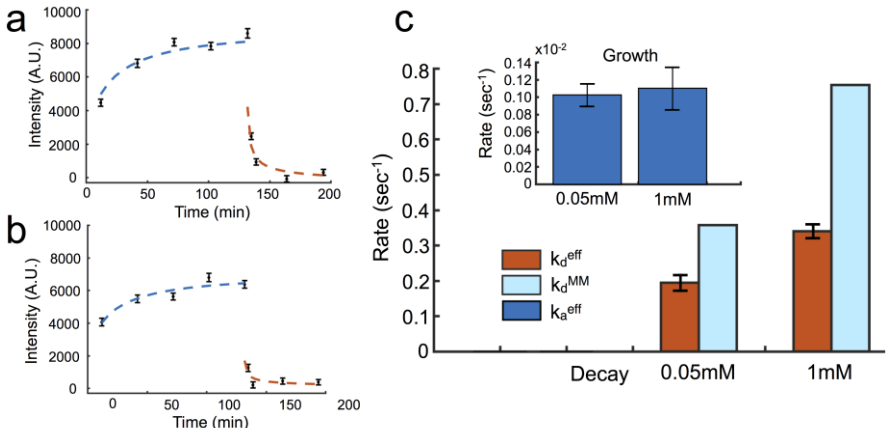

Figure 33. Membrane-coupled motors disassociate rapidly with the introduction of ATP. Experimental measurements of GFP intensity as a function of time for 45 microtubules using the methods described in Fig. 25. Data shown for (*a*) 0.05 mM and (*b*) 1 mM ATP, where ATP is introduced to induce gliding at 120 mins. Error bars indicate standard error of the mean. Theoretical fits (dashed lines) are performed separately for kinesin aggregation without ATP (Blue) and the decay of the microtubule-bound kinesin signal after ATP addition (Orange). (*c*) Rates $\boldsymbol{k_a^{eff}}$ (inset) and $\boldsymbol{k_d^{eff}}$ extracted from our fitting model (Equations 3b and 5b) for ATP concentrations 0.05mM and 1mM (Orange) show a general trend of increasing off rate ($\boldsymbol{k_d^{eff}}$) with increasing ATP concentration. Both growth rates ($\boldsymbol{k_a^{eff}}$) are approximately the same (dark blue). The fitted effective off-rates are compared with expected $\boldsymbol{k_d^{MM}}$ values calculated assuming Michaelis-Menten kinetics (light blue).

To further analyze the experimental data presented in Fig. 33a and compare the curves before and after ATP addition we constructed an analytical model for kinesin binding and unbinding onto the microtubules. In the absence of ATP, microtubules remain

static in space and as time passes the intensity of GFP-labeled kinesin grows. After the addition of ATP, the kinesin signal drops dramatically. We see that the two intrinsic rates that govern this process are very different, but also slow compared to the intrinsic motor on and off rates which are on the inverse second scale, suggesting that both rates may be influenced by a diffusion limited process.

Assuming the fluorescence intensity of kinesin in our images is directly proportional to the number density of kinesins on the microtubule, we can directly measure this density as a function of time. The dynamics governing the microtubule coverage σ (t) are coupled to the kinesin number density c (x,t) in the membrane and given by [93],

$$\frac{d\sigma}{dt} = k_a c(0,t)(1-\sigma) - k_d \sigma \tag{1a}$$

$$\frac{d\sigma}{dt} = D\frac{d}{dx}\Big[c(x,t)\Big]\Big|_{x=0} \tag{1b}$$

Where x is the distance away from a microtubule in the direction perpendicular to its axis. Note that we assume translational invariance parallel to the microtubule, i.e. we ignore edge effects, which seems reasonable given the fairly uniform coverage along the length. Here c (0,t) is the bath concentration of kinesin at the microtubule interface and k_a and k_d are the intrinsic kinesin association rate and disassociation at the microtubule surface respectively. The dissociation rate of kinesin, k_d, from the microtubule surface is ATP-dependent and hence can be turned off by removing ATP from the system. The flux at the interface between the surface bound kinesin and the microtubule is governed by Eq. 1a.

No ATP case: In the absence of ATP (k_d =0), Eq. 1a can be integrated, subject to the constraint in Eq. 1b, to find the microtubule coverage σ (t) in the diffusion-controlled regime [94](Eq. 2).

$$\sigma(t) = \sigma_m\left(1 - \exp\left(\frac{-2C_0}{\sigma_m}\sqrt{\frac{Dt}{\pi}}\right)\right) \tag{2}$$

Here σ_m is the saturated motor coverage that is controlled by the available binding sites on the microtubule. We can estimate the saturated value by considering that kinesin,

when attached to the microtubule, will occupy a distance along a protofilament of 8nm. Assuming that each kinesin occupies two neighboring beta subunits along the same protofilament and neighboring kinesin do not share beta subunits we calculate the coverage at saturation to be $\sigma_m \approx 93.3 \mu m^{-1}$. Here C_0 and D are the lipid bound motor concentration and the motor-lipid diffusion on the substrate respectively.

$$\sigma(t) = \sigma_m \left(1 - \exp\left(-\sqrt{k_a^{eff} t}\right)\right) \quad (3a)$$

$$k_a^{eff} = \frac{4DC_0^2}{\sigma_m^2 \pi} \quad (3b)$$

Fitting the observed increase in kinesin at the microtubule provides an estimate for the effective association rate, k_a^{eff} as defined in Eq. 3 a-b (Fig. 33c – inset). We found that the effective association rates are two orders of magnitude smaller than experimentally determined rates from single kinesin/microtubule systems [94]. It is also important to note that the saturation is controlled by an exponential that depends on the square root of *t* rather than *t*, which is qualitatively slower. This result shows that the diffusive effect of the lipid bilayer can control kinesin-microtubule association.

From the fit of Eq. 3a we may also estimate the number of surface DGS-NTA bound kinesin in our system from the effective association rate (Eq. 3b) using the diffusion constant determined in [56]. We find that the number density of the kinesin bound to DGS-NTA, $C_0 = 2.28 \pm 0.06\ \mu m^{-2}$, which is similar to previous studies [56].

Finally, we note that the process is diffusion controlled when the control parameter γ (Eq. 4) is small.

$$\gamma = \frac{DC_0}{k_a \sigma_m^2} \quad (4)$$

Using the values quoted above for *D*, C_0 and σ_m and using $k_a \sim 5 s^{-1}$ [94]we find that $\gamma \sim 7.4e\text{-}5$ signifying that we are well within the diffusion controlled regime.

ATP case: When the system becomes active by the addition of ATP, we have two more kinetic time constants at play. As motors begin to walk along a microtubule at each

step they have a chance to disassociate or walk off the end of the microtubule. Since the microtubule lengths (~20 μm) here are significantly longer than the typical motor run lengths (800 nm), the effective off rate would be expected to depend only on the intrinsic kinesin disassociation rate k_d. However, as we have seen in the adsorption process (previous section), the kinetics are diffusion controlled and we may expect a similar effect on the disassociation from the microtubule.

Equation 1a can also be exactly solved in this regime ($k_d > 0$, $\gamma << 1$), and in the long-time limit, the coverage is given by

$$\sigma(t) \sim \sigma_m \frac{k_a c_0}{k_d}\left(1 - \frac{1}{\sqrt{k_d^{eff} t}}\right) \quad (5a)$$

$$k_d^{eff} = \frac{D}{\sigma_m^2 k_a^2} k_d^2 \quad (5b)$$

Again, the diffusion controlled approach to steady state has a very different functional form from a normal exponential. Fitting the data (Fig. 33 a, b) after the addition of ATP (t >120min) using Eq. 5a, we obtain the value for the effective off-rate, k^{eff}_d (Fig. 33c). It is to be noted that, by assuming translational invariance, we are also implicitly ignoring the effect of the motion of the microtubule in this calculation. This is reasonable if the timescale set by the ratio of the microtubule length to the velocity (~60s) is large compared to the timescale of the effective off-rate (~3-5s).

Comparing the effective disassociation rate with the intrinsic rate expected from Michaelis-Menten kinetics at both ATP concentrations we see that they are very different, as indicated by Eq. 5b. The effective disassociation constant depends not only on the intrinsic disassociation rate but also on the diffusion constant, the association constant and the saturating motor concentration on the microtubule. This difference comes from the effect of the diffusivity of motors in the bilayer. Physically, this occurs because motors that disassociate from a microtubule persist in the area around the microtubule because the rate of diffusion is considerably slower than the rate of association, giving them a chance to rebind. This gives rise to an effectively lower disassociation rate of motors from the microtubule surface, which depends on the binding rate, saturating concentration and also the diffusion constant. Thus, the diffusion controlled process causes the fluorescence signal to remain higher than it should be as compared to kinetics where motors disassociate and are quickly assimilated into the bulk concentration.

4.4.2 Effects of Kinetics on Gliding Velocity After Long Time Scales

To quantify the effects of perturbing kinetics on membrane-based gliding in our system we studied steady state gliding velocity for three different ATP concentrations, 1 mM, 0.1 mM, and 0.05 mM (Fig 34). We observed no time dependence on gliding velocities after 100 minutes, and gliding velocity increases in magnitude as available ATP concentration in the system also increases. It is to be noted that ATP concentration is non-trivially coupled to the gliding velocity. Increasing the ATP concentration has two effects – it increases the intrinsic disassociation rate thereby reducing the steady state coverage of motors but also increases the speed of the individual motors. The gliding velocity is however directly proportional to the motor stepping speed but only weakly dependent on the steady state coverage at higher coverages[9]. Thus, as expected, the gliding velocity rises with ATP concentration consistent with Michaelis-Menten kinetics. We compared these steady state velocity values with the expected values obtained using our estimates for the steady state motor coverage $\sigma(t \rightarrow \infty)$ (Eq. 5a) and theoretical transport efficiencies given in [56]. We found very good agreement with our experimental gliding velocities (Fig. 33 a, c) for both 1 mM and 0.05 mM ATP concentrations, V_{MT} (1mM) ≈ 281.5$\frac{nm}{s}$ and V_{MT} (0.05mM) ≈ 133.2$\frac{nm}{s}$.

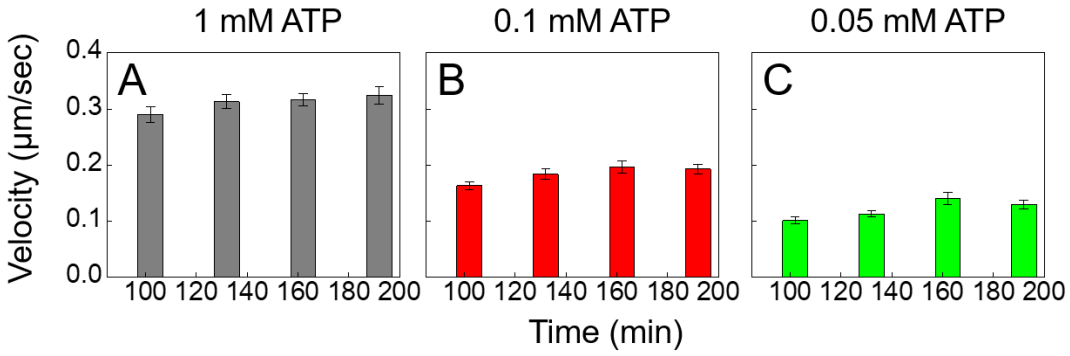

Figure 34. Membrane-coupled motors glide at lower speeds with lower ATP concentrations. Gliding experiments were carried out at 3 different ATP concentrations, 1mM (A), 0.1mM (B), and 0.05mM (C). Microtubule gliding velocities were recorded at steady state after 2 hours. Error bars represent the standard error of the mean. Estimates for gliding velocities at 1 mM and 0.05 mM ATP are V_{MT}(1mM)≈281.5$\frac{\boldsymbol{nm}}{\boldsymbol{s}}$ and V_{MT}(0.05mM)≈133.2$\frac{\boldsymbol{nm}}{\boldsymbol{s}}$.

4.4.3 Increasing Gliding Velocity Over Time Before Steady State

In their recent study, Grover et al. [56] investigated how kinesin-1 transport efficiency was impacted when bound to a lipid bilayer. Using gliding assays, they found that membrane-anchored motors exhibited reduced transport speeds at steady state and attributed the effect to motor slippage in the lipid bilayer. They also found that the steady state microtubule gliding velocity increased with increasing membrane-bound motor density. Our work builds on this past research and focuses on the kinetics of the process and the approach to steady state. Our results reveal that transport via membrane-bound motors is impacted by additional kinetic mechanisms. Both the effects of diffusion on motor binding and unbinding rates and the effect of ATP on the unbinding rate influence the steady state motor coverage. In a full model of motor transport, it will therefore be important to take the effects of motor diffusion into account.

We first examined kinesin binding rates in the absence of ATP to separate out the potential contribution of diffusion on transport. Without ATP on a non-diffusive substrate, the binding on-rate k_a should be zero, but in the case where kinesin is coupled to a fluid bilayer, motors can approach the static microtubule via diffusion, bind and build up on the microtubule while stationary, producing a diffusion controlled on-rate. Fluorescence microscopy allows us to observe this process clearly and plot kinesin accumulation on individual microtubules as time-dependent fluorescence intensity to a saturation point. Our theoretical modelling showed that this process is governed by diffusion and that the approach to saturation was exponential in $t^{1/2}$ with an effective on rate k_a^{eff} of approximately 0.1min^{-1}, which is an order of magnitude lower than what one would expect from a purely reaction controlled on-rate. It is interesting to note that the effective on rate in this diffusion controlled limit is independent of the intrinsic on rate but directly proportional to the diffusion constant (as in Eq. 3b), allowing the membrane fluidity to directly tune this on rate.

We next considered the effects of ATP. Kinesin off rates (k_d) are dependent on ATP concentration and our fitted results for the effective off rates were compared to purely theoretical values of k_d as determined by Michaelis-Menten Kinetics using the steady state maximum velocities obtained in Figure 34. We noticed that a simple Michaelis Menten model produced higher k_d values than those obtained from the fit to our analytical model. As indicated by Eq. 5b, the effective disassociation constant depends not only on the intrinsic disassociation rate but also on the diffusion constant (D), the association constant (k_a), and the saturating motor concentration on the microtubule (σ_m). This effect may be due to rapid rebinding of recently unbound motors surrounding the microtubule. Such an effect in vesicle transport where motors are coupled to a fluid membrane, could act to increase the number of active microtubule-bound motors and thus impact long-range transport in the cell.

It is interesting to note that the steady state coverage of motors (Eq. 5a at infinite t) is independent of the diffusion constant. Thus, while diffusion affects the effective on and off rates and hence the timescale of the transient approach to steady state, it does not

directly affect the steady state coverage for microtubules in a bath of motors. However, in the case of a vesicle being transported along a microtubule, the presence of diffusion makes a qualitative difference in allowing all the motors on the surface to become available for binding as opposed to the case of a rigid bead where only the motors within geometrical reach are available. Thus, the presence of diffusion breaks a common assumption about the availability of motors and significantly increases it. Transient time scales are also important in the vesicle case, because the time it takes for a second motor to bind the microtubule before the first motor disassociates is relevant for the probability of cargo disassociation. Finally, we note that ATP concentration can change the intrinsic off-rate which in turn changes the steady state concentration as well. Thus, for example, reducing ATP concentration decreases k_d which also increases steady state motor coverage – leading to more motors that could potentially lead to increases in run length.

The results from this study demonstrate that motor kinetics are an important determinant of transport that can be affected by membrane diffusion. Thus, more accurate models and experimental systems which incorporate the lipid bilayer are needed to increase our understanding of motor-based transport. Through this work, I identified the prospect of localized kinesin, as the proteins disassociation is a diffusion limited process. In my last project I will explore the potential for membrane bound filaments to produce an active nematic and how this kinesin localization produces unique physics.

Chapter 5

Active Nematics from Membrane Bound Microtubules

5.1 Introduction

In recent years the field of active matter has exploded, producing a rich variety of systems that exhibit collective behaviors. The variety of collective actions from anisotropic particles to proteins to the collective behavior of animals has significantly improved our knowledge of how the interaction between self-propelled particles can form unique phase behaviors. Of these systems, there is a class based on the driving of biofilaments by motor proteins. From these biofilament/motor systems there are a few paradigms. First the gliding of myosin/actin [62] or dynein/microtubule systems [63]. Secondly, the shearing of the kinesin/microtubule system has shown not only unique phase behavior [10, 11]. Thirdly when shearing systems are placed in three-dimensional vesicles, the system can deform its container and cause vesicle motion [22]. Until now kinesin/microtubule gliding systems have not been able to produce an active matter system without the addition of a depletant such as PEG, to exert a depletion force and induce collective motion [12]. Addition of PEG or any other additive is problematic however, in that the system is sensitive to their concentration, and more complex systems could be difficult to understand because of nonspecific binding or clumping of PEG to the system components.

Systems that are based on a depletion force require the additive of large molecules, typically polymers, into solution. These large molecules have an exclusion force due to their size, and their constant interaction with a microtubule will exert a pressure against the filament into the glass. This force prevents the microtubule head from going over another filament and increases the viscosity of the solution, reducing the filament velocity. By using a lipid membrane however, we propose a simpler system to prevent crossing that allows for a richer variety of behaviors. The work presented in chapter 2 and chapter 4 revealed two key characteristics that are applicable to the formation of an active nematic. The first is that when bound to a diffusive membrane, there is a tendency for filaments to "snuggle" [12] and not cross each other [56], due to the slippage of the membrane bound kinesin. The second is that motor proteins that unbind from a filament are diffusion limited and remain in close proximity to microtubules. This kinesin localization is indicative of how membrane bound transport of filaments is a two-way street, the gliding of filaments is driven by the motor protein, and the location of the motor protein is affected by the filaments.

In this study, we demonstrated not only that an active nematic will form from kinesin bound microtubules, but at microtubule densities that are too low to form an active nematic, we see interesting patterns of motion of local filament streams. These streams will persist for long time scales and exhibit global motion despite their local alignment. Even

more interesting, the structure of the active nematic is reflected in the membrane, where areas of increased fluorescence intensity indicate the localization of kinesin.

5.2 Methods

5.2.1 Materials

All lipids used in this chapter were purchased from Avanti Polar Lipids (Alabaster, AL, USA) in chloroform and used without further purification. They include 1,2-dioleoyl-sn-glycero-3-phophocholine (DOPC) and 1,2-dioleoyl-sn-glycero-3-[(N-(5-amino-1-carboxypentyl) iminodiacetic acid) succinyl] (nickel salt) (DGS-NTA(Ni)). Porcine tubulin was purified from pig brains by our lab and rhodamine labeled porcine tubulin (Cat. TL590M) was purchased from Cytoskeleton, Inc (Denver, CO, USA). Recombinant penta-histidine-tagged kinesin protein was purified from *E. coli*. All other chemicals were purchased from Sigma Aldrich (St. Louis, MO, USA).

5.2.2 Microtubule Purification and Preparation

Tubulin was obtained from pig brains provided by local butcher shops in the surrounding area, as the brains cannot be frozen or decomposed as this will denature the protein. Pig brains were then homogenized in a blender to break down the tissue. The mixture was then centrifuged to extract the protein, and GTP was added to polymerize the tubulin within the resuspended protein mix and form microtubules. After reformation, microtubules were extracted by centrifuging and re-homogenized with a dounce. Once they have been broken down, they were resuspended in a high salt bath to remove the MAPs and then centrifuged to separate the tubulin from other microtubule-associated proteins. This process is repeated twice until the final material is checked with a Western blot assay to confirm purity and flash frozen.

Labeled and unlabeled porcine tubulin stock is dissolved at a ratio of 1:5 at a concentration of 2.5 µg/µl in PEM80 (80 mM PIPES, 1 mM ethylene glycol bis(β-aminoethyl ether), 1 mM $MgSO_4$, pH 6.9), buffer and supplemented with 10mM GTP and 40 µM Taxol). The tubulin solution is then incubated in a 37 ℃ bath for 12 hours to allow for polymerization after which microtubules are then stored at room temperature in a dark box.

5.2.3 Motor Protein Purification and Preparation

For this project we purified our own kinesin. K560-GFP motor proteins that are of the kinesin-1 family, labeled with green fluorescent protein (GFP), and have a His-6 tag, were used. These motor proteins were purified over the course of a week from cultures of BL21 competent *E. coli* cells. The plasmid that codes for our motor proteins is taken up into the competent cells through heat shock treatment. During heat shock treatment our cells are kept on ice and after the addition of 5-10 ng of plasmid, the chilled vial is dropped into a 42 ℃ bath for 30 seconds. This flash heating causes the cell membrane to rapidly expand and uptake the plasmid. The culture is then mixed with Super Optimal broth with Catabolite repression (SOC) medium, a rich solution that has nutrients for the *E. coli* to grow in, and left at 37 ℃ on a shaking rack for an hour. After the culture has grown they are plated on Agar plates mixed with 10 mg/ml of ampicillin antibiotic. As our plasmid includes a resistance to the antibiotic, cells that did not uptake the plasmid for motor production will be killed off on the plate when left overnight at 37 ℃.

After growing on the plate, a single colony is then extracted and added to 15µl of Lysogeny broth and an additional 15µl of 100 mg/ml ampicillin and 150 µl of 20% glucose to both kill off any unwanted *E. coli* and to feed the colony. This mixture is again left at 37 ℃ in a shaking incubator for 12-18 hours. After the colony has grown we take 500 µl of sample and mix it with 500 µl of glycerol, so we can freeze our cells and store these cultures for later purification. The current stock of cells is then centrifuged out and resuspended in 1ml TPM media (8g Tryptone, 6g Yeast Extract, 1.6g NaCl, 0.8g Na_2HPO_4, and 0.4g KH_2PO_4) and left to grow at 37 ℃. This growth is measured by the optical density of the sample using a spectrophotometer, typically if the sample is turbid, the culture is at its desired population density and the sample is transferred to a medium with Isopropyl β-D-1-thiogalactopyranoside (IPTG) to induce expression of the kinesin protein.

The cell culture is centrifuged to condense cells and can be frozen for later usage. The cells are then resuspended in lysis buffer, rupturing the cells and releasing the protein into solution, and the cell remains are centrifuged out of solution. The supernatant containing the protein is then added to a Ni-Agarose bead solution, so that histidine tagged protein will bind to the bead and can be removed. Lastly the motor protein is extracted by pouring the beads into a gel column, where the beads rest on the gel. A wash buffer is then flowed through to unbind the motor protein from the beads and collect them on the second elution. Motor protein concentration is then assessed using Nanodrop analysis.

5.2.4 Lipid Membrane Preparation

Lipid mixtures of 91 mol% DOPC, and 9 mol% DGS-NTA(Ni), are mixed in chloroform then vacuum dried to remove all chloroform. Lipids were then rehydrated with water to final concentration of 2.5 mM. Small unilamellar vesicles were formed via tip

sonication and dropcast onto plasma cleaned glass constructed as a flow cell. The sample is incubated at 50 ℃ for 1 hour to allow for fusion of SUVs on the surface forming a single bilayer. DGS-NTA(Ni) was selected as a lipid to anchor motor proteins due to its similar tail structure to DOPC, and ability to partition into the fluid membrane phase.

5.2.5 Flow Cell Preparation

Flow cells are constructed by placing electrical tape on a glass slide cleaned in acetone, methanol, ethanol, and nanopure water that was then plasma cleaned immediately before use. After deposition of lipid membrane, a glass coverslip is placed on top of the tape and set in place with wax to form the flow cell with a volume of approximately 15 µl and sealed with vacuum grease once gliding has been established.

5.2.6 Dilute Microtubule Gliding Experiments

Kinesin solutions, 300 nM in PEM80 buffer, were introduced into the flow cell and left to adhere for 10 min. After allowing 10 minutes for the GFP labeled motors to adhere to the surface, we flowed in the 1:5 Rhodamine labelled microtubules diluted in PEM80 buffer at a concentration of .0125 mg/ml (10µM Taxol), which also removed excess motors. Microtubules were then given 10 minutes to adhere to the remaining motors bound on surface. Lastly a motility mix (PEM80 supplemented with 0.5mM ATP, 2mM DTT, 10 µM Taxol, 0.22 mg/ml glucose oxidase, 0.04 mg/ml catalase, 3.68 mg/ml glucose, 2 mM phosphocreatine and 70 µg/mL creatine phosphokinase) to provide a regenerative ATP source and reduce bleaching. This experiment was repeated in the same manner with ATP concentrations varied at 0.1mM and 0.05mM respectively.

5.2.7 Microtubule Gliding Experiments with Unlabeled Filaments

To induce an active nematic, the same protocol for dilute microtubule gliding was employed but with the addition of unlabeled filaments being added to the diluted microtubule mixture. The number of Rhodamine filaments was kept at .0125 µg/µl concentration while the final mix contained 2-10 µl of 5 µg/µl unlabeled microtubules instead of PEM80. Using this method, we can use the labeled filaments as tracers of the overall filament motility (Fig. 35). Filaments were pulsed back and forth in the flowcell to prevent initial alignment.

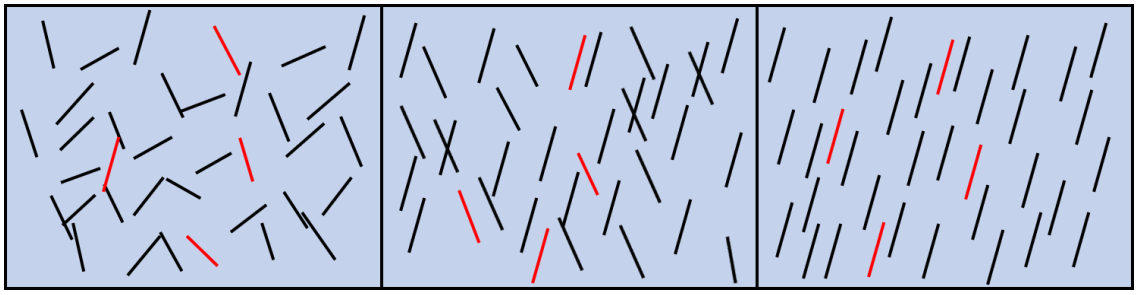

Figure 35. Labeled microtubules as tracers. Labeled filaments are dispersed with unlabeled filaments to show the general direction of flow, without producing to much fluorescence signal to obscure imaging.

5.3 Results

5.3.1 Formation of Active Nematic

Flowcells were prepared in the same manner as our experiments in chapter 4 with the exception that the membrane was left unsupported and only bound to the slide using a monovalent salt, NaCl. Motor proteins bound to a diffusive lipid membrane are able to move in-plane. Because of this diffusivity if the propelled filaments encounter an obstacle, the kinesin will be pushed back, reducing the net force applied by the filament. If the obstacle is another filament, then the filaments might not have enough force to cross each other due to the diffusivity of the membrane. We can see 3 filaments gliding into each other and aligning (Fig. 36). As the filaments are gliding bi-directionally these "snuggling events" are equally probable for filaments that are gliding in the same direction as those that encounter each other from opposite directions. This encounter can be measured by the increase in local fluorescence intensity of a bundle, with more filament encounters forming brighter bundles. These bundles only exist temporarily however, as there is no mechanism for them to become bound to each other or any external force that would keep two filaments together. Over time, bundles will deconstruct back into their constituent filaments. This tendency to "snuggle" is not absolute, and filaments are still able to occasionally cross each other, especially if they encounter each other at almost perpendicular angles. Despite this however, the alignment tendency is strong enough to form an active nematic if the filament density is high enough such that the number of interactions is large.

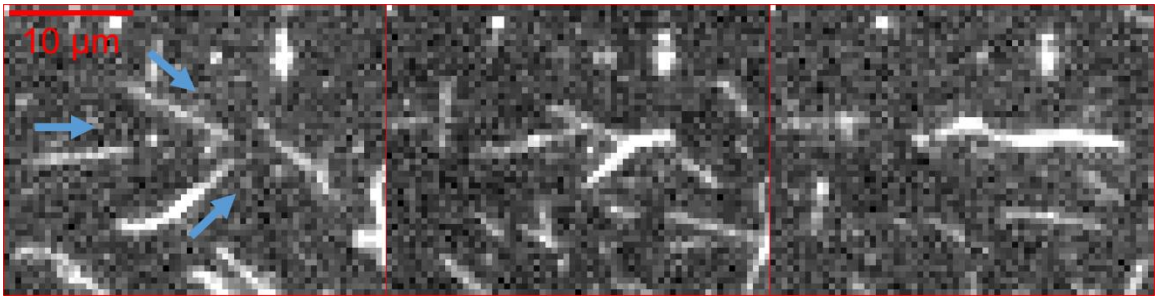

Figure 36. Transport of microtubules on membrane coupled kinesin can induce "snuggling". When filaments are bound to a membrane, the slippage of kinesin will result in an overall reduction of force [56]. If two or more filaments collide, then they may not have to force required to cross each other and align via "snuggling" [12].

When the concentration of microtubules is high enough, we see the formation of an active nematic from an isotropic mix of filaments. Having a larger concentration of filaments increases the number of "snuggling" events while decreasing the time that filaments spend before they encounter another filament. As they align with their neighbors over time they will exhibit a phase transition after ~30 minutes. To better visualize this we kept our original concentration of labeled filaments set at 0.0125 µg/µl, while adding unlabeled filaments to our sample to reach the required density.

In this system we achieved an active nematic when we added a solution of filaments with a density of 0.51 µg/µl and then added a motility mix with an ATP concentration of 0.5 mM. The benefit of this method is that the labeled filaments act as tracers showing the isotropic to nematic transition that occurs (Fig. 37 A, B), without having to deal with excessive fluorescence signal. As we can see there is an overall alignment of the filaments as they glide bidirectionally, and this can be better visualized if we take a t-stack of our gliding video. The t-stack consists of 10 frames that are 10 seconds apart for a total of 1 minute and 40 seconds of activity (Fig. 37 C), so that we can better see the gliding direction for filaments during their motion. This not only helps to illustrate the general direction of our filaments, but also shows some novel behavior in our active nematic, principally that our active nematic exhibits a sinusoid-like trajectory when it forms at this density. Once this active nematic has formed it remains in this phase for the duration of observation, 2 hours in total, and exhibits a global counter-clockwise rotation in orientation. The system can make a 180-degree rotation during this observation period, but the total rotation angle varies depending on the sample observed.

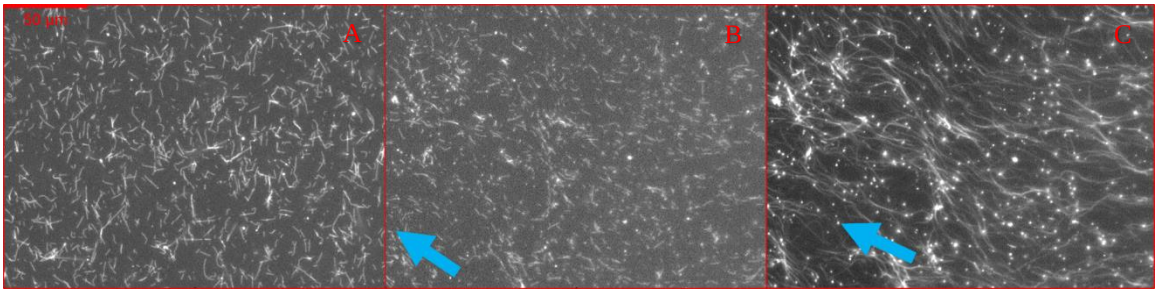

Figure 37. Formation of an active nematic from isotropic due to "snuggling" effect. When microtubules are initially added to the flow cell they are randomly mixed during initial gliding and form the active nematic after 40 minutes of gliding when gliding under the conditions of 0.5mM ATP and 0.51 µg/µl filament density. To better visualize this, we perform a z-stack of 10 frames to show the trajectory of the microtubules.

To test the hypothesis that the formation of this active nematic is due to the slippage of the motor protein on the membrane, and the resulting reduced force, the ATP concentration was reduced. By reducing the activity of the motor protein, the overall force exerted is reduced, increasing the tendency for filaments to "snuggle" against each other (Fig. 38). We can see that the active nematic phase is achievable at lower filament densities, as the lower number of interactions is compensated by the increased "snuggling" tendency. When filaments are gliding at a concentration of 0.1mM ATP, we can see that they form an active nematic at only 0.26 µg/µl by performing a t-stack of 20 frames (Fig. 38 B), almost half of the density of the 0.5 mM ATP samples. By reducing the ATP concentration to 0.05 mM, the activity is further reduced, and by taking a t-stack of 40 frames we can see that the filaments form an active nematic at 0.21 µg/µl microtubule density (Fig. 38 C). An interesting phenomenon is that while the active nematic still exhibit a counter clockwise rotation, the profile of the filament's trajectory is less wavy as the activity decreases, forming straighter lines of orientation.

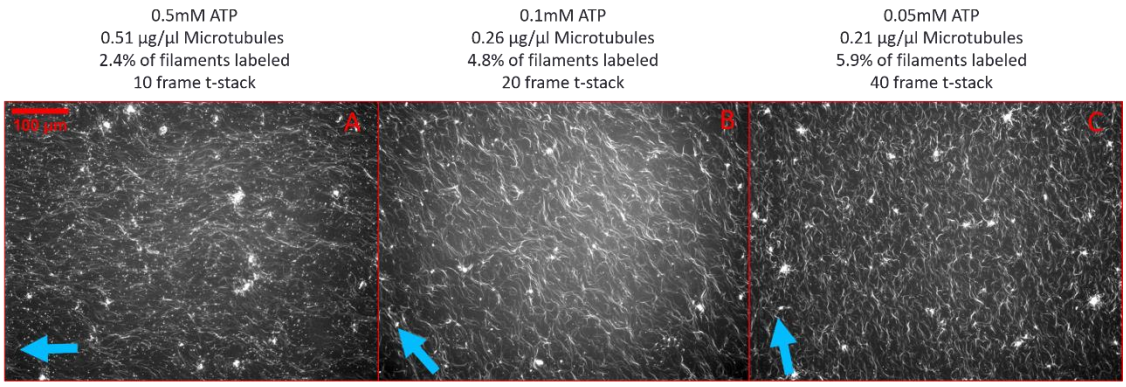

Figure 38. Activity dependence of active nematic phase. Our model for the formation of an active nematic is based on the reduction of motor activity. By reducing ATP concentration we can reduce the activity of kinesin and control the force of interactions. Comparing our initial active nematic (A), we find that by reducing the ATP concentration to 0.1 mM, an active nematic forms at reduced filament concentration (B, C).

5.3.2 Formation of the Network Phase

When gliding at a filament density of 0.26 µg/µl and an ATP concentration of 0.5 mM, we see the formation of a unique phase, termed the Network Phase (Fig. 39). In this phase, the filaments will converge and form bundles of filaments that have their own local orientation. This assemblage of bundles is akin to a network crisscrossing the field of view and will form on the same time scale as the formation of the active nematic phase at higher filaments concentrations. What is unique about these local streams of filaments, is that they will persist for time scales, longer than 30 minutes, and remain after the filaments that initially formed them have left the region. This result is in stark contrast to experiments in literature performed with filaments gliding under a depletion force, where filaments can form bundles but will disperse after their formation. The streams we observe are dynamic in their spatial distribution and can change their shapes and directions slowly overtime. This is most prominent when one observes that the system will still rotate clockwise in the same manner as the active nematic phase. During this rotation (Fig. 39 A-D), the streams of filaments, though independent in local orientation, will exhibit a global rotation. Not all streams will remain however, and some will instead become absorbed with neighboring streams, reforming into new ensembles.

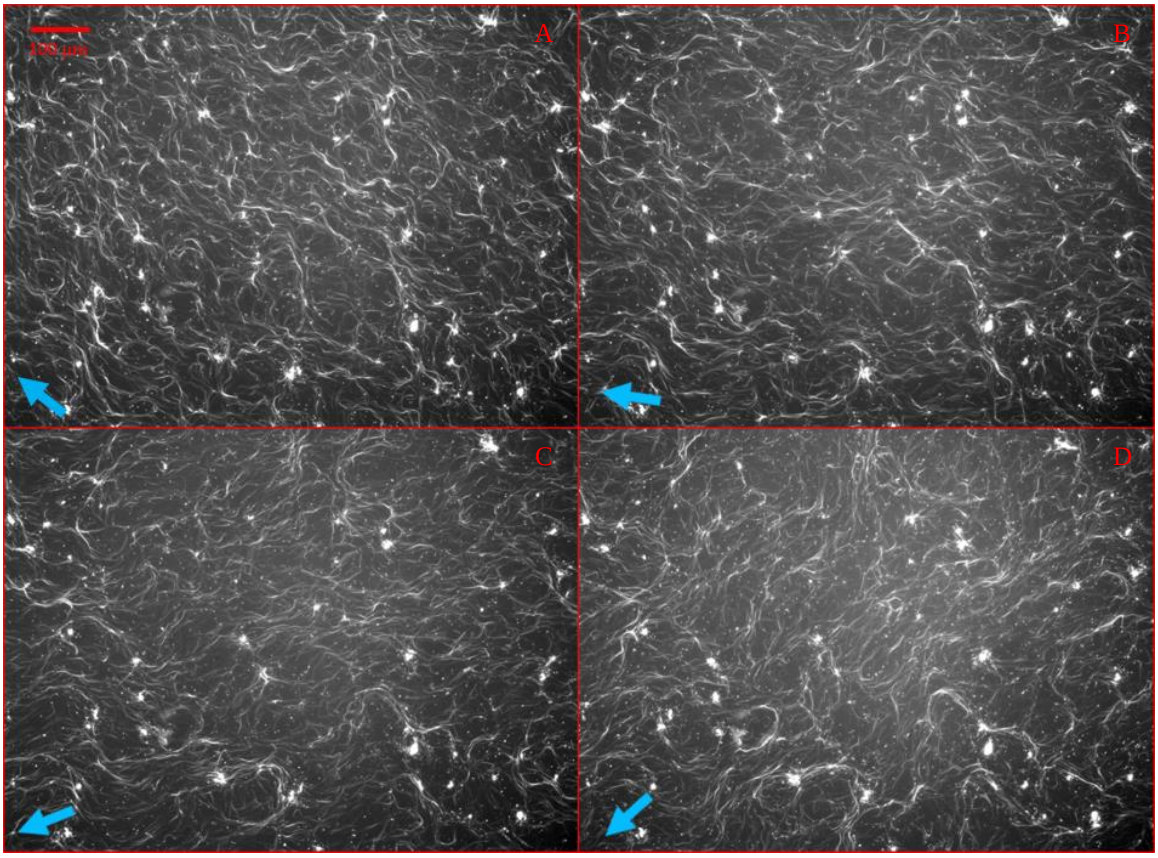

Figure 39. Intermediate network phase. When filament density is at 0.26 µg/ µl and an ATP concentration of 0.5mM the network phase occurs. This phase consists of streams of filaments that persist for long time scales and have local orientation (A). Over time these streams will exhibit a global rotation (B, C, D) that is counterclockwise. Image comprised of a z-stack of 10 frames taken 10 seconds apart.

The formation of different phases is therefore based on the activity of the motor protein and the density of filaments, forming an isotropic phase of random orientation in the dilute filament case, a network phase for certain combinations of motor activity and filament density, or an active nematic if filament density is high enough (Fig. 40).

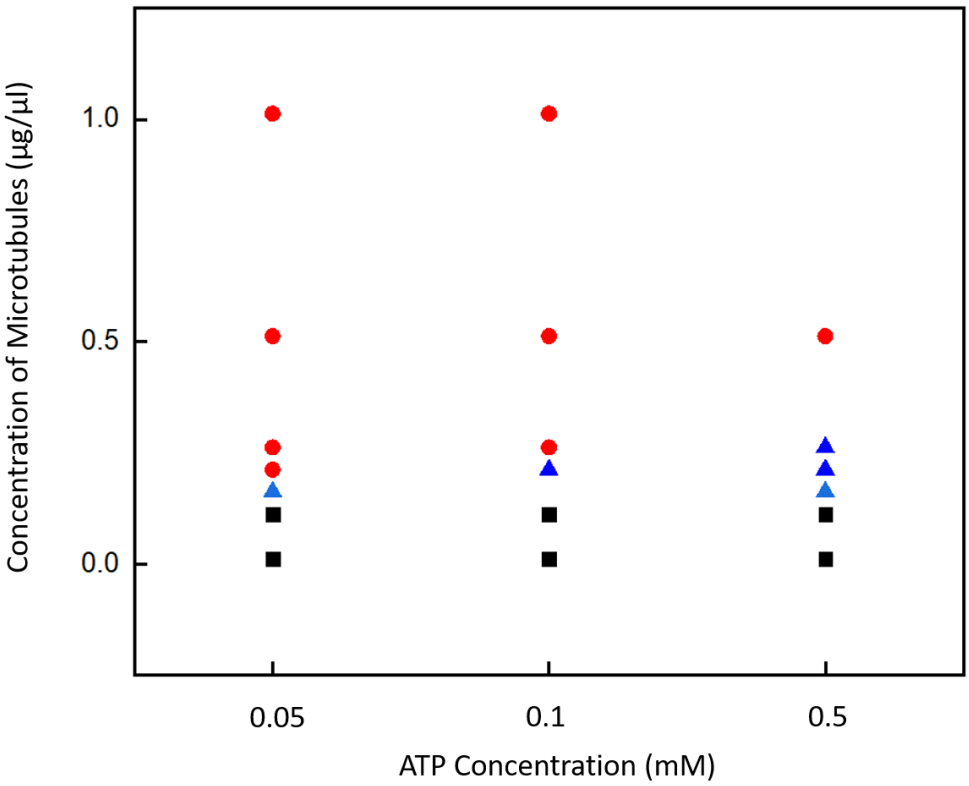

Figure 40. Qualitative Phase Diagram of Active Matter System. The red dots denote areas where the system is an active nematic, with an overall unified orientation. Blue triangles denote the existence of a network phase, where the filaments form streams of independent orientation. Black squares denote areas of isotropic flow, where filaments lack orientation.

The persistence of these streams and their re-orientation can also lead to the formation of vortices (Fig. 41). As the local filament streams move and encounter each other they can merge and form vortices that consist of individual filaments that move either counter clockwise or clockwise. These circular patterns made from bi-directional filaments can persist for tens of minutes. Taken together with the persistence of local streams theses filament patterns represent a unique characteristic of membrane bound active matter. To explain this behavior, we will turn our focus to the membrane.

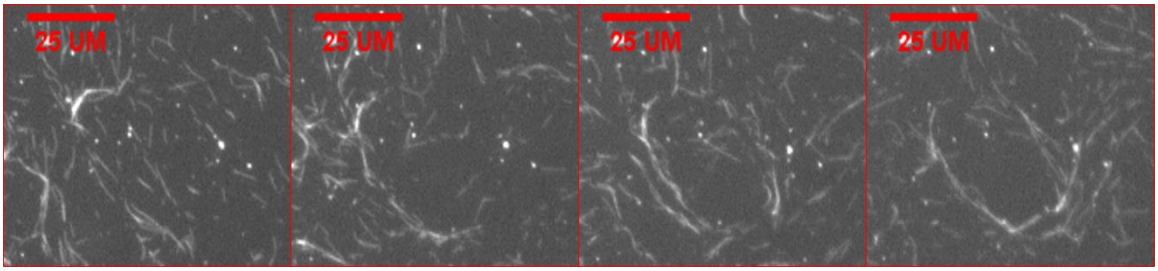

Figure 41. Formation of vortices in Network phase. In some instances, instead of forming streams of random local orientation, the filaments will form vortices that persist for tens of minutes.

5.3.3 Localization of Kinesin

Based on the work in chapter 4 on the disassociation of kinesin from microtubules, we concluded that the kinesin is diffusive on the surface of the membrane. This means that when a filament is gliding, kinesin that disassociates will remain in the region, as its motion is diffusion limited. On a hard glass substrate, the motor protein would remain fixed in its location. In contrast, on a fluid membrane, the motor protein can move and bind to filaments. For our active matter systems with increased filament density, this disassociation occurs writ-large, with hundreds of unlabeled filaments streaming and releasing motor proteins into the bulk membrane. Because of this, we wanted to test if once a large stream of filaments formed, would we see localization of motor proteins as they dissociated from the filaments. To test this hypothesis, we imaged our GFP-labeled motor proteins before gliding was initiated (Fig. 32 A) and saw that the motor distribution was uniform in nature. After gliding was initiated in a sample with 0.1 mM ATP, and 0.1625 mg/ml filament density we observed the formation of streams. After gliding for approximately 45 minutes, we then imaged the membrane bound kinesin in the GFP channel, where we saw that the signal intensity of the GFP was no longer homogenous. We could see not only local areas of high intensity, but these areas that corresponded to regions of dense filament streams (Fig. 32 C) in the Rhodamine channel. These streams were then monitored for 15 minutes, showing that the region is capable of growth at time scales in the tens of minutes (Fig. 32 D).

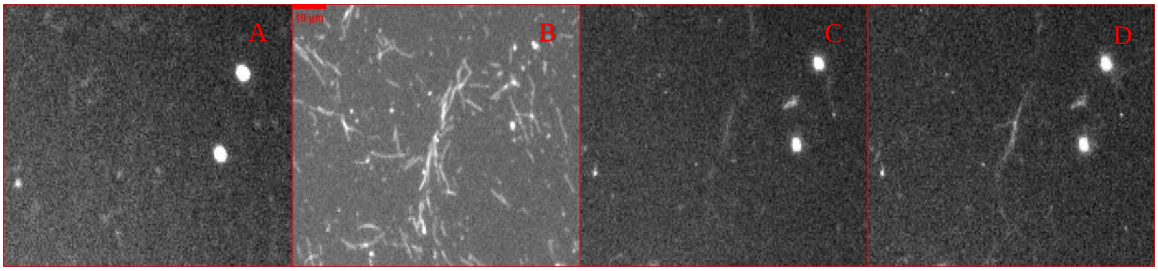

Figure 42. Localization of kinesin. At the start of gliding we can see that the fluorescent signal of our labeled kinesin is uniform (A). After the system has been gliding for a long time and streams of filaments form (B), we can see a localization of the GFP signal (C). After 15 minutes we can see that the GFP signal has grown in intensity and expanded (D).

5.4 Discussion

5.4.1 Membrane Based Active Nematic

In this research we wanted to form an active nematic using microtubules and kinesin bound to a lipid membrane. Previous research in forming active nematics using motor protein and biopolymers has followed one of two tracks: either shearing filaments in solution that can be confined to an interface [10, 11, 22] or filaments gliding on a hard substrate [12, 62, 63]. Both systems have yielded interesting dynamics, but gliding on a hard substrate has shown to be practically difficult to understand, as the nature of the system changes with the motor protein and filaments used. Experiments that have filament propelled by motor proteins have used myosin/actin filaments or dynein/microtubules to form active nematics, however kinesin/microtubule systems will not work on their own. For reasons currently not understood, microtubule filaments will not align on their own during gliding, and past work has required that an agent be added to solution. These agents such a PEG or methylcellulose, exert a depletion force on filaments, and theoretically will press them into the surface to prevent crossing.

In this system, we were able to form an active nematic without needing additional components that could interact with the protein or filaments. This was accomplished by the diffusivity of the membrane, reducing the momentum of filaments and preventing their crossing. When filaments reach a certain density, the mutual interactions from their motion will form a large-scale alignment, in the same way that depletion-force mitigated-interactions will. In a similar fashion, over time this system will exhibit a repeatable counterclockwise rotation that is characteristic of these systems [95]. This “snuggling” can then be tuned, by lowering the ATP concentrations we can increase their tendency to aligns and form an active nematic at lower filament densities.

This means of forming an active nematic opens up significant possibilities for exploring the collective behavior of filament particles. The most immediate application is

that we can tune the diffusivity and organization of our membrane. Lipid membranes are capable of a rich variety of lateral organization and can support a variety of phases. These phases can either affect the surface profile such as the ripple phase or affect the local diffusivity by forming lipid rafts. Another potential application is that we can place a lipid membrane on a variety of surfaces, not just planar ones, which could allow for more novel three-dimensional active phases. This membrane systems novelty extends beyond the active nematic phase and shows unique behavior at lower filament density that has not been reported for non-membrane bound systems.

5.4.2 Membrane Diffusivity and the Formation of Network Phase

When gliding below the density of an active nematic we see that streams of filaments form. These filament streams persist even in the absence of MAP proteins to bind them [12]. These streams exhibit a local orientation, with streams forming in all directions, connecting to each other in a manner reminiscent of a network. This contrasts with the results reported in depletion force experiments where filament bundles align with the overall direction of their neighbors [12]. Despite their local orientation these bundles can exhibit a global rotation [95], with some streams persisting for the entire rotation or reforming with other streams. These streams can form more complicated morphologies such as vortices that persist for long time scales.

An explanation for this behavior is not yet known, but we hypothesize that the time dependent localization of kinesin allows for stream persistence. As the microtubule glides, the work in chapter 4 established that gliding filaments are shedding kinesin at rate k_d^{eff} and are capable of absorbing motor proteins as they diffuse around the filament. This means that disassociated kinesin will remain in the local region and bind to other new filaments. For the dilute filament case this is not significant, but if we have hundreds of filaments streaming into a location and localizing the kinesin as we have observed, this could alter the filaments motion. Regions of higher motor density could change the local diffusivity of the membrane as well as make a motor protein gradient that steers filaments towards areas of higher motor density.

There are experimental challenges to investigation of this hypothesis, as imaging low concentrations of motor proteins is difficult with a standard fluorescent microscope. Future work with confocal or TIRF microscopy will be ideal. Additionally, the counterclockwise rotation in phases below the active nematic threshold is not well understood. Though this system is not completely understood, it has provided much important insight in the physics of active matter. Past experiments have demonstrated that forming an active matter system is an increasingly simple task, where one only needs to find particles that interact with each other and that are self-driven. What is more critical is to form systems of particles that don't just interact with each other but interact with the environment that in turn interacts with the particles. Living creatures, the highest form of active matter, do not just consume resources from their environment. We alter our

environment with our existence, and that alteration in turn changes us. By binding our kinesin and filaments to a diffusive membrane, we have formed an environment that induces a collective action by imposing the "snuggling" effect. However, the resulting properties of filaments then appear to in-turn affect the membrane, by localizing the bound kinesin to regions of high traffic. Exploring ways to better understand the underlying physics of this system will help us to better understand complex active matter. Eventually researchers could apply this first principles knowledge to the formation of synthetic, *ab initio* active matter systems indistinguishable from organic systems.

Conclusions and Future Work

In this thesis we covered 3 unique experiments relating to motor protein interactions with lipid membranes. The first experiment in chapter 3 used a simplified system to extract a nanotubule from a GUV. By pulling the GUV anchored by kinesin with a flow of fluid, the drag force induced will pull out tubules from the vesicles anchor points. This experiment found that the force required to extract a microtubule, 7.2 pN, confirming our hypothesis that only one to two motors are required to form a tubule from a fluid membrane. I used FRAP to characterize the membrane diffusivity coming to the determination that it's diffusion constant was D= 9.01 ± 0.58 $\frac{\mu m^2}{s}$. Beyond the results of this work we have the building blocks for the research presented in chapter 4 and 5, namely a way to bind motor proteins to a diffusive lipid membrane.

In chapter 4 we covered how membrane bound filament transport unique properties when compared to glass. In terms of active motion of filaments, we see that when microtubules are gliding on a diffusive membrane, they show significant increases in velocity over time. This increase in velocity requires that the filaments be bound to the membrane and is independent of their active gliding. To understand this property, we tested how motor proteins bound to a diffusive surface have a different interaction with the filament compared to glass and to our surprise we observed that the kinesin will diffuse and cluster onto a filament. When ATP is added to these clustered filaments the drop-in signal is modeled with a power law, not an inverse exponential, leading us to concluded that the disassociation of the motor is diffusion limited. This diffusion limitation could indicate that over long time scales the motor density is increasing on the filament. More importantly the implications of this work are that microtubules not only glide when bound to motor proteins on a membrane, but can in turn affect the kinesin itself, potentially localizing it.

In chapter 5 we used the results from chapter 4 to build an active nematic system. The "snuggling" behavior of our lipid bound filaments not only produced an active nematic, but at lower filament densities produced a phase with unique properties. Below this density the network phase is a unique combination of global and local properties, with filament streams orientated independent of each other yet rotate together. More interesting the active matter system seems to be capable of large-scale localization of kinesin, re-enforcing streams and extending their duration existence. Using a lipid membrane, I have made an active nematic that doesn't just have an environment forces particle interaction, but a system that in turn impacts its environment.

The course of the work in this thesis originally set out to understand the physics of kinesin-1 and their interactions with lipid membranes, principally how tubulation occurs and how the lipid membrane can alter the transport properties of filaments. In the course of that work however we discovered that that same lipid membrane could be used to form an active nematic, and more importantly be used as a model for an active matter system that is a product of its environment and in turn alters the environment. The advantage of

this system is twofold. Firstly, as a two-dimensional system it means that observing experiments is greatly simplified from observing systems composed of lipid vesicles that have three dimensions. Lastly, while the system is two-dimensional, the lipid membrane is still capable of hierarchies, where one could envision lipid rafts that confine the active matter. This hypothetical system could be driven by raft coalescence on one hand, as the system will want to reorganize itself to completely phase separate. On the other hand, the motion from the active matter bound to the rafts, when combined with another raft could drive them apart, presenting a system of growth and replication, as rafts absorb one another but then are driven towards division. Systems such as these will give us a better understanding of the first principles required to understand living systems, until a day comes were we can simplify them to the point where we will not need to rely on already extant proteins but can use analogs found abiotically.

References

[1] G. De Magistris and D. Marenduzzo, "An Introduction to the Physics of Active Matter," *Physica A: Satistical Mechanics and its Applications,* vol. 418, pp. 65-77, 2015.

[2] R. D. Vale, "The molecular motor toolbox for intracellular transport," *Cell,* vol. 112, no. 4, pp. 467-480, 2003.

[3] S. Thutupalli, M. Sun, F. Bunyak, K. Palaniappan and J. W. Shaevitz, "Directional reversals enable Myxococcus xanthus cells to produce collective one-dimensional streams during fruiting-body formation," *Journal of The Royal Society Interface,* vol. 12, no. 109, p. 20150049, 2015.

[4] J. Xu, S. J. King, M. Lapierre-Landry and B. Nemec, "Interplay between velocity and travel distance of kinesin-based transport in the presence of tau," *Biophysical journal,* vol. 105, no. 10, pp. L23-L25, 2013.

[5] T. Duke, T. E. Holy and S. Leibler, "" Gliding assays" for motor proteins: A theoretical analysis," *Physical review letters,* vol. 74, no. 2, p. 330, 1995.

[6] T. Korten and S. Diez, "Setting up roadblocks for kinesin-1: mechanism for the selective speed control of cargo carrying microtubules," *Lab on a Chip,* vol. 8, no. 9, pp. 1441-1447, 2008.

[7] Y. Okada, H. Yamazaki, Y. Sekine-Aizawa and N. Hirokawa, "The neuron-specific kinesin superfamily protein KIF1A is a unique monomeric motor for anterograde axonal transport of synaptic vesicle precursors," *Cell,* vol. 81, no. 5, pp. 769-780, 1995.

[8] C. Lor, J. D. Lopes, M. K. Mattson-Hoss, J. Xu and L. S. Hirst, "A Simple Experimental Model to Investigate Force Range for Membrane Nanotube Formation," *Frontiers in Materials,* vol. 3, no. 6, 2016.

[9] P. Bieling, I. A. Telley, J. Piehler and T. Surrey, "Processive kinesins require loose mechanical coupling for efficient collective motility," *EMBO reports,* vol. 9, no. 11, pp. 1121-1127, 2008.

[10] T. Sanchez, D. T. Chen, S. J. DeCamp, M. Heymann and Z. Dogic, "Spontaneous motion in hierarchically assembled active matter," *Nature,* vol. 491, no. 7424, p. 431, 2012.

[11] S. J. DeCamp, G. S. Redner, A. Baskaran, M. F. Hagan and Z. Dogic, "Orientational order of motile defects in active nematics," *Nature materials,* vol. 14, no. 11, p. 1110, 2015.

[12] D. Inoue, B. Mahmot, A. M. R. Kabir, T. I. Farhana, K. Tokuraku, K. Sada, A. Konagaya and A. Kakugo, "Depletion force induced collective motion of microtubules driven by kinesin," *Nanoscale,* vol. 7, no. 43, pp. 18054-18061, 2015.

[13] L. S. Hirst, Fundamentals of soft matter science, CRC Press, 2012.

[14] I. Buttinoni, G. Volpe, F. Kümmel, G. Volpe and C. Bechinger, "Active Brownian motion tunable by light," *Journal of Physics: Condensed Matter,* vol. 24, no. 28, p. 284129, 2012.

[15] M. Tennenbaum, Z. Liu, D. Hu and A. Fernandez-Nieves, "Mechanics of fire ant aggregations," *Nature materials,* vol. 15, no. 1, p. 54, 2016.

[16] R. Di Leonardo, "Active colloids: controlled collective motions," *Nature materials,* vol. 15, no. 10, p. 1057, 2016.

[17] D. Needleman and J. Brugues, "Determining physical principles of subcellular organization," *Developmental cell,* vol. 29, no. 2, pp. 135-138, 2014.

[18] R. M. Capito, H. S. Azevedo, Y. S. Velichko, A. Mata and S. I. Stupp, "Self-assembly of large and small molecules into hierarchically ordered sacs and membranes," *Science,* vol. 319, no. 5871, pp. 1812-1816, 2008.

[19] O. Lieleg, M. M. Claessens and A. R. Bausch, "Structure and dynamics of cross-linked actin networks," *Soft Matter,* vol. 6, no. 2, pp. 218-225, 2010.

[20] M. S. Cheung, "Where soft matter meets living matter—protein structure, stability, and folding in the cell," *Current opinion in structural biology,* vol. 23, no. 2, pp. 212-217, 2013.

[21] F. G. Woodhouse and R. E. Goldstein, "Spontaneous circulation of confined active suspensions," *Physical review letter,* vol. 109, no. 16, p. 168105, 2012.

[22] F. C. Keber, E. Loiseau, T. Sanchez, S. J. DeCamp, L. Giomi, M. J. Bowick, M. C. Marchetti, Z. Dogic and A. R. Bausch, "Topology and dynamics of active nematic vesicles," *Science,* vol. 345, no. 6201, pp. 1135-1139, 2014.

[23] R. Zimmermann, D. Küttner, L. Renner, M. Kaufmann, J. Zitzmann, M. Müller and C. Werner, "Charging and structure of zwitterionic supported bilayer lipid membranes studied by streaming current measurements, fluorescence microscopy,

and attenuated total reflection Fourier transform infrared spectroscopy," *Biointerphases,* vol. 4, no. 1, pp. 1-6, 2009.

[24] N. Sanghera and T. J. Pinheiro, "Unfolding and refolding of cytochrome c driven by the interaction with lipid micelles," *Protein Science,* vol. 9, no. 6, pp. 1194-1202, 2000.

[25] J. Jouhet, "Importance of the hexagonal lipid phase in biological membrane organization.," *Frontiers in plant science,* vol. 4, p. 494, 2013.

[26] M. Ashrafuzzaman and J. A. Tuszynski, Membrane Biophysics, Springer Science & business Media, 2012.

[27] W.-K. Fong, T. L. Hanley, B. Thierry, A. Tilley, N. Kirby, L. J. Waddington and B. J. Boyd, "Understanding the photothermal heating effect in non-lamellar liquid crystalline systems, and the design of new mixed lipid systems for photothermal on-demand drug delivery," *Physical Chemistry Chemical Physics,* vol. 16, no. 45, pp. 24936-24953, 2014.

[28] P. Uppamoochikkal, S. Tristram-Nagle and J. F. Nagle, "Orientation of tie-lines in the phase diagram of DOPC/DPPC/cholesterol model biomembranes," *Langmuir,* vol. 26, no. 22, pp. 17363-17368, 2010.

[29] M. Edidin, "The state of lipid rafts: from model membranes to cells," *Annual review of biophysics and biomolecular structure,* vol. 32, no. 1, pp. 257-283, 2003.

[30] L. S. Hirst, P. Uppamoochikkal and C. Lor, "Phase separation and critical phenomena in biomimetic ternary lipid mixtures," *Liquid Crystals,* vol. 38, no. 11-12, pp. 1735-1747, 2011.

[31] P. G. Saffman and M. Delbrück, "Brownian motion in biological membranes," *Proceedings of the National Academy of Sciences,* vol. 72, no. 8, pp. 3111-3113, 1975.

[32] D. Brown and E. London, "Functions of lipid rafts in biological membranes," *Annual review of cell and developmental biology,* vol. 14, no. 1, pp. 111-136, 1998.

[33] K. Jacobson, O. G. Mouritsen and R. G. Anderson, "Lipid rafts: at a crossroad between cell biology and physics," *Nature cell biology,* vol. 9, no. 1, p. 7, 2007.

[34] H. Xiao, P. Verdier-Pinard, N. Fernandez-Fuentes, B. Burd, R. Angeletti, A. Fiser, S. B. Horwitz and G. A. Orr, "Insights into the mechanism of microtubule stabilization by Taxol," *Proceedings of the National Academy of Sciences,* vol. 103, no. 27, pp. 10166-10173, 2006.

[35] K. S. Burbank and T. J. Mitchison, "Microtubule dynamic instability," *Current Biology,* vol. 16, no. 14, pp. R516-R517, 2006.

[36] A. Desai and T. J. Mitchison, "Microtubule polymerization dynamics," *Annual review of cell and developmental biology,* vol. 13, no. 1, pp. 83-117, 1997.

[37] T. Mitchison and M. Kirschner, "Dynamic instability of microtubule growth," *nature,* vol. 312, no. 5991, p. 237, 1984.

[38] E. Nogales, "Structural insights into microtubule function," *Annual review of biochemistry,* vol. 69, no. 1, pp. 277-302, 2000.

[39] T. Horio and T. Murata, "The role of dynamic instability in microtubule organization," *Frontiers in plant science,* vol. 5, p. 511, 2014.

[40] R. Stracke, K. J. Böhm, J. Burgold, H.-J. Schacht and E. Unger, "Physical and technical parameters determining the functioning of a kinesin-based cell-free motor system," *Nanotechnology,* vol. 11, no. 2, p. 52, 2000.

[41] K. Visscher, M. J. Schnitzer and S. M. Block, "Single kinesin molecules studied with a molecular force clamp," *Nature,* vol. 400, no. 6740, p. 184, 1999.

[42] L. Jia, S. G. Moorjani, T. N. Jackson and W. O. Hancock, "Microscale transport and sorting by kinesin molecular motors," *Biomedical microdevices,* vol. 6, no. 1, pp. 67-74, 2004.

[43] H. Hess and V. Vogel, "Molecular shuttles based on motor proteins: active transport in synthetic environments," *Reviews in Molecular Biotechnology,* vol. 82, no. 1, pp. 67-85, 2001.

[44] D. H. Mengistu, E. E. Kooijman and S. May, "Ionization properties of mixed lipid membranes: A Gouy–Chapman model of the electrostatic–hydrogen bond switch," *Biochimica et Biophysica Acta (BBA)-Biomembranes,* vol. 1808, no. 8, pp. 1985-1992, 2011.

[45] R. D. Vale, T. S. Reese and M. P. Sheetz, "Identification of a novel force-generating protein, kinesin, involved in microtubule-based motility," *Cell,* vol. 42, no. 1, pp. 39-50, 1985.

[46] N. J. Carter and R. A. Cross, "Mechanics of the kinesin step," *Nature,* vol. 435, no. 7040, p. 308, 2005.

[47] J. Rousselet, L. Salome, A. Ajdari and J. Prostt, "Directional motion of Brownian particles induced by a periodic asymmetric potential," *Nature,* vol. 370, no. 6489, p. 446, 1994.

[48] C. Appert-Rolland, M. Ebbinghaus and L. Santen, "Intracellular transport driven by cytoskeletal motors: General mechanisms and defects," *Physics Reports,* vol. 593, pp. 1-59, 2015.

[49] M. J. Schnitzer and S. M. Block, "Kinesin hydrolyses one ATP per 8-nm step," *Nature,* vol. 388, no. 6640, p. 386, 1997.

[50] R. D. Vale and R. A. Milligan, "The way things move: looking under the hood of molecular motor proteins," *Science,* vol. 288, no. 5463, pp. 88-95, 2000.

[51] N. Hirokawa, Y. Noda, Y. Tanaka and S. Niwa, "Kinesin superfamily motor proteins and intracellular transport," *Nature reviews Molecular cell biology,* vol. 10, no. 10, p. 682, 2009.

[52] S. Klumpp and R. Lipowsky, "Cooperative cargo transport by several molecular motors," *Proceedings of the National Academy of Science,* vol. 102, no. 48, pp. 17284-17289, 2005.

[53] J. T. Finer, R. M. Simmons and J. A. Spudich, "Single myosin molecule mechanics: piconewton forces and nanometre steps," *Nature,* vol. 368, no. 6467, p. 113, 1994.

[54] S. R. Nelson, K. M. Trybus and D. M. Warshaw, "Motor coupling through lipid membranes enhances transport velocities for ensembles of myosin Va," *Proceedings of the National Academy of Sciences,* vol. 111, no. 38, pp. E3986-E3995, 2014.

[55] Q. Li, K.-F. Tseng, S. J. King, W. Qiu and J. Xu, "A fluid membrane enhances the velocity of cargo transport by small teams of kinesin-1," *The Journal of chemical physics,* vol. 148, no. 12, p. 123318, 2018.

[56] R. Grover, J. Fischer, F. W. Schwarz, W. J. Walter, P. Schwille and S. Diez, "Transport efficiency of membrane-anchored kinesin-1 motors depends on motor density and diffusivity," *Proceedings of the National Academy of Sciences,* vol. 113, no. 46, pp. E7185-E7193, 2016.

[57] M. C. Marchetti, J.-F. Joanny, S. Ramaswamy, T. B. Liverpool, J. Prost, M. Rao and R. A. Simha, "Hydrodynamics of soft active matter," *Reviews of Modern Physics,* vol. 85, no. 3, p. 1143, 2013.

[58] F. G. Woodhouse and R. E. Goldstein, "Spontaneous circulation of confined active suspensions," *Physical review letters,* vol. 109, no. 16, p. 168105, 2012.

[59] D. Needleman and Z. Dogic, "Active matter at the interface between materials science and cell biology," *Nature Reviews Materials,* vol. 2, no. 9, p. 17048, 2017.

[60] T. H. Jukes and M. Kimura, "Evolutionary constraints and the neutral theory," *Journal of molecular evolution,* vol. 21, no. 1, pp. 90-92, 1984.

[61] T. Surrey, F. Nédélec, S. Leibler and E. Karsent, "Physical properties determining self-organization of motors and microtubules," *Science,* vol. 292, no. 5519, pp. 1167-1171, 2001.

[62] V. Schaller, C. Weber, C. Semmrich, E. Frey and A. R. Bausch, "Polar patterns of driven filaments," *Nature,* vol. 467, no. 7311, p. 73, 2010.

[63] Y. Sumino, K. H. Nagai, Y. Shitaka, D. Tanaka, K. Yoshikawa, H. Chaté and K. Oiwa, "Large-scale vortex lattice emerging from collectively moving microtubules," *Nature,* vol. 483, no. 7390, p. 448, 2012.

[64] T. Vicsek, A. Czirók, E. Ben-Jacob, I. Cohen and O. Shochet, "Novel type of phase transition in a system of self-driven particles," *Physical review letters,* vol. 75, no. 6, p. 1226, 1995.

[65] M. Terasaki, L. B. Chen and K. Fujiwara, "Microtubules and the endoplasmic reticulum are highly interdependent structures," *The Journal of cell biology,* vol. 103, no. 4, pp. 1557-1568, 1986.

[66] R. D. Vale and H. Hotani, "Formation of membrane networks in vitro by kinesin-driven microtubule movement," *The Journal of Cell Biology,* vol. 107, no. 6, pp. 2233-2241, 1988.

[67] D. Axelrod, D. E. Koppel, J. Schlessinger, E. Elson and W. W. Webb, "Mobility measurement by analysis of fluorescence photobleaching recovery kinetics," *Biophysical journal,* vol. 16, no. 9, pp. 1055-1069, 1976.

[68] S. Uemura, K. Kawaguchi, J. Yajima, M. Edamatsu, Y. Y. Toyoshima and S. Ishiwata, "Kinesin-microtubule binding depends on both nucleotide state and loading direction," *Proceedings of the National Academy of Sciences,* vol. 99, no. 9, pp. 5977-5981, 2002.

[69] Q. P. Su, W. Du, Q. Ji, B. Xue, D. Jiang, Y. Zhu, H. Ren, C. Zhang, J. Lou, L. Yu and Y. Sun, "Vesicle size regulates nanotube formation in the cell," *Scientific Reports,* vol. 6, p. 24002, 2016.

[70] J.-B. Manneville, P. Bassereau, S. Ramaswamy and J. Prost, "Active membrane fluctuations studied by micropipette aspiration," *Physical Review E,* vol. 64, no. 2, p. 021908, 2001.

[71] H. J. Deuling and W. Helfrich, "Red blood cell shapes as explained on the basis of curvature elasticity," *Biophysical journal* , vol. 16, no. 8, pp. 861-868, 1976.

[72] J. Happel and H. Brenner, Low Reynolds number hydrodynamics: with special applications to particulate media (Vol. 1), Springer Science & Business Media, 2012.

[73] E. Schäffer, S. F. Nørrelykke and J. Howard, "Surface forces and drag coefficients of microspheres near a plane surface measured with optical tweezers," *Langmuir,* vol. 23, no. 7, pp. 3654-3665, 2007.

[74] D. Cuvelier, I. Derényi, P. Bassereau and P. Nassoy, "Coalescence of membrane tethers: experiments, theory, and applications," *Biophysical journal,* vol. 88, no. 4, pp. 2714-2726, 2005.

[75] W. Rawicz, K. C. Olbrich, T. McIntosh, D. Needham and E. Evans, "Effect of chain length and unsaturation on elasticity of lipid bilayers," *Biophysical journal,* vol. 79, no. 1, pp. 328-339, 2000.

[76] C.-H. Lee, W.-C. Lin and J. Wang, "Measuring the bending rigidity of giant unilamellar liposomes with differential confocal microscopy," *Conference on Lasers and Electro-Optics,* p. CFF7, 2000.

[77] J. Xu, Z. Shu, S. J. King and S. P. Gross, "Tuning multiple motor travel via single motor velocity," *Traffic,* vol. 13, no. 9, pp. 1198-1205, 2012.

[78] T. Pott, H. Bouvrais and P. Méléard, "Long-range transport of giant vesicles along microtubule networks," *Chemistry and physics of lipids,* vol. 154, no. 2, pp. 115-119, 2008.

[79] D. M. Soumpasis, "Theoretical analysis of fluorescence photobleaching recovery experiments," *Biophysical journal,* vol. 41, no. 1, pp. 95-97, 1983.

[80] F. Harb, A. Simon and B. Tinland, "Ripple formation in unilamellar-supported lipid bilayer revealed by FRAPP," *The European Physical Journal E,* vol. 36, no. 12, p. 140, 2013.

[81] L. S. Hirst, A. Ossowski, M. Fraser, J. Geng, J. V. Selinger and R. L. Selinger, "Morphology transition in lipid vesicles due to in-plane order and topological

defects," *Proceedings of the National Academy of Sciences,* vol. 110, no. 9, pp. 3242-3247, 2013.

[82] A. Roux, G. Cappello, J. Cartaud, J. Prost, B. Goud and P. Bassereau, "A minimal system allowing tubulation with molecular motors pulling on giant liposomes," *Proceedings of the National Academy of Sciences,* vol. 99, no. 8, pp. 5394-5399, 2002.

[83] M. Tokarz, B. Hakonen, P. Dommersnes, O. Orwar and B. Åkerman, "Electrophoretic transport of latex particles in lipid nanotubes," *Langmuir,* vol. 23, no. 14, pp. 7652-7658, 2007.

[84] N. Stepanyants, G. D. Jeffries, O. Orwar and A. Jesorka, "Radial sizing of lipid nanotubes using membrane displacement analysis," *Nano letters,* vol. 12, no. 3, pp. 1372-1378, 2012.

[85] N. Hirokawa, "Kinesin and dynein superfamily proteins and the mechanism of organelle transport," *Science,* vol. 279, no. 5350, pp. 519-526, 1998.

[86] R. D. Allen, D. G. Weiss, J. H. Hayden, D. T. Brown, H. Fujiwake and M. Simpson, "Gliding movement of and bidirectional transport along single native microtubules from squid axoplasm: evidence for an active role of microtubules in cytoplasmic transport," *The Journal of Cell Biology,* vol. 100, no. 5, pp. 1736-1752, 1985.

[87] A. J. Tan, D. E. Chapman, L. S. Hirst and J. Xu, "Understanding the role of transport velocity in biomotor-powered microtubule spool assembly," *RSC Advances,* vol. 6, no. 82, pp. 79143-79146, 2016.

[88] T. A. Schroer, B. J. Schnapp, T. S. Reese and M. P. Sheetz, "The role of kinesin and other soluble factors in organelle movement along microtubules," *The Journal of cell biology,* vol. 107, no. 5, pp. 1785-1792, 1988.

[89] M. Setou, T. Nakagawa, D.-H. Seog and N. Hirokawa, "Kinesin superfamily motor protein KIF17 and mLin-10 in NMDA receptor-containing vesicle transport," *Science,* vol. 288, no. 5472, pp. 1796-1802, 2000.

[90] J. J. Keya, D. Inoue, Y. Suzuki, T. Kozai, D. Ishikuro, N. Kodera, T. Uchihashi, A. M. R. Kabir, M. Endo, K. Sada and A. Kakugo, "High-Resolution imaging of a single gliding protofilament of tubulins by HS-AFM," *Scientific Reports,* vol. 7, no. 1, p. 6166, 2017.

[91] R. F. Flewelling and W. L. Hubbell, "Hydrophobic ion interactions with membranes. Thermodynamic analysis of tetraphenylphosphonium binding to vesicles," *Biophysica journal,* vol. 49, no. 2, pp. 531-540, 1986.

[92] J. B. Pawley, Handbook of biological confocal microscopy, Springer Science & Business Media, 2010.

[93] T. Miura and K. Seki, "Diffusion influenced adsorption kinetics," *The Journal of Physical Chemistry B,* vol. 119, no. 34, pp. 10954-10961, 2015.

[94] C. Leduc, O. Campàs, K. B. Zeldovich, A. Roux, P. Jolimaitre, L. Bourel-Bonnet, B. Goud, J.-F. Joanny, P. Bassereau and J. Prost, "Cooperative extraction of membrane nanotubes by molecular motors," *Proceedings of the National Academy of Sciences,* vol. 101, no. 49, pp. 17096-17101, 2004.

[95] K. Kim, N. Yoshinaga, S. Bhattacharyya, H. Nakazawa, M. Umetsu and W. Teizer, "Large-scale chirality in an active layer of microtubules and kinesin motor proteins," *Soft Matter,* vol. 14, no. 17, pp. 3221-3231, 2018.

[96] F. Pampaloni, G. Lattanzi, A. Jonáš, T. Surrey, E. Frey and E.-L. Florin, "Thermal fluctuations of grafted microtubules provide evidence of a length-dependent persistence length," *Proceedings of the National Academy of Sciences,* vol. 103, no. 27, pp. 10248-10253, 2006.

[97] C. Herold, C. Leduc, R. Stock, S. Diez and P. Schwille, "Long-range transport of giant vesicles along microtubule networks," *ChemPhysChem,* vol. 13, no. 4, pp. 1001-1006, 2012.